Anomalous speed correlations in starling flocks: from microscopic models to field theory

Scuola di dottorato Vito Volterra

Dottorato di Ricerca in Fisica – XXXIV Ciclo

Candidate
Antonio Culla
ID number 1604296

Thesis Advisor
Andrea Cavagna

February 11, 2022

Thesis defended on 11/02/2022
in front of a Board of Examiners composed by:

Roberto Di Leonardo (chairman)

Roberto Benzi

José Lorenzana

Abstract

From the analysis of experimental data about starling flocks we can find some key properties of these biological systems. First of all, flocks are highly polarized systems, i.e. every individual's velocity, within one flock, deviates very little from the average flock velocity; secondly, every flocks has a stable average speed of flight of about $12m/s$, which does not depend on the size of the flock or on the number of individuals that compose the flock; finally, the most peculiar property, fluctuations in the vector velocities and speed fluctuations are scale-free correlated. This means that the correlation length of both directional and speed fluctuations scales with the linear size of the system. The coexistence of scale-free correlations and moderate speed fluctuations is an issue of general relevance for collective behaviour, be it of biological or artificial nature, and yet these two traits set conflicting constraints on the mechanism controlling the speed of each agent, as the factors boosting correlations tend to amplify fluctuations, and vice versa.

In this thesis I present and study a new model that is capable of reproducing all this features without a strong fine-tuning of its parameters. This new theory, the marginal model, relies on a zero temperature critical point that ensures scale-free correlations of all the velocities' degrees of freedom, in the symmetry-broken phase. This property is achieved by confining the speed of each particle with a flat-minimum potential, which means that the minimum of the speed-bounding potential has a vanishing second derivative.

First of all I study the marginal theory at equilibrium, using the mean-field fully-connected approximation and I find that it displays a divergent susceptibility for vanishing temperature, which confirms the idea of a zero temperature critical point. After defining and studying the model from a theoretical point of view, I validate the theory through numerical simulations of the microscopic self-propelled marginal model and by comparison with the experiments. I show that the marginal theory is the only one, so far, compatible with experimental data of natural flocks. Finally, I derive a statistical field theory for the marginal model and I study it using momentum-shell renormalization group (RG) at one loop, for vanishing temperature. I compute the critical exponents that are checked by finite-size scaling analysis of equilibrium on-lattice simulations.

Acknowledgments

I would like to thank my advisor, Andrea, for his invaluable guidance and supervision in these three years of PhD. I would like also to thank Irene and Tomás for their advice and contribution. I want to thank my two thesis referees: William Bialek, for his opinions on this work, and Víctor Martín Mayor, for his lessons in Madrid and his opinions about this thesis.

For the times when we worked together I thank Luca and Giulia, it was fun thinking, discussing and sometimes arguing. I would like also to thank all the other people of the COBBS group, in particular Stefania, Leonardo, Massimiliano and Federica for many useful discussions.

For countless chats about my work, I would like to thank all the people I have interacted with in these three years, I think this work would have been less rich without their untraceable contribution.

Contents

Guide for the reader

Among the possible topics of interest in physics nowadays, "collective systems" are widely studied. This name refers to systems that are composed by a usually large number of elements that interact in a non-trivial way, giving rise to interesting collective phenomena and showing different characteristic scales in space and time. The reductionist approach alone is not enough to explain a collective system [2, 37] and a specific study is needed to understand a phenomenon that is "more than the sum of its parts". Spin glasses [82, 89], growing surfaces [71], earth's climate [11, 57, 77], artificial neural networks [46, 90] are just some examples of this vast field of study that was born more than fifty years ago and it keeps growing. In the latest years, many collective systems that traditionally belonged to the field of biology have been studied by physicists, using the theoretical tools of statistical mechanics and the experimental expertise of biology, physics, informatics and engineering altogether. Some of these systems, which pose interesting and fundamental physics problems, are bacteria [39, 44], animals' neural networks [80, 81, 105], immune system [65, 86] and, going to macroscopic sizes, groups of animals [3, 13, 19, 31, 51, 58].

Among the great variety of problems that belong to the "physics of life" category, collective motion of animal groups stands out for its complexity and arises some fundamental theoretical questions. One of the main points to be investigated is how to include these systems in the framework of non-equilibrium statistical mechanics [123]. Furthermore it is crucial to determine if some kind of fluctuation-dissipation relations [78] hold for these systems; even if correlations can be measured [3, 24], response experiments are tricky, as controlled perturbations are difficult to perform. Another important point to understand is whether collective behaviour in biological systems is comparable to ferromagnetic criticality, hence it requires fine-tuning, or it does not require any precise combination of physical parameters to happen [34, 83]. To address these questions and many others, several models have been developed by physicists, biologists and mathematicians. These models are often called self-propelled particles (SPP) models, because they have to include some mechanism of self-propulsion for their components to mimic the motion of a living being. One of the first SPP models is the Vicsek model [49, 111], which can be thought as a self-propelled version of a ferromagnet, where spins become velocities and individuals move according to a set of evolution equations. The Vicsek model has been adapted and modified in many ways to describe different kinds of systems [35, 49, 101] and following the Vicsek model's example, many other theories have been developed to capture the fundamental features of collective motion in biological systems [33, 34, 38, 60, 106, 108].

This thesis starts from the experimental evidence on common starling (*Sturnus*

vulgaris) flocks. In the last decades, observations of starling flocks have been made [7, 32, 34, 54] and what emerges from them is that flocks move coherently, which means that each bird's velocity is very similar to the average flock's velocity. Furthermore, also each bird's speed (which is the velocity's modulus) is close to the average speed of the flock that does not vary much from flock to flock [34]. Another striking experimental finding is that, within a flock, directional and speed fluctuations are correlated over large scales, comparable with the system's size [24]; to be more precise, when computed for every flock, the correlation lengths of directional and speed fluctuations scale with the linear size of the system [24]. These experimental evidences seem to be intuitively very plausible for a collective group of animals, yet they are difficult to reproduce all within one simple SPP model. The literature gives us many examples of equilibrium models [102, 122] and non-equilibrium models [33, 110] that possess a polarized phase with orientational scale-free correlations. This phenomenon occurs due to the fact that, when the system is polarized, long-wavelength orientational fluctuations are easy to perform, since they involve a little energy cost. This property has been studied deeply for equilibrium systems and it is described by the Goldstone theorem [52, 53]. However, if we want to combine this phenomenology with also modulus (or speed) scale-free correlations, while keeping mild speed fluctuations, the task is not easy. In the equilibrium context, when the thermodynamic limit is valid, we know that a certain degree of freedom displays scale-free correlations when the Gibbs free energy of the system becomes flat (i.e. has zero second derivative) in the direction of that degree of freedom. This is exactly what happens when a system undergoes a phase transition; at the critical point the minimum of the total Gibbs free energy, which depends on the total magnetization of the system, is flat in all the possible directions, hence every degree of freedom is scale-free correlated [91]. However, when we go deep in the symmetry-broken phase, which is the phase of flocks, the Gibbs free energy curvature (in the minimum) of standard models is non-vanishing in the modulus' direction, which implies short-range correlations for modulus' fluctuations [17, 93]. A partial solution to this situation was find using the pseudo-Gaussian model of [12]; the idea was to reduce the overall speed-bounding potential amplitude in order to reduce minimum's curvature too, but this approach causes other inconsistencies with experiments, namely too large values for average speed and fluctuations.

A possible and interesting solution to this problem is a new model that we call "marginal model". This name is due to the fact that the speed-bounding microscopic potential has a zero-curvature minimum [27, 34], hence the adjective "marginal". The idea behind this model is the following: to obtain scale-free correlations, together with high polarization, we need a model with a Gibbs free energy that has a flat minimum in the modulus direction, for low temperature. When the temperature vanishes, we know that so does the entropy contribution to the free energy; this means that this thermodynamic potential resembles the bare potential of the theory. Hence, if we want our low-temperature total free energy to be "marginal" in the modulus direction we have to choose a bare potential that already possesses this property. The phenomenology that we expect to see is that, when the temperature is different from zero, the model has a positive curvature minimum in the modulus direction and it behaves for all intents and purposes like a standard theory in its symmetry-broken phase but, as the temperature vanishes, the entropic contribution

to the free energy becomes zero and the free energy resembles the flat-minimum potential of the bare pseudo-Hamiltonian. In this way we hope to obtain a model that can reproduce speed scale-free correlations for vanishing temperature, with a sharp potential that limits the average speed and its fluctuations to plausible values. In this thesis I will analyze the marginal theory and compare it with experimental data, to test the soundness of our idea and to verify that it can describe all the phenomenology encountered in starling flocks.

In the first chapter I present the main experimental findings about starling flocks, together with the definition of the experimental observables (e.g. average velocity and speed, correlation length) [30]. Afterwards, in the second chapter, I describe the standard theories for equilibrium models of systems with a high-polarization (or symmetry-broken) phase [17, 18, 92, 93]. Later, in the third chapter I present an initial effort to reproduce speed scale-free correlations, the pseudo-Gaussian model [12], and then I introduce and perform a first theoretical analysis of our new proposal: the marginal model [27, 34]. In order to check the soundness of our new model, in chapter four I compare experiments, the pseudo-Gaussian model and the marginal model [34]. Finally, in the last chapter, I study the equilibrium version of the marginal model using the momentum-shell renormalization group (RG) to investigate the critical properties of our model for vanishing temperature [28].

Finding an appropriate model to describe the flocking phenomenon lets us investigate on many questions about biological systems. First of all we need to comprehend which framework of statistical mechanics is the most appropriate to describe biological systems [13]. We can ask ourselves which role plays the out-of-equilibrium nature of these systems in their dynamics and how much it is appropriate to consider a flock at local equilibrium [85]. Another important point to address is the role of symmetries in such systems, whether the consequences of symmetries and their breaking, which we know to be valid for equilibrium ferromagnetic systems [52, 100], are still valid for flocks or not. Finally, if we are able to create an efficient model for the flocking phenomenon, it will be possible to develop practical applications, for example in the field of robotics [47].

Publications and contribution

In this brief section I point out the publications of my PhD. I will also point out which parts of this thesis are made by the author and which parts are taken from previous works and publications.

A first introduction to the marginal model with its mean-field analysis (here in chapter 3) and a first set of simulations on a cubic lattice to find the critical exponents (last section of chapter 5) can be found in [27]. The comparison between theoretical models (the marginal SPP model and the pseudo-Gaussian SPP model) and experimental data (here in chapter 4) is explained in [34], which is under review for Nature Communications. The RG analysis of the equilibrium marginal model (here in chapter 5), starting from the mean-field Gibbs free energy, is in [28], which is currently under preparation.

All the experimental finding of chapter 1 can be found in [24], my work consisted in extending the analysis, which was only made to the experimental data of the

Starflag project [31, 32], to all the experimental data that we have now. The keystone result of this analysis is shown in Fig. 1.6 and it is coherent with the analysis already made in [24]. All the explanations about how to compute correlations are taken from the review [30]. In chapter 2 I review the most important results, obtained in [92, 93] by A. Patashinski and V. Pokrovsky and in [17, 18] by K.G. Wilson, E. Brézin and D.J. Wallace, about systems with a continuous symmetry. All the calculations and the main results are taken from the papers and the book I have just cited above, the last section was made by extending a result of [100]. My original contribution of this chapter consisted in writing the code and performing the analysis of Monte-Carlo simulations, to verify the relation between longitudinal and transverse susceptibility. These results are summed up in Fig. 2.4. The whole part of chapter 3 that concerns the theoretical equilibrium study of the marginal model (from section 3.3 up to the end of the chapter) is entirely original and made by me [27]. The first part about the pseudo-Gaussian model is an improvement on the analysis already performed in [12]. For what concerns chapter 4, the presentation of the Vicsek model is taken from [30, 49], the comparison between models and experimental data is original and it was made by me [34]. All the SPP simulations presented in this chapter were made by adapting a code of Tomás S. Grigera. The simulations and the RG analysis of chapter 5 were made entirely by me. I have done all my work under the supervision of Andrea Cavagna (my PhD supervisor), Irene Giardina and Tomás S. Grigera. A part of the development and analysis on the simulations presented in the chapters 3 and 4 were made in collaboration with other PhD students of our group, Luca Di Carlo and Giulia Pisegna.

Chapter 1

Introduction Part I: Experimental data on natural flocks of birds

My work starts from the experimental findings about natural flocks of starlings. In this chapter I will explain some of the main features that have been found in starling flocks and why a new model is necessary in order to correctly reproduce them. I will briefly recall the most important information about experimental observations, then I will present the observables we measure in flocking experiments, with a particular focus on connected correlation functions and correlation length. In the end I will show the main findings about scale-free correlations of the full velocity vector fluctuations and speed fluctuations and I will explain why it is nontrivial to have simultaneously an average speed that is constant over all the measured systems together with scale-free correlations of speed fluctuations.

1.1 Experiments

Observations of starlings (*Sturnus vulgaris*) have been performed in Rome, from the rooftop of Palazzo Massimo alle Terme, in front of the Termini railway station, where there is a large roosting site. Multiple synchronized video-sequences of every flocking event are acquired from different observation points, using a calibrated multi-camera video-acquisition system [26]. Videos are analyzed using a specifically developed tracking software [5] that is able to reconstruct 3D trajectories for each individual within the flock.

The data that we present here were taken over several experimental campaigns, using different experimental systems that we briefly present. The first field observations were made between 2007 and 2010, within the Starflag project [32, 31], using Canon D1-Mark II cameras shooting at 10 frames-per-second (FPS) with a resolution of 8.2 Megapixels (MP). A second series of observations was performed between 2011 and 2012, using IDT M5 cameras, shooting at 170 FPS with a resolution of 5 MP. Finally, the most recent observations were made between 2019 and the first months of 2020, with IDT OS10-4K cameras, shooting at 155 FPS with a resolution of 9.2 MP.
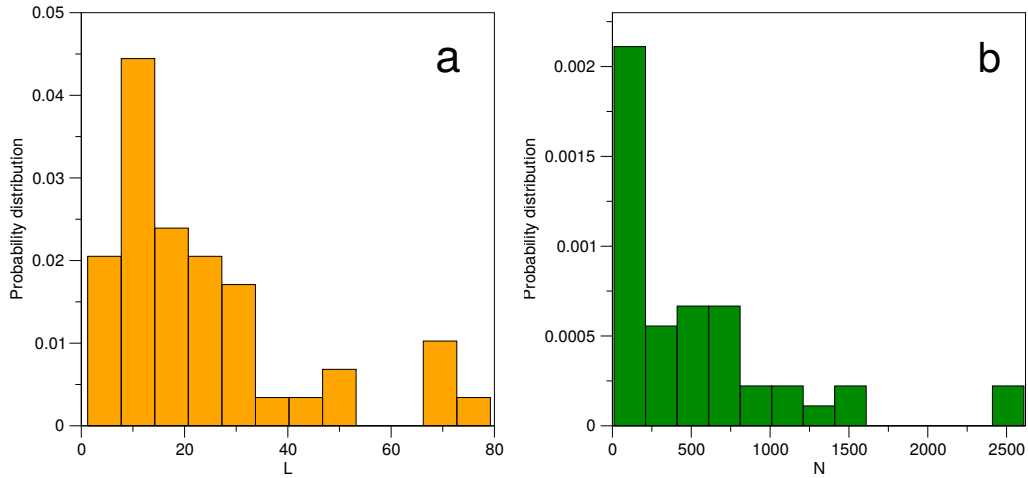
Figure 1.1. Linear size and number of individuals. a: Histogram of the flock sizes, the minimum size is about $1\ m$ and the maximum size is $77\ m$. Every size is the median size between all the frames of a single flocking event. **b**: Histogram of the number of individuals through all the flocking events, the minimum number is 10 and the maximum is 2559. Every N is the median number of individuals between all the frames in a single flocking event. The aspect ratio of flocks is non-trivial [7], so a generic relation between L and N cannot be found.

Considering all the data at our disposal, we have flocks ranging from 10 to about 2500 individuals, with a linear size of flocks going from 1 to about 80 meters. We would like to stress that a crucial part of our analysis, namely the fact that the average speed is constant for every system's size (Fig. 1.3), is possible because of the new data of the experimental campaigns of 2011-2012 and 2019-2020, which gave us information about the smallest flocks. This large range of sizes is extremely useful to investigate the correlation between measurable quantities and systems' size or number of individuals.

Every observation was made using trifocal geometry [56] with a three camera system. The reconstruction of individuals' trajectory was performed for the first series of data with the method of [31, 32], while the most advanced algorithm of [5] was used for second and third generation data.

1.2   Basic observables

From flocks' trajectories we can compute some simple observables that describe the most important and intuitive features of our systems. From each frame of each flocking event we can compute the system's linear size L as the distance between the furthest individuals in the flock. We also compute N, the number of individuals within the flock, and use it to compute averages,

$$\boldsymbol{v} = \frac{1}{N}\sum_{i=1}^{N} \boldsymbol{v}_i \qquad \text{average velocity} \tag{1.1}$$

$$s = \frac{1}{N} \sum_{i=1}^{N} v_i \qquad \text{average speed} \tag{1.2}$$

$$\phi = \frac{1}{N} \left| \sum_{i=1}^{N} \frac{\boldsymbol{v}_i}{v_i} \right| \qquad \text{polarization} \tag{1.3}$$

where $\boldsymbol{v}_i$ is the velocity vector of bird i and $v_i = |\boldsymbol{v}_i|$. In the end, we can consider all the quantities (1.1), (1.2), (1.3), L and N from each frame of a single flocking event and take the median over all the frames. We prefer the median with respect to the mean because it is more outlier-resistant.

From Fig. (1.1) we can clearly see that the linear sizes of our flocks extend across two orders of magnitude (from 1m to 80m) and the number of individuals too (from ~ 10 to ~ 2500 individuals). This might seem surprising, because one could expect that the number of individuals scales as $N \sim L^d$ where d is the space dimension (in this case $d = 3$). In fact, starling flocks have peculiar aspect ratios [7] and the scaling relation between L and N does not hold. The aspect ratio fluctuates a lot from flock to flock and also from frame to frame of the same flocking event, but this is not a problem for our analysis , because the main properties of this system do not depend strongly on aspect ratios [7, 24].

From the distributions in Fig. (1.2) we notice in panel **a** that the average speed do not varies much, from flock to flock. In particular we see that the speed has a mean value of 11.9 m/s m/s and a standard deviation of 2.3 m/s. This is not surprising, because the speed of flight of each individual, and therefore their average, is strongly constrained by the physiology of birds. In order to fly efficiently they cannot move too slow, but also, due to mechanics of their body, they cannot move too fast. From panel **b** of the same figure, we see that flocks have a high polarization, i.e. the quantity defined in eq. (1.3) is close to its limit value of 1. This implies that the whole flock is moving coherently in one direction, with small fluctuations in the velocity of the individuals. To uniform our language with statistical physics, we can say that this biological system is in a symmetry-broken phase. We can think that every direction of flight is energetically equivalent but the system is in a non-symmetric state with respect to the rotational symmetry.

In Fig. (1.3) we see another important feature of starling flocks, the average speed does not depend on the system's number of individuals. Regardless of flock's size no correlation has been found between the average speed and the size of the flock. This property would seem quite trivial, but we will see that it is fundamental to determine which model is the most appropriate to describe experimental data. The new data of the last two experimental campaigns (presented also in [34]) were fundamental to populate the section of this plot in the region between $N \sim 10$ and $N \sim 100$, that will be of particular importance to determine which theory describes in the most accurate way the experimental phenomenology. Not all the theories that presented in this thesis are able to reproduce a constant average speed through all the system's sizes and if they fail, they will fail in the small-N region.
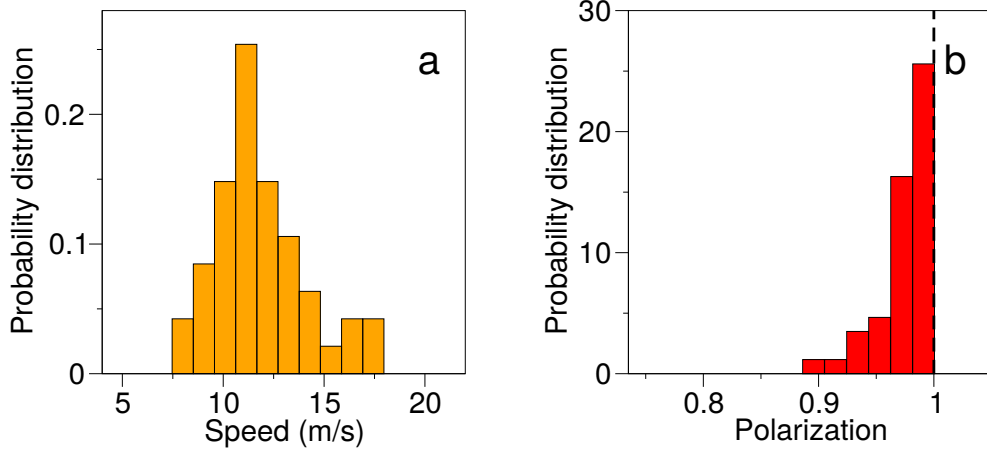
Figure 1.2. Histograms of average speed and polarization. a: Probability distribution of average speed, eq.(1.2). Every s is the median over all the frames of a single flock recording. The mean s is 11.9 m/s with a standard deviation of 2.3 m/s. **b**:Probability distribution of polarization (1.3). Every polarization is a median between all the frames of a single flocking event. All the flocks are in the ordered phase, the lowest polarization is 0.89.

1.3   Connected correlation functions

After the basic measurements explained before, we proceed computing spatial connected correlation functions [30] for the full velocity and for the speed,

$$C(r) = \frac{\sum\limits_{i,j=1}^{N} \delta\boldsymbol{v}_i \cdot \delta\boldsymbol{v}_j \delta(r_{ij} - r)}{\sum\limits_{i,j=1}^{N} \delta(r_{ij} - r)} \qquad\qquad \delta\boldsymbol{v}_i \equiv \boldsymbol{v}_i - \boldsymbol{v} \qquad (1.4)$$

$$C_s(r) = \frac{\sum\limits_{i,j=1}^{N} \delta s_i \delta s_j \delta(r_{ij} - r)}{\sum\limits_{i,j=1}^{N} \delta(r_{ij} - r)} \qquad\qquad \delta s_i \equiv v_i - s \qquad (1.5)$$

where the δ-function counts the number of couples that have a distance $r_{ij} = r$. To practically compute these functions we define a bin width Δr and each δ-function is equal to 1 for all the distances r_{ij} that are in the interval $[r, r + \Delta r]$, and 0 otherwise. The width of the interval Δr is chosen such that the functions $C(r)$ and $C_s(r)$ appear as smooth as possible, more details can be found in the appendix 1.A. We have an example in Fig. (1.4) of both correlation functions, we can see that they have a zero, which is always true, because, from the definition (1.4),

$$\int_0^L \mathrm{d}r\, C(r) \sum_{i,j=1}^{N} \delta(r_{ij} - r) = \int_0^L \mathrm{d}r\, \sum_{i,j=1}^{N} \delta\boldsymbol{v}_i \cdot \delta\boldsymbol{v}_j \delta(r_{ij} - r) = \sum_{i,j=1}^{N} \delta\boldsymbol{v}_i \cdot \delta\boldsymbol{v}_j = 0$$

$$(1.6)$$
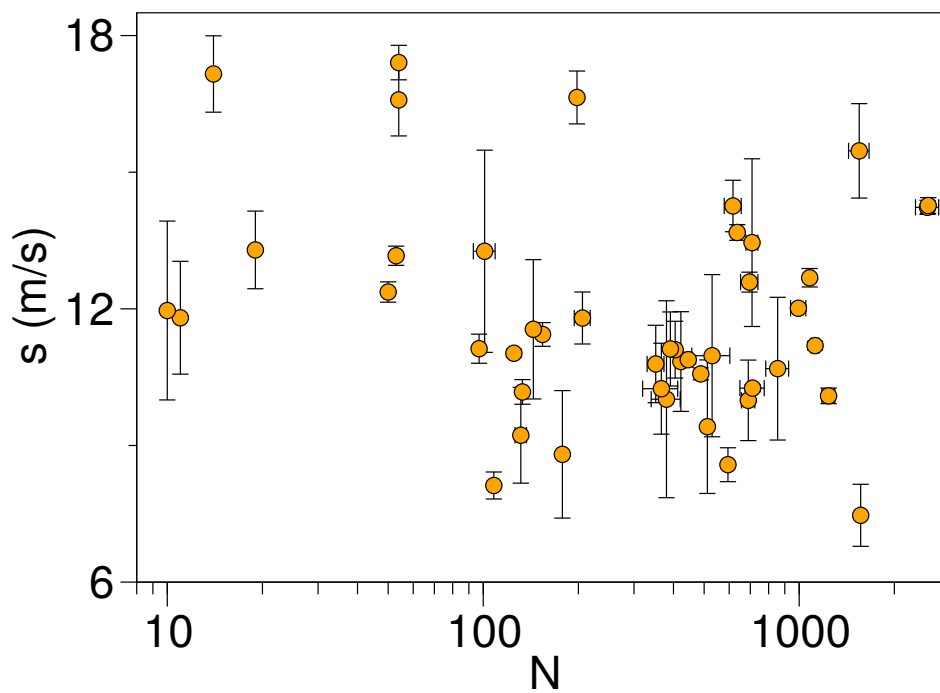
Figure 1.3. Average speed VS number of individuals in the system Scatter plot of average speed versus number of individuals in the system. The average speed, defined in eq. 1.2, is not correlated with the number of individuals. Spearman coefficient: $r_S = -0.13$ P-value: $p = 0.21$. The mean speed over all the flocks is $s = 11.9m/s$ with a standard deviation of $2.3m/s$.
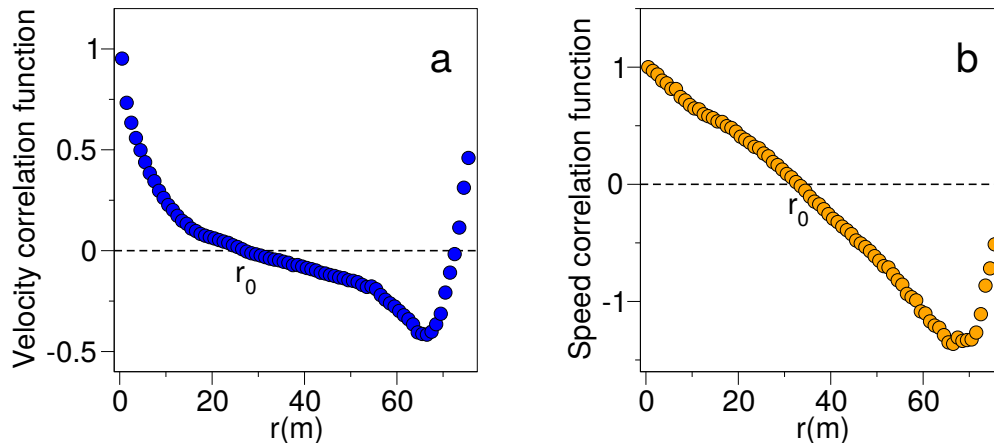
Figure 1.4. Experimental connected correlation functions. a: A connected correlation function of the full velocity vector, as it is defined in eq. (1.4), for a flock with $L = 76.1$ m. **b**: A speed connected correlation function, as it is defined in eq. (1.5), for the same flock. The functions are normalized such that $C(r = 0) = C_s(r = 0) = 1$, every function has at least one zero in the interval $[0, L]$ at a certain $r = r_0$.

since the factor $\sum_{i,j=1}^{N} \delta(r_{ij} - r)$ is always positive and the $C(r)$ is not equal to zero through the whole interval of definition, from the passages above we conclude that the correlation function must have a zero in its interval of definition $[0, L]$. The same holds for the $C_s(r)$.

1.3.1   Spatial average and phase average

We could have defined fluctuations in a different way, namely,

$$\delta \boldsymbol{v}_i = \boldsymbol{v}_i - \langle \boldsymbol{v}_i \rangle \tag{1.7}$$

$$\delta s_i = s_i - \langle s_i \rangle \tag{1.8}$$

where $\langle \cdot \rangle$ stands for the phase average, i.e. a mean value over a certain stationary probability distribution. The practical way to compute the average over a certain observable A would have been to simply compute $\langle A \rangle = 1/\bar{t} \sum_{t=1}^{\bar{t}} A(t)$ where $\bar{t}$ is the total number of system's configurations to which we have access. In fact, this is the way to compute averages and fluctuations over observables in numerical equilibrium simulations. When we deal with biological experimental data or with self-propelled particle (SPP) simulations we cannot use this procedure. The reason is that our system is intrinsically out of equilibrium [123], we are not guaranteed that a stationary distribution exists and even if it existed we do not know if the actual flock we are observing has reached that stationary state. Moreover, the sequence of frames that we have to compute an average for a local quantity is not long enough to grant a fair sampling. Hence, focusing on a single individual to compute a time average of its velocity (or speed) over all the frames of the experimental acquisition

is not sensible. On the other hand, a spatial average can be performed to see in every particular frame the correlation function of fluctuations with respect to the spatial average, like we do using eq.s (1.4) and (1.5). In the case of an equilibrium system, the two different average definitions (phase average and space average) bear qualitatively similar results for the conneccted correlation functions and they can be linked easily to each other, as it is explained in [30].

1.3.2 Correlation length

Using the definition of connected correlation function eq.s (1.4) and (1.5), we can define the correlation length ξ, that is a measure of the size of a correlated region, i.e. a region in which velocity fluctuations have the same direction or speed fluctuations have the same sign. This quantity can be computed on data in many ways [1, 20, 21, 91], one of them is $\xi = r_0$, as it was used in [24]. We find that the most practical definition for our purposes, which can be used both for experimental data and for simulations, is the following [34],

$$\xi = \frac{\int\limits_0^{r_0} \mathrm{d}r \; r \; C(r)}{\int\limits_0^{r_0} \mathrm{d}r \; C(r)} \tag{1.9}$$

$$\xi_s = \frac{\int\limits_0^{r_0} \mathrm{d}r \; r \; C_s(r)}{\int\limits_0^{r_0} \mathrm{d}r \; C_s(r)} \tag{1.10}$$

where r_0 is the first point of zero-crossing of the connected correlation functions, defined in eq.s (1.4) and (1.5). We choose this practical definition for the correlation function because it gives sensible results in any possible regime of our system. We could have used simply $\xi = r_0$ (or $\xi_s = r_0$), and this choice works very well for scale-free systems that have long range correlations, see Fig. 1.5-**b** and [24] but, if the system has short-range correlations, it becomes difficult to determine the value of r_0 because the shape of the correlation function becomes almost an exponential, see Fig. 1.5-**a** and [30]. On the other hand, if we choose to use an exponential fit with the functional form $C(r) \sim e^{-r/a}$ and we define the correlation length as $\xi = a$, it works fine for systems with short-range correlations (Fig. 1.5-**a** and [30]) while it performs poorly when correlations are long-ranged and the functional form of the correlation functions is not exponential (Fig. 1.5-**b** and [24]). Therefore we decide to use the definitions (1.9) and (1.10), because they capture the range of correlation given by r_0; they are integrals, hence they are more resistant to fluctuations then a simple value as r_0 and their value depends on the shape of the whole correlation function up to r_0 [34].

Now that we have defined the interesting quantities to measure correlations, we can explain what results we can expect from the connected correlation functions. We can write a generic connected correlation function for a certain observable as [1, 91, 116],

$$C(r) \sim r^{-\alpha} f\left(\frac{r}{\xi}, \frac{a}{L}, \frac{\xi}{L}\right) \tag{1.11}$$
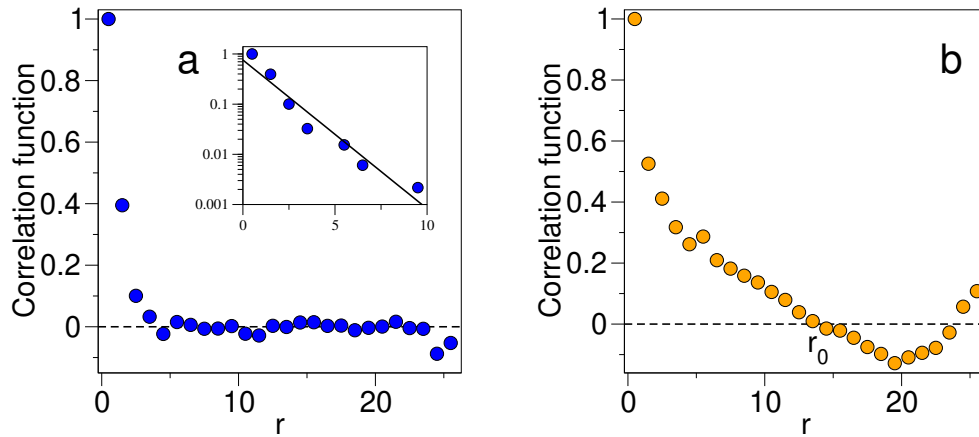
Figure 1.5. Speed correlation functions in different regimes. a: Speed correlation function in a short-range correlation regime [30]. Lattice simulations using the pseudo-Gaussian model of [12] with $g = 1$, system's size $L = 30$, on a cubic box. The form of this function is exponential, hence it is easy to find a correlation length via a linear fit in log scale (solid line in the inset), while the exact location of the zero-crossing point r_0 is difficult to determine, due to fluctuations. **b**: Speed correlation function in a long-range (or scale-free) correlation regime. The shape of the function is not exponential, hence a fit to determine the correlation length is unfeasible, however the zero-crossing point r_0 is easy to determine. Lattice simulations using the pseudo-Gaussian model of [12] with $g = 10^{-3}$, system's size $L = 30$, on a cubic box. The definition of correlation length of eq. (1.10) is applicable to both these cases. Correlation functions are normalized in order to have $C(r = 0) = 1$.

This function has two contribution, a scale-free one $r^{-\alpha}$, with $\alpha > 0$, and the scaling function f that captures the dependence of correlations from the correlation length, the system's size L and the microscopic interaction range a. To have any kind of correlation at all, an interaction between the microscopic components of the system is needed. The value of a represents the spatial range of this interaction, it can be short-range, as it is in many classic statistical mechanics models [91], or it can be long-range, as in the case of electromagnetic interaction [66]. In our case we assume that our biological system interacts in a short-ranged fashion [8, 59, 111] and that the system's size is sufficiently larger than the interaction range [8], so that we can drop the dependence of the scaling function on a/L. The meaningful scales that we have are: the correlation length ξ, which depends on the observable we are studying, and the trivial scale L, which is the size of the system. If the correlation length is proportional to the size of the system we say that the system is scale-free [24], the only meaningful scale left is the system's size and the correlation function can be written as simply,

$$C(r) \sim r^{-\alpha} f\left(\frac{r}{L}\right) \tag{1.12}$$

the reason of this definition is that, in the thermodynamic limit $L \to \infty$ [63] the system is "truly" scale-free, in the sense that its correlation function only displays the scale-free power law behaviour $C(r) \sim r^{-\alpha}$. The physical sense of the scale-free condition for a finite-size system is that, no matter what the size of the system, the fluctuations of the degree of freedom that we are analyzing are correlated over macro-regions that span a large portion of the whole system, eventually growing up to infinite size when the system's size itself goes to infinity. Scale-free correlations of the order parameter are a key feature of a system at a critical point [91]. A similar phenomenon happens when a system is in a phase where a continuous symmetry is spontaneously broken [52]; we will see later the differences between this two cases.

1.4   Scale-free correlations in starling flocks

With the definitions of the correlation functions (1.4), (1.5) and the correlation lengths definitions (1.9) and (1.10) we can investigate the behaviour of correlations in starling flocks [24]. We compute the correlation lengths for both velocity fluctuations $\delta \boldsymbol{v}_i$ and speed fluctuations δs_i, taking the median over all the frames of each flocking event, and we plot them against the systems' sizes. We find that the correlation length is proportional to the size of the system. This is true both for the full velocity correlation length (Fig. (1.6)-**a**) and for the speed correlation length (Fig. (1.6)-**b**).

There is another way to verify that a system's observable has scale-free correlations, if we use eq. (1.12), that is a scale-free correlation function, we can see that,

$$C(x)/C(x=0) = x^{-\alpha} f(x) \tag{1.13}$$

where $x = r/L$. This equation means that, if a system is scale free and we plot the normalized correlation functions at various sizes L as a function of the rescaled space x, we should see all the functions collapsing onto each other. This is the case
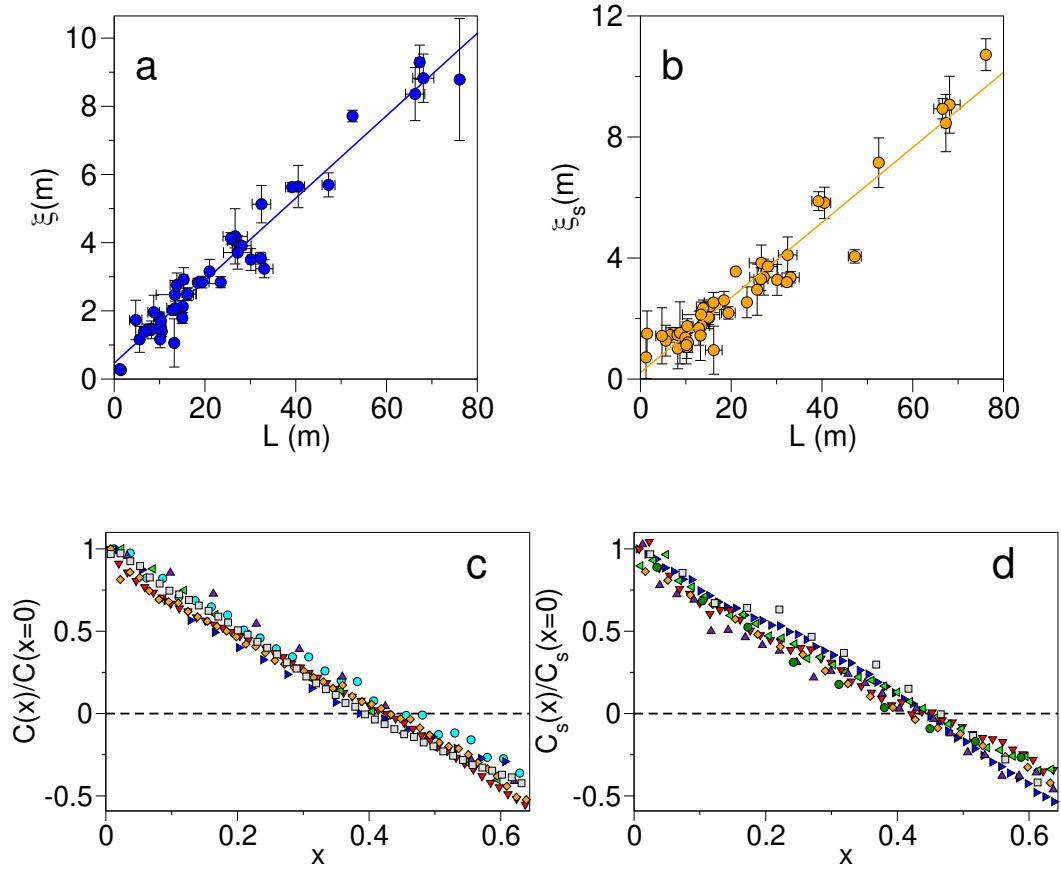
Figure 1.6. Scale-free velocity and speed correlations in starling flocks. a: Velocity correlation length (1.9) as a function of the system's size. We can clearly see that the correlation length scales with the size of the system [24]. **b**: Speed correlation length (1.9) as a function of the system's size. We can clearly see that the correlation length scales with the size of the system [24, 34]. **c**:Velocity connected correlation functions (1.4) as a function of $x = r/L$ for different system's sizes. All the correlation functions collapse onto each other. This means that the correlation range is proportional to the size of the system. **d**:Speed connected correlation functions (1.4) as a function of $x = r/L$ for different system's sizes. All the correlation functions collapse onto each other. This means that the correlation range is proportional to the size of the system. All the reported values for correlation lengths are medians on the frames of a single flocking event, while the displayed error bars are median absolute errors.

for starling flocks, as we can see in Fig. (1.6)-**c,d**, where the velocities normalized correlation functions collapse on top of each other and the same happens for speeds'. We can conclude that, in starling flocks, the velocity vector fluctuations with respect to the average velocity are scale-free correlated (Fig. (1.6)-**a,c**) and speed fluctuations too are scale-free correlated (Fig. (1.6)-**b,d**).

Given the fact that starling flocks are in a polarized phase, we are not surprised about the scale-free correlations of the whole velocity vector's fluctuations. Since every direction of flight is equivalent, we can imagine that large wavelength fluctuations of the orientational degree of freedom are easy to perform, due to the fact that their energy cost is very low. In equilibrium systems, due to the Goldstone modes [52, 53] that emerge when a continuous symmetry is spontaneously broken, we find that the phase modes have scale-free correlations [93, 100] once we lower the temperature enough such that the system is in the ordered phase. We can think that for starling flocks, even if they are not equilibrium systems, a similar mechanism could be taking place.

This means that, without invoking any out-of-equilibrium feature, we can easily reproduce velocity orientational scale-free correlations with an equilibrium model in its low-temperature ordered phase. However, a further in-depth analysis is needed if we want to have a clear picture of how the Goldstone mechanism works. It is non-trivial to understand the behaviour of longitudinal and transverse fluctuations and how they are linked with phase and modulus fluctuations [17, 93]. We will discuss and explain these topics in the next chapter.

1.4.1   The anomaly of speed

We have found that natural flocks are polarized systems and that they show scale-free orientational correlations; even if it is interesting, this last property was not completely unexpected. Standard equilibrium ferromagnetic systems with an Hamiltonian that possesses a continuous symmetry, due to the Goldstone theorem [53], also show this property, which is linked to the lack of symmetry of the equilibrium state of the system, in the low-temperature phase. Scale-free speed correlations, however, are rather surprising; in standard systems with a continuous order parameter (e.g. Heisenberg model, $O(n)$ models [102]) the modulus degree of freedom remains short-range correlated in the whole polarized phase [93, 100]. If the order parameter has n dimensions, the Gibbs free energy minimization condition defines a $n-1$-dimensional hypersurface of minima with the same energy and the same modulus but, if we perturb the minimum outside of the surface of minima, the energy cost rises, hence the modulus mode remains "massive". In other words, if the system is far away from the phase transition, the modulus mode, which is equivalent to the speed of starling flocks, is always short-range correlated. All the degrees of freedom of a classical spin system become scale-free correlated only at the critical point, but polarization at the critical point is zero (in the thermodynamic limit), hence it cannot be compatible with highly ordered flocks. A new idea is needed if we want a polarized system with scale-free modulus (i.e. speed) correlations, as we observe in experimental data. A previous attempt has been made using inference [12] but, as we will explain later, it cannot describe properly all the phenomenology that we can observe in experimental data, from smallest to largest flocks, without

recurring to fine-tuning. We will introduce in chapter 3 a new theory, the marginal model, that is capable of reproducing all the experimental features, keeping the number of parameters involved as low as possible. Our new model does not involve an explicit fine-tuning of the parameters such that the system is at a sort of critical point, different for each observed size.

1.A   Appendix: coarse-graining scale for the correlation functions

In this appendix we explain the heuristic procedure that we used to choose a suitable binning size Δr to compute the correlation functions in eq. (1.4) and eq. (1.5). As we can see from Fig. 1.7, if we choose a really small bin size (green line $\Delta r = 10^{-2}m$) we capture a lot of noise in the correlation value, this feature of the correlation function has two side effects: it can make extremely difficult to find a good estimate of the point at which the correlation function crosses zero and enlarges drastically the time needed to numerically integrate the correlation function (as we need to do to compute an estimate of the correlation length, see eq.s (1.9) and (1.10)). To avoid these problems we increase the bin size, in this way we preserve the shape of the correlation function but we average out fluctuations (black line of Fig. 1.7). Therefore we easily find the zero-crossing point of the correlation function and we can quickly integrate it. If we had increased too much the value of the bin Δr, we would have lost details about the shape of the correlation function. Following this ideas we chose $\Delta r = 1\ m$ for all the flocks that we analyzed (both for the velocity and for the speed correlation function), since it guarantees, for all the experimental data, enough information about the correlation function's shape, without including too much noise.

The reason why $\Delta r = 1\ m$ is suitable for all our data is that, on average, in a flock the nearest neighbours distance is $\sim 1\ m$ [34]. This means that the "lattice spacing" of this system should be considered of order $\sim 1\ m$ and that it is not sensible to try to measure differences in correlations below this length-scale.
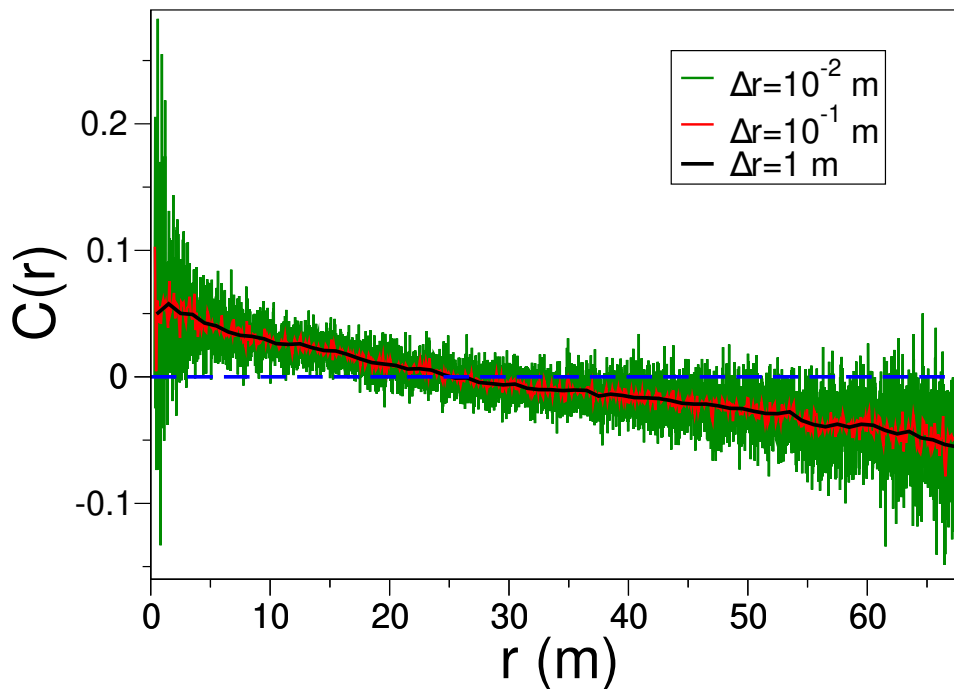
Figure 1.7. Correlation function for different choices of binning Δr. We plot the unnormalized velocity correlation function (1.4) for a typical flock of linear size 68.1 m and about 1500 individuals, using different bin sizes. We can see that if the bin size is too small with respect to the nearest neighbours average distance of $\sim 1\ m$(green and red line) we obtain large fluctuations that do not add any useful information in the computation of correlation. Once we choose a bin size close to the nearest neighbours average distance (black line) we average out the fluctuations retaining the shape of the correlation function.

Chapter 2

Introduction Part II: Breaking a continuous symmetry

In the previous chapter we discussed experimental data about natural flocks of starlings; we have seen that we have data for systems of a wide range of linear sizes (from $1\ m$ to $76\ m$) and number of individuals (from 10 to 2600). We pointed out that the average speed of every flock does not depend on the flock's size and its mean value is around $11.9\ m/s$. Another key feature of the data is that starling flocks are in a deeply polarized state and they show simultaneously scale-free correlations for the orientational degrees of freedom (the velocity) and for the modulus (the speed).

In order to build a model that is capable of reproducing what we have found in experimental data, we start our discussion in the field of equilibrium ferromagnetic systems with continuous rotation symmetry. In this chapter we delineate the main features of such models [52, 100, 93], using as a reference the $O(n)$ model [102] because it is general, yet simple enough.

During this whole chapter, we will also make connections with the phenomenology of flocks (see sections 2.2.1, 2.3.4 and 2.4.1), in order to show how the ferromagnetic equilibrium models are capable of reproducing the experimental features of natural flocks.

The choice of starting our work from equilibrium models, even if the observed experimental system is out-of-equilibrium, has two main reasons. First of all, we want to start from simpler models and then add more complex off-equilibrium features, if they are needed to capture fundamental aspects of flocking systems. Secondly, we know from previous studies [85] that individuals in a flock can be considered in a condition of local equilibrium, which means that the local relaxation time is far shorter then the time needed to rearrange the interaction network. This property justifies an equilibrium approach and explains why some non-trivial key features of flocks can be explained by simple ferromagnetic models, e.g. orientational scale-free correlations. However, as we shall see, standard ferromagnetic models will not be able to explain *all* the properties of flocks.

2.1   The $O(n)$ model

The Landau-Ginzburg Hamiltonian [73, 91] of the $O(n)$ model is,

$$\mathcal{H} = \int_V \mathrm{d}^d r \left\{ \frac{1}{2} \left(\nabla \boldsymbol{\varphi} \left(\boldsymbol{r} \right) \right)^2 + \frac{t}{2} \varphi^2 \left(\boldsymbol{r} \right) + u\varphi^4 \left(\boldsymbol{r} \right) - \boldsymbol{h} \cdot \boldsymbol{\varphi} \left(\boldsymbol{r} \right) \right\} \tag{2.1}$$

where $\boldsymbol{\varphi}$ is a mesoscopic statistical field with n components, $\varphi = |\boldsymbol{\varphi}|$, the gradient term is $(\nabla \boldsymbol{\varphi})^2 = \sum_{\alpha,\beta} \left(\frac{\partial \varphi_\alpha}{\partial r_\beta} \right)^2$ where $\alpha = 1, ..., n$ and $\beta = 1, ..., d$, t is proportional to the distance of the temperature from the bare critical temperature $t \sim T - T_0$ (in traditional nomenclature: t is the "bare mass" of the theory [95]), u is the coupling constant, $\boldsymbol{h}$ is an external space-independent magnetic field and V is the total volume of the system. We choose a volume large enough to consider our system in the thermodynamic limit, such that we can observe its spontaneous symmetry-breaking properties [91]. At equilibrium, the probability distribution of $\boldsymbol{\varphi}$ is the Boltzmann-Gibbs distribution [63],

$$P[\boldsymbol{\varphi}] = \frac{1}{Z} e^{-\beta \mathcal{H}[\boldsymbol{\varphi}]} \tag{2.2}$$

where β is $1/(k_B T)$, with T as the temperature and k_B as the Boltzmann constant [63] that we define to be equal to one. Z is the partition function and it is defined as the functional integral $Z = \int \mathrm{D}\boldsymbol{\varphi} \; e^{-\beta \mathcal{H}[\varphi]}$.

Our system, at a microscopic level, is made up of n-dimensional spins and $\boldsymbol{\varphi}$ is a local average of microscopic spins over a volume that is large enough to contain a large number of spins but small if compared to the total volume of the system, i.e. our field theory (2.1) is a coarse-graining of an underlying microscopic theory. We can immediately see that all the terms, except for the external field term $\boldsymbol{h} \cdot \boldsymbol{\varphi}$, are $O(n)$-symmetric i.e. they are symmetric over a space-independent rotation of $\boldsymbol{\varphi}$ in the n-dimensional internal space. The external field term explicitly breaks the $O(n)$ symmetry and forces the magnetization $\boldsymbol{m}$ to be non-zero and parallel to the external field $\boldsymbol{h}$.

We can study our model, without the external field ($\boldsymbol{h} = 0$) in the thermodynamic limit $V \to \infty$, at a Landau level, neglecting all the fluctuations. To do so, we consider $\boldsymbol{\varphi}$ of equation (2.1) to be constant in space, then to obtain the magnetization $\boldsymbol{m}$ we just minimize the Landau potential,

$$V(\varphi) = \frac{t}{2} \varphi^2 + u\varphi^4 \tag{2.3}$$

If we call φ_0 the modulus of the minimum, which is our equilibrium magnetization, we have

$$\varphi_0 = \begin{cases} 0 & t \geq 0 \\ \sqrt{\frac{|t|}{4u}} & t < 0 \end{cases} \tag{2.4}$$

the situation is depicted in Fig. 2.1. When $t > 0$ (panel **a**) we are above the bare critical temperature, hence the magnetization is 0 and the potential has only one minimum at $\boldsymbol{\varphi} = 0$, the system is in its disordered state. When $t = 0$ (panel **b**)
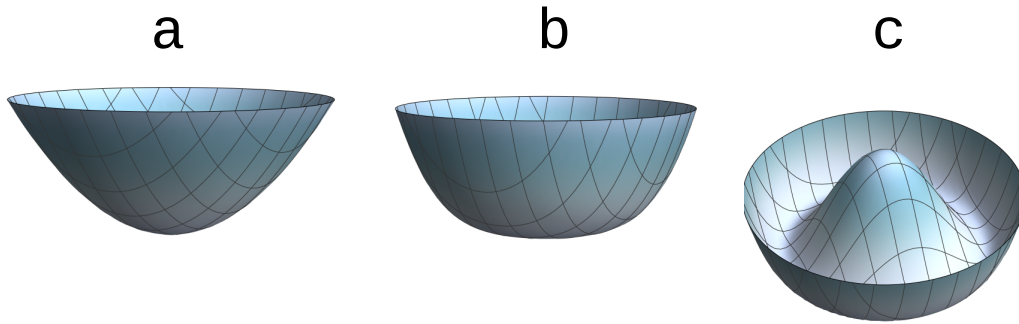
Figure 2.1. O(n) Landau potential for $n = 2$. **a**: Potential shape for $t > 0$. There is only one minimum at $\boldsymbol{\varphi} = 0$. **b**: Potential shape for $t = 0$. There is only one flat minimum at $\boldsymbol{\varphi} = 0$, with zero curvature. **c**: Potential shape for $t < 0$, we have a circumference of minima, everyone with the same distance from the origin. The point $\boldsymbol{\varphi} = 0$ is a maximum.

the system is at its critical temperature (at least at bare level), the minimum is at $\boldsymbol{\varphi} = 0$ and we have also that the minimum is "flat" (or marginal), which means that if we compute the first three derivatives of the potential at the minimum, they are all equal to zero. When we go below $t = 0$ (panel **c**) we are in the ordered symmetry-broken phase, where the potential develops a manifold of minima with $\varphi = \sqrt{\frac{|t|}{4u}}$ and the point $\boldsymbol{\varphi} = 0$ becomes a maximum. The symmetry is broken in the sense that our system will be in one state of the infinitely many compatible with $\varphi = \sqrt{\frac{|t|}{4u}}$, this state is not symmetric with respect to the whole $O(n)$ symmetry, but only with respect to a smaller subgroup (i.e. the subgroup of rotations in the planes defined by all the couples of axes that are both perpendicular to the equilibrium magnetization). To understand what happens at the critical point $t = 0$, we compute the scalar susceptibility for $t > 0$ and $h = 0$,

$$\chi = \left.\frac{\partial m}{\partial h}\right|_{h=0} \tag{2.5}$$

that is the variation of the magnetization if we apply a small external magnetic field in the disordered phase of the system, in the limit of vanishing external field. To compute it we consider a small external field $\boldsymbol{h}$ pointing along one of the n possible axes, the Landau potential will be,

$$V(\varphi) = \frac{t}{2}\varphi^2 + u\varphi^4 - \boldsymbol{h} \cdot \boldsymbol{\varphi} \tag{2.6}$$

if we minimize if with respect to φ we obtain the equation, for the component of φ_0 that is parallel to $\boldsymbol{h}$,

$$t\varphi_0 + 4u\varphi_0^3 - h = 0 \tag{2.7}$$

while all the other components follow the (2.4), hence the are zero. If we take the derivative with respect to h of the above equation, and then we set $h = 0$, we find an explicit form for the scalar susceptibility,

$$\chi = \frac{1}{2t} \sim t^{-1} \tag{2.8}$$

We conclude that, even neglecting the fluctuations with the Landau approximation, at the phase transition point $t = 0$ our system has a diverging susceptibility. The behaviour with t tells us that at Landau level, the critical exponent γ [91] is equal to 1. The susceptibility's divergence implies, using the fluctuation-dissipation relation (see appendix 2.A and [78]),

$$\chi = \beta \int \mathrm{d}^d r \; C(r) \sim \int \mathrm{d}^d r \; \frac{f(r/\xi)}{r^{d-2+\eta}} \sim \xi^{2-\eta} \tag{2.9}$$

from the Gaussian approximation of eq. 2.1 we know that $\eta = 0$, hence using eq.s 2.8 and 2.9 we find that the correlation length diverges,

$$\xi \sim t^{-1/2} \tag{2.10}$$

which means that the critical exponent $\nu = 1/2$ at bare level. This critical point can be studied, using the Renormalization Group [114, 115] and the epsilon expansion [117, 118] to find a better estimate for critical exponents.

2.2   Ward identities and Goldstone modes

Using the symmetry properties of our Hamiltonian, we will now derive the Ward identities [1, 104, 112] that can be used to derive an important property of correlations in the symmetry-broken phase. We can write the Hamiltonian (2.1) in this fashion,

$$\mathcal{H}[\boldsymbol{\varphi}] = \mathcal{H}_s[\boldsymbol{\varphi}] - \boldsymbol{h} \cdot \int \mathrm{d}^d r \; \boldsymbol{\varphi}(\boldsymbol{r}) \tag{2.11}$$

where $\mathcal{H}_s[\varphi]$ is the $O(n)$-symmetric part of the Hamiltonian. By definition, if $\mathcal{R}$ is a generic rotation in the n-dimensional space of $\boldsymbol{\varphi}$, the following holds,

$$\mathcal{H}_s[\mathcal{R}\boldsymbol{\varphi}] = \mathcal{H}_s[\boldsymbol{\varphi}] \tag{2.12}$$

This implies that the per-particle Helmholtz free-energy [63],

$$f(\boldsymbol{h}) = -\frac{1}{\beta V} \ln \int \mathrm{D}\boldsymbol{\varphi} \; e^{-\beta \mathcal{H}[\boldsymbol{\varphi}]}$$

$$= -\frac{1}{\beta V} \ln \int \mathrm{D}\boldsymbol{\varphi} \; e^{-\beta \mathcal{H}_s[\boldsymbol{\varphi}]+\beta \boldsymbol{h} \cdot \int \mathrm{d}^d r \; \boldsymbol{\varphi}(\boldsymbol{r})} \tag{2.13}$$

is symmetric too. To show that, we simply compute f in $\mathcal{R}\boldsymbol{h}$, we use the symmetry of the Hamiltonian and a change of variable $\boldsymbol{\varphi}' = \mathcal{R}\boldsymbol{\varphi}$ in the functional integral.

$$f(\mathcal{R}\boldsymbol{h}) = -\frac{1}{\beta V} \ln \int \mathrm{D}\boldsymbol{\varphi}' \; e^{-\beta \mathcal{H}_s[\boldsymbol{\varphi}']+\beta \mathcal{R}\boldsymbol{h} \cdot \int \mathrm{d}^d r \; \boldsymbol{\varphi}'(\boldsymbol{r})}$$

$$= -\frac{1}{\beta V} \ln \int \mathrm{D}\boldsymbol{\varphi} \; e^{-\beta \mathcal{H}_s[\mathcal{R}\boldsymbol{\varphi}]+\beta \mathcal{R}\boldsymbol{h} \cdot \int \mathrm{d}^d r \; \mathcal{R}\boldsymbol{\varphi}(\boldsymbol{r})}$$

$$= -\frac{1}{\beta V} \ln \int \mathrm{D}\boldsymbol{\varphi} \; e^{-\beta \mathcal{H}_s[\boldsymbol{\varphi}]+\beta \boldsymbol{h} \cdot \int \mathrm{d}^d r \; \boldsymbol{\varphi}(\boldsymbol{r})}$$

$$= f(\boldsymbol{h}) \tag{2.14}$$

where $\mathrm{D}\boldsymbol{\varphi}' = \mathrm{D}\boldsymbol{\varphi}$ because the transformation $\mathcal{R}$ has a Jacobian with unitary determinant and also $\mathcal{R}^T\mathcal{R} = \mathbb{I}$ because rotations preserve the scalar product. We have shown that the Helmholtz free-energy is $O(n)$-symmetric in its argument $\boldsymbol{h}$, just like the Hamiltonian is symmetric in $\boldsymbol{\varphi}$. We now perform an infinitesimal rotation $\mathcal{R}$. This is possible because rotations are continuous transformations and any arbitrarily small rotation can be written as [120],

$$\mathcal{R} \simeq \mathbb{I} + \sum_{k=1}^{n(n-1)/2} \epsilon_k A_k \tag{2.15}$$

where $\mathbb{I}$ is the identity transformation, the A_ks are the symmetry's generators and the ϵ_ks are the generalized angles in the n-dimensional space. We can represent the generators A_k as antisymmetric $n \times n$ matrices, they can be constructed following the procedure: fill a $n \times n$ matrix with zeroes, choose a matrix entry in the upper triangular half and place a 1 in it, place a -1 in the symmetric entry, repeat for all the entries in the upper triangular half of the matrix. A generic A_k matrix will look like,

$$A_k = \begin{pmatrix} 0 & 0 & 0 & 0 & \dots \\ 0 & 0 & 1 & 0 & \dots \\ 0 & -1 & 0 & 0 & \dots \\ 0 & 0 & 0 & \ddots & \ddots \\ \vdots & \vdots & \vdots & \ddots & \ddots \end{pmatrix} \tag{2.16}$$

From the invariance of the Gibbs free energy (2.14) we have,

$$\delta f = f(\mathcal{R}\boldsymbol{h}) - f(\boldsymbol{h}) = 0 \tag{2.17}$$

If we substitute the generic $\mathcal{R}$ with its expansion (2.15) and we stop at first order in the ϵ_k we have,

$$0 = \delta f = \left(\sum_k \epsilon_k A_k \boldsymbol{h} \right) \cdot \frac{\partial f}{\partial \boldsymbol{h}} \tag{2.18}$$

We obtained the Ward-Takahashi identity [1, 73] only using the symmetry properties of the Hamiltonian, hence it holds for any value of the temperature, at any level of perturbation theory, both in the symmetric phase and in the symmetry-broken phase. If we use directly the (2.18), given that the average magnetization $\boldsymbol{m} = -\frac{\partial f}{\partial \boldsymbol{h}}$ [63] and that the ϵ_ks are arbitrary, we find,

$$(A_k \boldsymbol{h}) \cdot \boldsymbol{m} = 0 \qquad \forall\, k \tag{2.19}$$

To understand the meaning of this equation we have to remember the form of the A_ks matrices (2.16) and figure out the effect on the vector $\boldsymbol{h}$. Essentially, if a certain matrix A_k has a 1 only at column i and row j (and consequently a -1 at column j and row i), it projects the vector $\boldsymbol{h}$ on the plane spanned by its components h_i and h_j and then computes a vector h_k that is orthogonal to the projection, remaining on the same plane. If $\boldsymbol{m}$ is orthogonal to all the vectors h_k, such as it is implied by the

(2.19), this means that $\boldsymbol{m}$ is parallel to $\boldsymbol{h}$. Hence from this Ward-Takahashi identity we simply obtained that the magnetization is always parallel to the external field. If we derive once the (2.19) with respect to the external field $\boldsymbol{h}$ we have,

$$0 = (A_k)_{\alpha\beta}\, \delta_{\beta\mu} m_\alpha + (A_k)_{\alpha\beta}\, h_\beta \chi_{\alpha\mu} \qquad \forall\, k \tag{2.20}$$

where we are writing the matrices and vectors components with the Einstein convention of summing over repeated indices. Given that the susceptibility matrix is symmetric i.e. $\chi_{\alpha\beta} = \chi_{\beta\alpha}$ and the rotation's generators are antisymmetric i.e. $(A_k)_{\alpha\beta} = -(A_k)_{\beta\alpha}$, we find,

$$-A_k \boldsymbol{m} + \chi A_k \boldsymbol{h} = 0 \qquad \forall\, k \tag{2.21}$$

where we switched back to matrix notation. From the (2.19) we know that the magnetization and the external field are parallel, hence we can write $\boldsymbol{m} = \frac{m}{h}\boldsymbol{h}$, plugging it into the previous equation we find,

$$\left(\chi - \frac{m}{h}\right)(A_k \boldsymbol{h}) = 0 \qquad \forall\, k \tag{2.22}$$

from this Ward identity we learn an important property of the susceptibility. This equation gives us an eigenvalue ($\frac{m}{h}$) and its eigenvectors ($(A_k \boldsymbol{h})$ for every k) for the susceptibility matrix χ. For all the directions spanned by the set of vectors $h_k = (A_k \boldsymbol{h})$, the susceptibility is $\frac{m}{h}$. Since the A_k are a basis of the space of all the antisymmetric $n \times n$ matrices we can say that the space spanned by the h_k is the space orthogonal to $\boldsymbol{h}$. In other words, we find that the susceptibility in the directions that are orthogonal to the magnetic field (and the equilibrium magnetization) is,

$$\chi_\perp = \frac{m}{h} \tag{2.23}$$

In the symmetry-broken phase, where the equilibrium magnetization is different from zero even in absence of an external field, the transverse susceptibility (2.23) diverges for vanishing magnetic field. This means, via the fluctuation-dissipation relation, that also the correlation length of transverse fluctuations diverges in the symmetry-broken phase. At zero external field, below the critical temperature $\xi_\perp = \infty$. The physical meaning of this phenomenon is the following, if we are in the polarized phase, even a small external field that is orthogonal to the equilibrium magnetization at zero field causes a divergent response in the system. This means that it is energetically very easy to perturb the magnetization in a direction that is orthogonal to the magnetization itself. If we look at Fig. 2.1-c it is clear why this is possible, we are perturbing the magnetization (at least in the linear approximation) along the "valley" of minima, where every point belongs to the same level curve, i.e. we can change a little the magnetization along the circumference of minima without raising the energy of the system.

Using the fluctuation-dissipation relation [78] we understand that the transverse fluctuations are scale-free correlated, we are in the presence of Goldstone modes [52, 53], i.e. scale-free modes (or massless modes) that appear in the symmetry-broken phase, at zero external field. These modes involve the transverse fluctuations,

which are orthogonal with respect to the equilibrium magnetization, and, in the case of our $O(n)$ rotational symmetry, they are $n - 1$. More generally, following the Goldstone theorem [53], we can determine the number of Goldstone modes that emerges in the symmetry-broken phase of a theory in the following way. A system that in symmetric under a certain group transformation H in its symmetric phase (both in the Hamiltonian and in its equilibrium state), may have a phase transition and posses a certain phase where its equilibrium state is symmetric only with respect to a subgroup G of the initial group H. The number of Goldstone modes that emerge in this symmetry-broken phase is then equal to the number of generators of the full symmetry H minus the number of generators of the subgroup G [100]. We apply now this theorem to our case, we have that H is the group of rotations in a n-dimensional space, thus the number of its generators is $N_H = n(n-1)/2$ (that is also the dimension of the vector space of all the $n \times n$ antisymmetric matrices). In the symmetry-broken phase this group reduces to the rotations along the planes that are orthogonal to the equilibrium magnetization, that is G. The number of planes orthogonal to a certain axis is $N_G = (n-1)(n-2)/2$ hence the number of Goldstone modes is,

$$\text{\# Goldstone modes} = N_H - N_G = \frac{1}{2}\left[n(n-1) - (n-1)(n-2)\right] = n - 1 \quad (2.24)$$

as we stated in the beginning. A direct consequence of Goldstone modes is the Mermin-Wagner theorem [79] which states that a system with a continuous symmetry undergoes a phase transition from a disordered state to an ordered one only for $d > 2$. If $d = 2$ and $n = 2$, even if the system has not an ordered phase, it possesses a Kosterlitz-Thouless phase transition [72], but we are not interested in this peculiar situation since our biological system lives in a $3D$ space [23] where $n = d = 3$.

Fluctuations Hamiltonian

A more intuitive approach to find Goldstone modes for our $O(n)$ Landau-Ginzburg model (2.1) is to expand the Hamiltonian of the fluctuations around the Landau minimum [91],

$$\boldsymbol{\varphi} = \varphi_0 \hat{\boldsymbol{n}} + \delta\varphi_{\parallel}\left(\boldsymbol{r}\right) \hat{\boldsymbol{n}} + \delta\boldsymbol{\varphi}_{\perp}\left(\boldsymbol{r}\right) \quad (2.25)$$

$$\varphi_0 \simeq \sqrt{\frac{|t|}{4u}} + \frac{h}{2|t|} \quad (2.26)$$

where we computed φ_0 using the eq. (2.7) for $t < 0$, $\hat{\boldsymbol{n}}$ is the direction of the mean-field magnetization (and of the external field $\boldsymbol{h}$), $\delta\varphi_{\parallel}$ is the magnitude of the fluctuation that is parallel to the Landau magnetization $\varphi_0\hat{\boldsymbol{n}}$ while $\delta\boldsymbol{\varphi}_{\perp}$ is the perpendicular fluctuation. If we substitute the (2.25) and the (2.26) into the (2.1) we obtain the Hamiltonian,

$$\mathcal{H} = \text{const} + \int_V \mathrm{d}^d r \left\{ \frac{1}{2}\left(\nabla\delta\varphi_{\parallel}\right)^2 + \frac{1}{2}\left(\nabla\delta\boldsymbol{\varphi}_{\perp}\right)^2 + \frac{t_{\parallel}}{2}\delta\varphi_{\parallel}^2 + \frac{t_{\perp}}{2}\delta\varphi_{\perp}^2 + \right.$$

$$\left. + u\left(\delta\varphi_{\parallel}^2 + \delta\varphi_{\perp}^2\right)^2 + u_3\delta\varphi_{\parallel}^3 + u_3\delta\varphi_{\parallel}\delta\varphi_{\perp}^2 \right\} \quad (2.27)$$

where, up to order h, we have,

$$t_\parallel = 2|t| + \frac{3h}{\varphi_0} \qquad\qquad t_\perp = \frac{h}{\varphi_0} \qquad\qquad u_3 = 4u\varphi_0 \qquad (2.28)$$

If use the Hamiltonian (2.27) to compute the Gaussian propagators in momentum space for the longitudinal ($\parallel$) and transverse ($\perp$) fluctuations we find,

$$G^0_\parallel (p) = \frac{T}{p^2 + 2|t| + \frac{3h}{\varphi_0}} \qquad\qquad G^0_\perp (p) = \frac{T}{p^2 + \frac{h}{\varphi_0}} \qquad (2.29)$$

where we have the T in the numerator because our distribution is the (2.2), this factor here is harmless because it is just a total scaling of the propagators' amplitudes. Using the fluctuation-dissipation relation [78] we can compute the longitudinal susceptibility and the transverse susceptibility at tree level,

$$\chi_\parallel = \beta G^0_\parallel(p = 0) = \frac{1}{2|t| + \frac{3h}{\varphi_0}} \qquad\qquad \chi_\perp = \beta G^0_\perp(p = 0) = \frac{\varphi_0}{h} \qquad (2.30)$$

At this level of approximation, we find in the (2.30) the same result that we find using the Ward identity (2.22), the transverse susceptibility diverges in the symmetry-broken phase, when the external field vanishes.

From eq. (2.30) we note a differing point: at tree level, the longitudinal susceptibility does not diverge, even for $h = 0$. In fact, while the divergence of the transverse susceptibility is a general result, which is valid at all perturbative orders, because it is a consequence of a Ward identity (2.22), that descends from a symmetry of the Hamiltonian, eq. (2.30) is just derived using the Gaussian approximation of the fluctuations' Hamiltonian (2.27), hence we are not guaranteed that the longitudinal susceptibility will be finite for $h = 0$ and $t < 0$, if we improve our approximation. In fact, in the next section we will see that this result only holds at tree level. From (2.28) and (2.29) we find that we have two distinct correlation lengths for the transverse degrees of freedom and the longitudinal one. Because of the fact that the transverse fluctuations have $n - 1$ components, we also recover that this theory has $n - 1$ Goldstone modes [52], as we find above using the Goldstone theorem.

If we set the external field to zero and then we approach the bare critical temperature $t = 0$, we find that both susceptibilities (2.30) diverge, as it should be because we are approaching the critical point, where all the degrees of freedom of our system become scale-free. Notice that the longitudinal susceptibility diverges with the same exponent $\gamma = 1$ as its scalar counterpart (2.8), that we defined in the symmetric phase $t > 0$. We cannot use the above equations to describe our system directly at the critical point, we should have set $t = 0$ from the start in eq. (2.7), doing so we obtain that, at the bare critical point ,our magnetization is,

$$\varphi_0 = \left(\frac{h}{4u}\right)^{1/3} \sim h^{1/3} \qquad (2.31)$$

hence we obtain another bare critical exponent $\delta = 3$ [91].

2.2.1 Back to flocks # 1: Goldstone modes in starling flocks

We want now to connect what we discussed so far with the phenomenology of flocks. In order to compare the model we have discussed in this section with flocks we can identify the microscopic spins of the $O(n)$ model with starlings' velocities. It becomes immediately apparent that, in order to achieve high polarization (which corresponds to high magnetization φ), we must be in the symmetry-broken (SB), low-temperature phase with $t < 0$. We can now explain the panels **a** and **c** of Fig. 1.6, using the Goldstone modes theory. As we find using the Ward identity (2.22) and also the fluctuation expansion (2.25), a system with short-range interactions and a continuous symmetry develops scale-free transverse modes in its polarized (or symmetry-broken) phase. Hence we are not surprised to see that in our polarized (see Fig. 1.2) biological system, the full velocity fluctuations' correlations, that contain also the transverse contribution, are scale-free. Any model with a $O(3)$ symmetry, that lives in $d = 3$, is capable of reproducing full velocities' scale-free correlations as we discovered them in starling flocks [13].

Before tackling the scale-free modulus correlations problem (i.e. the speed scale-free correlations as we can see in panels **b** and **d** of Fig. 1.6) we need to carefully understand what happens with the longitudinal correlations. We only have the result of eq. (2.30) that is the equivalent of a mean-field approximation that often does not give accurate results in the regime of strong fluctuations [91].

We also must underline the fact that the longitudinal susceptibility of eq. 2.30, which is linked to the correlation length of longitudinal fluctuations, does not coincides with the modulus susceptibility, which is linked to the modulus correlation length that we measured in data (Fig. 1.6-**b**). The Cartesian decomposition of fluctuations (longitudinal and transverse) is different from the spherical decomposition (modulus and phases) and correlation properties depend on which kind of decomposition we are performing, as we shall see later.

The role of gravity and symmetry

We pointed out in the section above that we can describe flocks using a O(3)-symmetric model. Given the presence of gravity and its importance in the dynamics of avian flight, this choice is not obvious at all. We support it with two arguments: one concerning the average velocity of a flock and another concerning the nature of fluctuations.

First of all we can imagine that the center of mass velocity of a flock can point in a direction outside the horizontal plane, it is common for flocks to increase or decrease their altitude during the flight. However some directions are highly unlikely to be chosen (for example the vertical axis direction upward or downward) due to the mechanics of flight and the physiology of birds. This means that the average velocity of a flock, which is the order parameter, is a vector that belongs to the whole $3D$ space but only some directions are actually energetically equivalent (approximately). We could think this situation as an intermediate case between a $O(2)$ symmetry and a $O(3)$ symmetry for the order parameter.

Secondly, if we plot all the velocity fluctuations for every individual in a flock, during the whole flocking event (see Fig. 2.2) we can see that fluctuations are
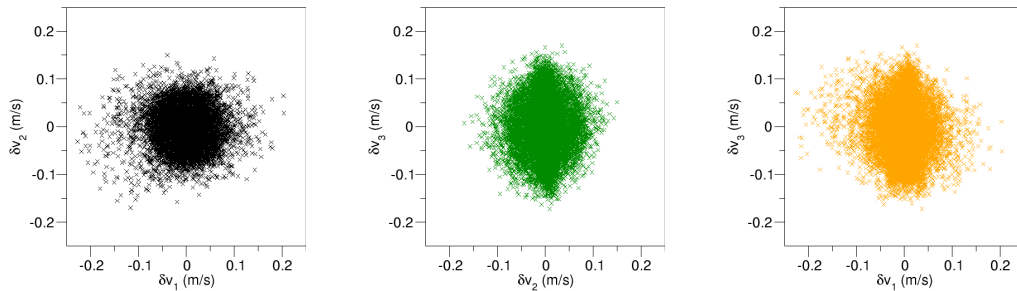
Figure 2.2. Projections of velocity fluctuations with respect to the average velocity for a typical flock. We can see in the plot the projection onto three perpendicular planes of the single-individual velocity fluctuations with respect to the average velocity of the flock (in each frame). The flock has a linear size of $68m$ and is composed of 1548 individuals. None of the three axes δv_1, δv_2 and δv_3 can be identified with the vertical axis. We can see that fluctuations are present in the whole $3D$ space, even if they are denser along the δv_3 axis.

present in the whole $3D$ space. This evidence means that, at least on the time scale of single-bird fluctuations, there is no preferred plane for fluctuations, hence there is not an explicit breaking of the $O(3)$ symmetry in favor of a $O(2)$ symmetry. However, we can see that fluctuations are denser in some directions (see Fig. 2.2, second and third panel, along the δv_3 axis), which can make us think that also from this point of view we are in an intermediate situation between the $O(2)$ case and the $O(3)$ case.

Overall, we choose to approximately describe the system with a $O(3)$-symmetric theory since this extremely simplifies our discussion with respect to considering the more accurate description of an intermediate symmetry between $O(2)$ and $O(3)$ and also because our model has proved to be able to describe correctly experimental data [27, 34].

2.3   The longitudinal susceptibility's divergence

We will now prove that the longitudinal susceptibility too diverges, meaning that longitudinal fluctuations too are scale-free correlated [17, 18, 92, 93]. However, this does not give us any information about modulus fluctuations correlations, on the contrary the relation that we will find between longitudinal and transverse susceptibility (and that I verified with simulations) is based on the fact that we can neglect modulus fluctuations amplitude [18, 92].

2.3.1   The large-n expansion

Following [17], we compute perturbatively the two susceptibilities, that we previously computed at tree level in eq. (2.30), using the following setting. First of all we include the inverse temperature β that appears in the definition (2.2) in the field's definition, so that $P \sim e^{-\mathcal{H}}$, this will lighten the notation. Then we work in the limit of large n; to be consistent and have all the terms in the Hamiltonian of the same

order in n we choose u to be of order $\frac{1}{n}$. We choose the field $\boldsymbol{h}$ to point along the first of the n possible axes and we change variable in the Hamiltonian (2.1) using,

$$L(\boldsymbol{x}) = \varphi_1(\boldsymbol{x}) - M \tag{2.32}$$

where M is the average of $\varphi_1(\boldsymbol{x})$, computed using the full probability distribution. M is of order $\sqrt{n}$, in order to be coherent with the bare approximation of eq. (2.26). Then we can write the Hamiltonian as a free part,

$$\mathcal{H}_0 = \frac{1}{2} \int \mathrm{d}^d r \left\{ (\nabla L)^2 + \sum_{\alpha=2}^{n} (\nabla \varphi_\alpha)^2 + \chi_\parallel^{-1} L^2 + \chi_\perp^{-1} \sum_{\alpha=2}^{n} \varphi_\alpha^2 \right\} \tag{2.33}$$

and an interaction part

$$\mathcal{H}_I = \int \mathrm{d}^d r \left\{ \frac{1}{2} \left(t - \chi_\parallel^{-1} + 12 M^2 u \right) L^2 + \frac{1}{2} \left(t - \chi_\perp^{-1} + 4 M^2 u \right) \sum_{\alpha=2}^{n} \varphi_\alpha^2 + \right.$$

$$+ u \left(L^2 + \sum_{\alpha=2}^{n} \varphi_\alpha^2 \right)^2 + 4 u M \left(L^3 + L \sum_{\alpha=2}^{n} \varphi_\alpha^2 \right) +$$

$$\left. + L M \left(t + 4 u M^2 \right) - h L \right\} \tag{2.34}$$

with the sum and subtraction of the quantities $\chi_\perp^{-1} \sum_{\alpha=2}^{n} \varphi_\alpha^2$ and $\chi_\parallel^{-1} L^2$, where we define the longitudinal susceptibility as $\chi_\parallel = \frac{\partial M}{\partial h}$ (coherently with our previous calculations of eq. (2.30)) and the transverse susceptibility using the Ward identity (eq. (2.23)) $\chi_\perp = M/h$. We use this procedure of summing and subtracting the inverse susceptibilities (or "dressed" masses [95]), in order to automatically sum all the possible insertions of loops on a leg L or φ_α with $\alpha > 1$ [14]. To investigate the relation between the two susceptibilities we use the equation,

$$\langle L \rangle = 0 \tag{2.35}$$

that follows from the definition (2.32). We compute the equation above expanding the exponential of the interaction Hamiltonian eq. (2.34) and computing the Gaussian averages $\langle \cdot \rangle_0$ using the free Hamiltonian (2.33). We stop at leading order, hence including in our expansion only the largest order terms in n, that is $O(\sqrt{n})$ and the smallest order terms in u. We must also include only the odd interaction terms, in order to obtain non-vanishing Gaussian averages, once we multiply them for L in the above equation. If we represent the equation above through diagrams, we have the leg that represents L of the above equation,

$$\tag{2.36}$$
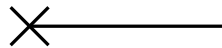
where the solid line represent the field L and the cross on the left indicates that we can only attach other legs, which will be connected from the interaction vertices, on

the right. Of all the potential contributions from the interaction Hamiltonian (2.34), we must consider only the odd vertices,

$$4uM$$

$$tM+4uM^3\text{-}h$$

(2.37)

which are of the highest order in n (which is $\sqrt{n}$) and of the lowest order in u. In the vertex on the left the dashed lines represent the transverse field φ_α, hence if we connect them in a diagram we have to consider a factor $n-1$, that in our limit of large n can be considered as $\sim n$. In the end, the diagrams that give a contribution to eq. (2.35) are,

(2.38)

In formulas we have,

$$4uM \left\langle L^2 \right\rangle_0 \left\langle \sum_{\alpha=2}^{n} \varphi_\alpha^2 \right\rangle_0 + M \left(t + 4uM^2 \right) \left\langle L^2 \right\rangle_0 - h \left\langle L^2 \right\rangle_0 = 0 \qquad (2.39)$$

that can be rewritten as

$$4u \left\langle \sum_{\alpha=2}^{n} \varphi_\alpha^2 \right\rangle_0 + t + 4uM^2 - \frac{h}{M} = 0 \qquad (2.40)$$

because both M and $\left\langle L^2 \right\rangle_0$ are always non-vanishing in the symmetry-broken phase. Now we compute the above equation at the critical point, where $t = t_C$ will be the distance between the critical temperature at our order of approximation and the bare critical temperature and where $\chi_\parallel^{-1} = \chi_\perp^{-1} = h = M = 0$. We first send h to zero while we remain in the ordered phase, and then we let the inverse susceptibilities and the magnetization vanish at the critical point. We obtain:

$$4u \left\langle \sum_{\alpha=2}^{n} \varphi_\alpha^2 \right\rangle_{0C} + t_C = 0 \qquad (2.41)$$

where the average $\langle \cdot \rangle_{0C}$ is made using the Gaussian Hamiltonian (2.33) with $\chi_\perp^{-1} = 0$. Now we subtract eq. (2.41) from (2.40) and we obtain,

$$\frac{h}{M} = t_R + 4uM^2 + 4un \int \frac{\mathrm{d}^d k}{(2\pi)^d} \left[\frac{1}{k^2 + \chi_\perp^{-1}} - \frac{1}{k^2} \right] \qquad (2.42)$$

where $t_R = t - t_C$ is the distance between the temperature of the system and the critical temperature at our level of approximation. The integral in the expression above is the explicit expression for $\langle \sum_{\alpha=2}^{n} \varphi_\alpha^2 \rangle_0 - \langle \sum_{\alpha=2}^{n} \varphi_\alpha^2 \rangle_{0C}$, using the free Hamiltonian (2.33). We can perform it for $d < 4$, letting $\boldsymbol{k}$ span the whole d-dimensional space,

$$
\begin{aligned}
I &= \int \frac{\mathrm{d}^d k}{(2\pi)^d} \left[\frac{1}{k^2 + \chi_\perp^{-1}} - \frac{1}{k^2} \right] = -\frac{\chi_\perp^{1-d/2}\Omega_d}{(2\pi)^d} \int_0^\infty \mathrm{d}x \, \frac{x^{d-3}}{x^2+1} \\
&= -\frac{\chi_\perp^{1-d/2}\Omega_d}{(2\pi)^d} \int_0^\infty \mathrm{d}\alpha \, e^{-\alpha} \int_0^\infty \mathrm{d}x \, x^{d-3} e^{-\alpha x^2} \\
&= -\frac{\chi_\perp^{1-d/2}\Omega_d}{2(2\pi)^d} \int_0^\infty \mathrm{d}\alpha \, \alpha^{1-d/2} e^{-\alpha} \int_0^\infty \mathrm{d}t \, t^{d/2-2} e^{-t} \\
&= -\frac{(h/M)^{1-\epsilon/2}\Omega_{4-\epsilon}}{2(2\pi)^{4-\epsilon}} \int_0^\infty \mathrm{d}\alpha \, \alpha^{\epsilon/2-1} e^{-\alpha} \int_0^\infty \mathrm{d}t \, t^{-\epsilon/2} e^{-t} \\
&= -\frac{(h/M)^{1-\epsilon/2}\pi^{2-\epsilon/2}\Gamma(\epsilon/2)\Gamma(1-\epsilon/2)}{(2\pi)^{4-\epsilon}\, \Gamma(2-\epsilon/2)} \\
&= -\left(\frac{h}{M}\right)^{1-\epsilon/2} \frac{\pi^{3-\epsilon/2}}{(2\pi)^{4-\epsilon}\, \Gamma(2-\epsilon/2)\sin\left(\pi\epsilon/2\right)}
\end{aligned}
\tag{2.43}
$$

where we use the substitution $x = k\sqrt{\chi_\perp}$ and we express the fraction $1/(x^2+1)$ using the integral,

$$
\frac{1}{(x^2+1)^p} = \frac{1}{\Gamma(p)} \int_0^\infty \mathrm{d}\alpha \, \alpha^{p-1} e^{-\alpha(x^2+1)}
\tag{2.44}
$$

After that, we perform another substitution $t = \alpha x^2$, then we write the dimension as $d = 4 - \epsilon$ and the transverse susceptibility $\chi_\perp = M/h$, following eq. (2.22). In the end we express the final integrals in α and in t using the Euler Gamma function,

$$
\Gamma(z) = \int_0^\infty \mathrm{d}y \, y^{z-1} e^{-y}
\tag{2.45}
$$

and we use the in the last passage the Euler reflection formula,

$$
\Gamma(z)\Gamma(1-z) = \frac{\pi}{\sin(\pi z)}
\tag{2.46}
$$

The state equation (2.42) then becomes, using the solution of the integral (2.43)

$$
\frac{h}{M} = t_R + 4uM^2 - 4un \left(\frac{h}{M}\right)^{1-\epsilon/2} \frac{\pi^{3-\epsilon/2}}{(2\pi)^{4-\epsilon}\Gamma(2-\epsilon/2)\sin\left(\pi\epsilon/2\right)}
\tag{2.47}
$$

By rescaling the φ_α fields and the temperature t_R, we get rid of the constants in eq. (2.47). In the symmetry-broken phase, with $h \to 0$, $t < 0$ and $M \neq 0$, we can write the previous equation as,

$$
t_R = -M^2 + \left(\frac{h}{M}\right)^{1-\epsilon/2}
\tag{2.48}
$$

from which we can compute the critical exponent $\beta = 1/2$ [17], by setting $h = 0$, and the critical exponent $\delta = 3 + \epsilon$ [17], by setting $t_R = 0$. If we take the derivative with respect to h of the equation above, we obtain,

$$0 = -2M\chi_\parallel + (1 - \epsilon/2)\, M^{-1} \left(1 - \chi_\parallel/\chi_\perp\right) \chi_\perp^{\epsilon/2} \tag{2.49}$$

Now we make the assumption that $\chi_\parallel/\chi_\perp \ll 1$, which is reasonable, given that at tree level the longitudinal susceptibility does not diverge (see eq. (2.30)) and that we expect the transverse fluctuations to cost less energy with respect to the longitudinal ones, as one can imagine by looking at the bare potential of the theory Fig. (2.1). Following the consequences of the assumption, we can disregard the term $\chi_\parallel/\chi_\perp$, hence the above equation becomes

$$\chi_\parallel = \frac{1}{2} M^{-2}(1 - \epsilon/2)\chi_\perp^{\epsilon/2}$$
$$\chi_\parallel \sim \chi_\perp^{\epsilon/2} \tag{2.50}$$

that is consistent with the observation $\chi_\perp \gg \chi_\parallel$ and tells us that, even if more weakly, the longitudinal susceptibility too diverges in the symmetry-broken phase, for vanishing external field. The reason of this divergence can be found in the coupling between the longitudinal degree of freedom L and the transverse one φ_α (for $\alpha > 1$) that is expressed in the interaction vertex on the left of eq. (2.37). If we compute the longitudinal correlation function $\langle L^2 \rangle$ at $k = 0$ and $h = 0$ (that corresponds to the longitudinal susceptibility via the fluctuation-dissipation theorem, see appendix 2.A), at tree level we have the non-divergent result of eq. (2.30), but if we include the one-loop diagram built with two cubic vertices (2.37),

$$\tag{2.51}$$

we see that this one-loop correction, because of the internal lines that are transverse (hence massless, see eq. (2.29)) propagators, is infrared divergent at zero external field [18]. The explicit expression of the diagram above at zero external momentum is,

$$D \sim \int \frac{\mathrm{d}^d p}{(2\pi)^d} \frac{1}{(p^2 + \chi_\perp^{-1})^2} \sim \chi_\perp^\epsilon \tag{2.52}$$

hence it is infrared divergent for $d < 4$. At this level we find just a perturbative result, in the limit of large n and small coupling u but, if we perform a Monte Carlo simulation of a $O(3)$-symmetric system, we can see that the scaling of eq. (2.50) holds quite well (see section 2.3.3). We could think that this is a general property of systems with a continuous symmetry in a symmetry-broken phase, hence in the following subsection we will consider the problem from a wider point of view.

2.3.2 The longitudinal susceptibility for any n

We will now follow the calculations of [93], generalizing them for any $d < 4$. A $O(n)$-symmetric system, which is coupled with an external symmetry-breaking field, can be described using its generalized Gibbs free energy (per unit volume),

$$\hat{f}(\boldsymbol{m}) = g(m^2) - \boldsymbol{h} \cdot \boldsymbol{m} \tag{2.53}$$

where $g(m^2)$ is the Gibbs free energy, that has the same symmetry of the system. The variable $\boldsymbol{m}$ is the spatial average over the whole system of the fluctuating fields $\boldsymbol{\varphi}(\boldsymbol{x})$, hence it is the fluctuating variable that describes the total magnetization per unit volume of the system. The minimum of $\hat{f}(\boldsymbol{m})$ identifies the equilibrium magnetization of the system $\boldsymbol{m}_0$,

$$\boldsymbol{h} = 2\boldsymbol{m}_0 g'(m_0^2) \tag{2.54}$$

and thus expresses the relation between the equilibrium magnetization and the external field $\boldsymbol{h}$. In principle, using the equation above, we can express the spontaneous magnetization as a function of the external field $\boldsymbol{m}_0 = \boldsymbol{m}_0(\boldsymbol{h})$, plug it in eq. (2.53), and find the Helmholtz free energy $\hat{f}(\boldsymbol{m}_0(\boldsymbol{h})) = f(h^2)$, that is also $O(n)$-symmetric in its argument $\boldsymbol{h}$. In the symmetry-broken phase at zero field, the spontaneous equilibrium magnetization modulus is fixed by the above equation, which simplifies to,

$$g'(m_0^2) = 0 \tag{2.55}$$

where we have discarded the solution $m_0 = 0$ since we already know that below the critical temperature we have non-vanishing spontaneous equilibrium magnetization. Deriving equation (2.54) with respect to the component $m_{0\beta}$ we can find an expression for the inverse susceptibility matrix,

$$\chi_{\alpha\beta}^{-1} = \frac{\partial h_\alpha}{\partial m_{0\beta}} = 2\delta_{\alpha\beta} g'(m_0^2) + 4m_{0\alpha} m_{0\beta} g''(m_0^2)$$
$$= \left[4m_0^2 g''(m_0^2) + 2g'(m_0^2)\right] n_\alpha n_\beta + \left[2g'(m_0^2)\right] (\delta_{\alpha\beta} - n_\alpha n_\beta) \tag{2.56}$$

where $\delta_{\alpha\beta}$ is the Kronecker delta and $\boldsymbol{n} = \boldsymbol{h}/h = \boldsymbol{m}_0/m_0$. From the susceptibility matrix in this form, we can easily identify the transverse and the longitudinal inverse susceptibilities,

$$\chi_\perp^{-1} = 2g'(m_0^2) = \frac{h}{m_0} \tag{2.57}$$
$$\chi_\parallel^{-1} = 4m_0^2 g''(m_0^2) + 2g'(m_0^2) \tag{2.58}$$

where we recovered, using eq. (2.54), the Ward identity (2.22). Given that we want to investigate the properties of longitudinal and transverse fluctuations, we expand the generalized thermodynamic potential (2.53) near the minimum $\boldsymbol{m}_0$, we express $\boldsymbol{m}$ as,

$$\boldsymbol{m} = \boldsymbol{m}_0 + \delta\boldsymbol{m} = \boldsymbol{m}_0 + \delta m_\parallel \boldsymbol{n} + \delta\boldsymbol{m}_\perp \tag{2.59}$$
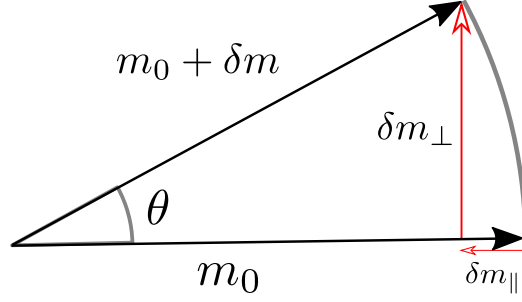
Figure 2.3. Magnetization fluctuations decomposed A generic phase fluctuation for $n = 2$ is decomposed into its longitudinal and transverse component. We can see that both kinds of fluctuations have a non-zero contribution from a phase fluctuation. The longitudinal one is smaller $\sim \theta^2$, while the transverse one is bigger $\sim \theta$ for $\theta \ll 1$.

where $\delta m_\parallel \boldsymbol{n}$ and $\delta \boldsymbol{m}_\perp$ are, respectively, the parallel fluctuation to the equilibrium magnetization and the orthogonal fluctuation to the equilibrium magnetization. The change in the potential is, at quadratic order,

$$\delta \hat{f} = f(\boldsymbol{m}) - f(\boldsymbol{m}_0) = \frac{1}{2} \frac{\partial^2 \hat{f}}{\partial m_\alpha \partial m_\beta}\bigg|_{\boldsymbol{m}_0} \delta m_\alpha \delta m_\beta = \frac{1}{2} \frac{\partial^2 g}{\partial m_\alpha \partial m_\beta}\bigg|_{\boldsymbol{m}_0} \delta m_\alpha \delta m_\beta$$

$$= \frac{1}{2} \chi_{\alpha\beta}^{-1} \delta m_\alpha \delta m_\beta = \frac{1}{2} \left(\chi_\perp^{-1} \delta m_\perp^2 + \chi_\parallel^{-1} \delta m_\parallel^2 \right) \tag{2.60}$$

where we are summing over repeated indices (from now on, if not stated otherwise, we always imply the sum over repeated indices). From this expression we can see that energetic fluctuations are linked to magnetization's fluctuations through the two susceptibilities. For vanishing field, the inverse transverse susceptibility vanishes too. hence it is extremely easy to perform a transverse fluctuation of the magnetization, because at least at quadratic level, it does not cost in energy terms.

The principle of modulus conservation

To refine our study of fluctuations around the thermodynamic potential minimum (2.53), we now assume that the "principle of modulus conservation" [92, 93] can be applied. We will find later that this assumption is reasonable and leads to self-consistent results. This principle states that the fluctuations of m^2 are negligible, which means,

$$\delta(\boldsymbol{m} \cdot \boldsymbol{m}) = \boldsymbol{m} \cdot \boldsymbol{m} - m_0^2 \simeq 0 \tag{2.61}$$

Using eq. (2.59) and the fact that in the limit of small fluctuations we can neglect $\delta m_\parallel^2$ because it is much smaller than $\delta m_\parallel$, the above equation transforms into,

$$\delta(\boldsymbol{m} \cdot \boldsymbol{m}) \simeq 2 m_0 \delta m_\parallel + \delta m_\perp^2 \simeq 0 \tag{2.62}$$

that gives us an important information about the relative magnitude of fluctuations, namely that $\delta m_\parallel \sim \delta m_\perp^2$. The geometrical reason of this relation can be understood by looking at Fig. 2.3; if we neglect modulus fluctuations, only phase fluctuations of

a certain angular amplitude θ are permitted and we can write both the longitudinal contribution and the transverse contribution as functions of the angle θ,

$$\delta m_\perp = m_0 \sin(\theta) \sim \theta \tag{2.63}$$

$$\delta m_\parallel = m_0 - m_0 \cos(\theta) \sim \theta^2 \tag{2.64}$$

that implies

$$\delta m_\parallel \sim \delta m_\perp^2 \tag{2.65}$$

Moreover, we find that, if we assume the conservation of the modulus (2.61), the scalar product of longitudinal fluctuations and the equilibrium magnetization have opposite direction, i.e $\boldsymbol{m}_0 \cdot \delta m_\parallel \boldsymbol{n} < 0$ (from eq. (2.62)). This property can be clearly seen in Fig. 2.3, where a phase fluctuation generates a longitudinal fluctuation that is always opposite with respect to the equilibrium magnetization. Now that we know how to compare longitudinal and transverse fluctuations, we proceed expanding up to the fourth order in $\delta m_\perp$ (i.e. the second order in $\delta m_\parallel$) the generalized Gibbs free energy (2.53). We already have the quadratic contribution from eq. (2.60), hence we only need to compute the third order contribution,

$$\delta \hat{f}_3 = \frac{1}{6} \left. \frac{\partial^3 \hat{f}}{\partial m_\alpha \partial m_\beta \partial m_\mu} \right|_{\boldsymbol{m}_0} \delta m_\alpha \delta m_\beta \delta m_\mu \tag{2.66}$$

and the fourth order contribution.

$$\delta \hat{f}_4 = \frac{1}{24} \left. \frac{\partial^4 \hat{f}}{\partial m_\alpha \partial m_\beta \partial m_\mu \partial m_\nu} \right|_{\boldsymbol{m}_0} \delta m_\alpha \delta m_\beta \delta m_\mu \delta m_\nu \tag{2.67}$$

Starting with $\delta \hat{f}_3$ we have to compute,

$$\left. \frac{\partial^3 \hat{f}}{\partial m_\alpha \partial m_\beta \partial m_\mu} \right|_{\boldsymbol{m}_0} = \left. \frac{\partial^3 g}{\partial m_\alpha \partial m_\beta \partial m_\mu} \right|_{\boldsymbol{m}_0} = 12 \delta_{\alpha\beta} m_{0\mu} g'' + 8 m_{0\alpha} m_{0\beta} m_{0\mu} g''' \tag{2.68}$$

where we are simply writing explicitly all the derivatives with respect to the various components m_α, we also omit the argument m_0^2 of g and its derivatives to lighten the notation. Plugging the result into the (2.66) we obtain,

$$\delta \hat{f}_3 = 2 g'' m_0 \delta m_\parallel \left(\delta m_\parallel^2 + \delta m_\perp^2 \right) + \frac{4}{3} g''' m_0^3 \delta m_\parallel^3 \tag{2.69}$$

where we consider only the term $2 g'' m_0 \delta m_\parallel \delta m_\perp^2$ that is the only one, considering eq. (2.65), of order $\delta m_\perp^4$. All the other terms of the above equation are of higher order. Going on to the contribution of eq. (2.67) we have to compute,

$$\left. \frac{\partial^4 \hat{f}}{\partial m_\alpha \partial m_\beta \partial m_\mu \partial m_\nu} \right|_{\boldsymbol{m}_0} = \left. \frac{\partial^4 g}{\partial m_\alpha \partial m_\beta \partial m_\mu \partial m_\nu} \right|_{\boldsymbol{m}_0}$$

$$= 12 \delta_{\alpha\beta} \delta_{\mu\nu} g'' + 48 \delta_{\alpha\beta} m_\mu m_\nu g''' + 16 m_\alpha m_\beta m_\mu m_\nu g'''' \tag{2.70}$$

and then, plugging it into eq. (2.67), we have,

$$\delta \hat{f}_4 = \frac{1}{2} g'' \left(\delta m_\parallel^2 + \delta m_\perp^2 \right)^2 + 2 g''' m_0^2 \delta m_\parallel^2 \left(\delta m_\parallel^2 + \delta m_\perp^2 \right) + \frac{2}{3} g'''' m_0^4 \delta m_\parallel^4 \qquad (2.71)$$

where we consider only the term $\frac{1}{2} g'' \delta m_\perp^4$, because all the others exceed the order $\delta m_\perp^4$. Putting together all the terms we have computed so far, up to order $\delta m_\perp^4$, we have,

$$\begin{aligned} \delta \hat{f} &= g' \delta m_\perp^2 + (g' + 2 m_0 g'') \delta m_\parallel^2 + 2 m_0 g'' \left[\delta m_\parallel \delta m_\perp^2 / m_0 + \delta m_\perp^4 / (4 m_0^2) \right] \\ &= \frac{1}{2} \chi_\perp^{-1} \delta m_\perp^2 + \frac{1}{2} \chi_\parallel^{-1} \left[\delta m_\parallel^2 + \delta m_\parallel \delta m_\perp^2 / m_0 + \delta m_\perp^4 / (4 m_0) \right] \\ &= \frac{1}{2} \left[\frac{\delta m_\perp^2}{\chi_\perp} + \frac{[\delta(\boldsymbol{m} \cdot \boldsymbol{m})]^2}{4 m_0^2 \chi_\parallel} \right] \end{aligned} \qquad (2.72)$$

where we have made the approximation $\chi_\parallel^{-1} \simeq 2 m_0 g''$ from eq. (2.58), because we want to investigate the limit of $h \to 0$, hence we know from eq. (2.54) that the first derivative of the Gibbs free energy g' vanishes like $\sim h$. We are essentially using the same assumption that we use to go from eq. (2.49) to eq. (2.50), that is, for a small enough h, $\chi_\parallel / \chi_\perp \ll 1$. If we use eq.s (2.57) and (2.58), we find,

$$\chi_\parallel / \chi_\perp = \frac{g'}{g' + m_0 g''} \ll 1 \qquad (2.73)$$

that implies,

$$g'' \gg g' \qquad (2.74)$$

because, even for $h = 0$, the equilibrium magnetization m_0 is a finite quantity.

We now check if our initial assumption eq. (2.61) is sensible. From eq. (2.72) we can easily compute the above quantities because, from the definition of generalized Gibbs free energy [63], we have that the probability distribution of our variables is,

$$P \left(\delta \boldsymbol{m}_\perp, \delta(\boldsymbol{m} \cdot \boldsymbol{m}) \right) \sim \exp \left\{ -V \beta \delta \hat{f} \left(\delta \boldsymbol{m}_\perp, \delta(\boldsymbol{m} \cdot \boldsymbol{m}) \right) \right\} \qquad (2.75)$$

where V is the system's volume and $\beta = 1/(k_B T)$ with $k_B = 1$. To find the correct distribution we have also to compute the Jacobian of the transformation $\left(\delta \boldsymbol{m}_\perp, \delta m_\parallel \right) \to (\delta \boldsymbol{m}_\perp, \delta(\boldsymbol{m} \cdot \boldsymbol{m}))$, it can be done using eq. (2.62), and it is only a harmless constant $\mathcal{J} = 1/(2 m_0)$. From the equation above we have,

$$\left\langle \delta m_\perp^2 \right\rangle = (n-1) \frac{T \chi_\perp}{V} \qquad \qquad \left\langle [\delta(\boldsymbol{m} \cdot \boldsymbol{m})]^2 \right\rangle = \frac{4 m_0^2 T \chi_\parallel}{V} \qquad (2.76)$$

The principle of conservation of the modulus, expressed by eq.s (2.61) and (2.62), is equivalent to say that squared modulus fluctuations of equation (2.61) are much smaller than transverse fluctuations squared. Hence, if we square eq. (2.62) we can see that the following must hold,

$$\left\langle [\delta(\boldsymbol{m} \cdot \boldsymbol{m})]^2 \right\rangle \ll \left\langle \delta m_\perp^2 \right\rangle^2 \qquad (2.77)$$

where we used the fact that $\delta m_\perp$ is a Gaussian variable (see eq. (2.72)), thus from Wick's theorem we have $\langle \delta m_\perp^4 \rangle \sim \langle \delta m_\perp^2 \rangle^2$. Combining eq.s (2.76) and (2.77) we have a condition for the system's volume,

$$V \ll (n-1)^2 \frac{T\chi_\perp^2}{4m_0^2 \chi_\parallel} \tag{2.78}$$

Another condition on the validity of our approximation is that the largest fluctuations (i.e. the transverse ones) must be small with respect to the equilibrium magnetization,

$$\left\langle \delta m_\perp^2 \right\rangle \ll m_0^2 \tag{2.79}$$

that becomes another condition on the volume, using eq. (2.76),

$$V \gg (n-1) \frac{T\chi_\perp}{m_0^2} \tag{2.80}$$

We can see that, if $\chi_\parallel$ does not grow too fast for $h \to 0$, given a certain volume V, we can choose an external field h small enough so that both eq. (2.78) and (2.80) hold, hence validating both the expansion for small fluctuations (2.59) and the principle of modulus conservation (2.61). The validity of this principle tells us that, for systems with a continuous symmetry that becomes spontaneously broken, the modulus' fluctuations in the ordered phase are negligible with respect to the other degrees of freedom's fluctuations. Following [93], we can think of extending this principle to non-homogeneous fluctuations with large enough wavelength i.e. we extend the principle that we verified for the macroscopic quantity $\boldsymbol{m}$ to the mesoscopic fields $\boldsymbol{\varphi}(\boldsymbol{r})$, in the limit of momentum k close to 0. The idea that modulus fluctuations can be neglected is common in continuous spin models, some of them fix the vectors moduli, at mesoscopic level (non linear σ-model [122]) and even at microscopic level (classic Heisenberg model [103]).

Longitudinal susceptibility's asymptotic behaviour

We compute now the longitudinal susceptibility, applying the principle of modulus conservation (2.62) to mesoscopic fields. We expand eq. (2.53), bearing in mind the principle of modulus conservation, and use it as a proxy for a field theory for fluctuations. Using eq. (2.53) and eq. (2.72) we see that, if we were to expand further the potential $\hat{f}$, we would only obtain higher powers of the squared modulus fluctuations,

$$\begin{aligned}
\delta\hat{f} &= g\left(m_0^2 + \delta(\boldsymbol{m}\cdot\boldsymbol{m})\right) - g\left(m_0^2\right) - \boldsymbol{h}\cdot\delta\boldsymbol{m} \\
&= \frac{1}{2}\left[\frac{\delta m_\perp^2}{\chi_\perp} + \frac{[\delta(\boldsymbol{m}\cdot\boldsymbol{m})]^2}{4m_0^2\chi_\parallel}\right] + g'''\left[\delta(\boldsymbol{m}\cdot\boldsymbol{m})\right]^3 + g''''\left[\delta(\boldsymbol{m}\cdot\boldsymbol{m})\right]^4 + ... \\
&\simeq \frac{1}{2}\frac{\delta m_\perp^2}{\chi_\perp} \tag{2.81}
\end{aligned}$$

Following the above result, we see that the transverse fluctuations decouple from the negligible squared modulus fluctuations, hence we promote the homogeneous

magnetization transverse fluctuations $\delta m_\perp$ to a field $\delta\varphi_\perp(\boldsymbol{r})$ and we write the Hamiltonian,

$$\mathcal{H}_\perp = \frac{1}{2}\int \mathrm{d}r \left[\frac{1}{\chi_\perp}\delta\varphi_\perp^2 + c\,(\nabla\delta\varphi_\perp)^2\right] \tag{2.82}$$

where the gradient term takes into account the non-homogeneous transverse fluctuations. In principle we could add, in the above Hamiltonian, any gradient-dependent term but we stick to the lowest order because we are interested in the long-wavelength fluctuations of the system. The constant c is the stiffness of the system, which quantifies the rigidity of the system with respect to non-homogeneous transverse fluctuations. From the above equation, using the Boltzmann distribution [63], we can compute the transverse correlation function, in momentum space,

$$G_\perp(q) = \frac{T}{cq^2 + \chi_\perp^{-1}} = \frac{T}{cq^2 + \frac{h}{\varphi_0}} \tag{2.83}$$

The principle of modulus conservation for fields translates from (2.62) to,

$$2\varphi_0\delta\varphi_\parallel(\boldsymbol{r}) + \delta\varphi_\perp^2(\boldsymbol{r}) = 0 \tag{2.84}$$

where φ_0 is the equilibrium value of the field. The above equations (2.84) and (2.83) can be used to compute the longitudinal susceptibility,

$$\begin{aligned}
\chi_\parallel &= \frac{\partial\left\langle\delta\varphi_\parallel(\boldsymbol{r}=0)\right\rangle}{\partial h} = -\frac{1}{2\varphi_0}\frac{\partial\left\langle\delta\varphi_\perp^2(\boldsymbol{r}=0)\right\rangle}{\partial h} \\
&= -\frac{1}{2\varphi_0}(n-1)\int\frac{\mathrm{d}^d q}{(2\pi)^d}\frac{\partial G_\perp(q)}{\partial h} \\
&= \frac{(n-1)\Omega_d}{2(2\pi)^d h^2}\int_0^\infty \mathrm{d}q\,\frac{q^{d-1}}{\left(\frac{c\varphi_0}{h}q^2 + 1\right)^2} \\
&= \frac{(n-1)\Omega_d}{2(2\pi)^d(c\varphi_0)^{d/2}}\left[\int_0^\infty\mathrm{d}x\,\frac{x^{d-1}}{(x^2+1)^2}\right]h^{-\epsilon/2} \\
&\sim \chi_\perp^{\epsilon/2}
\end{aligned} \tag{2.85}$$

where we performed the substitution $x = q\sqrt{c\varphi_0/h}$. The integral in x can be computed using eq. (2.44) and then using the Euler Gamma function to express the dimension-less integrals; it bears a finite result for any $d < 4$. The above calculation states that, for *any n*,

$$\chi_\parallel \sim \chi_\perp^{\epsilon/2} \tag{2.86}$$

In the end, using only the $O(n)$ symmetry of the theory and assuming that modulus fluctuations are negligible with respect to the transverse ones, we find that the longitudinal susceptibility diverges for vanishing external field. Given that its divergence is weaker than the transverse susceptibility's, both eq.s (2.78) and (2.80) are legitimate, for a small enough field h. The whole calculation is indeed self-consistent and generalizes the result of eq. (2.50) for any n and any $O(n)$-symmetric theory.
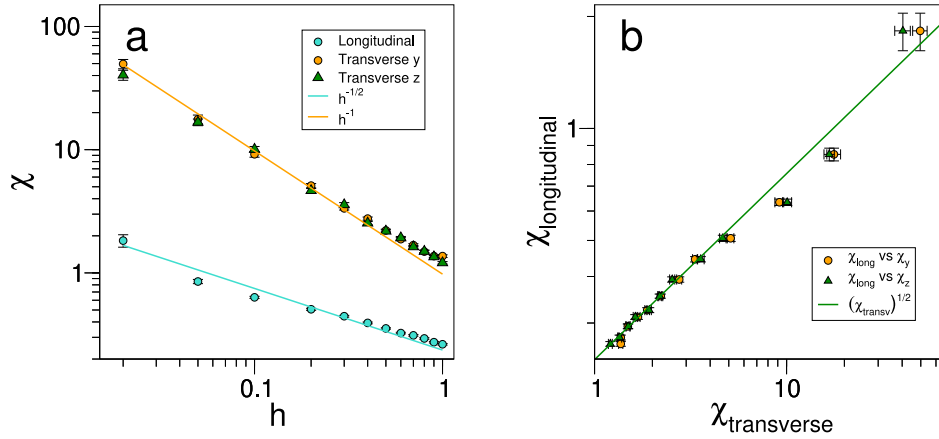
Figure 2.4. Longitudinal and transverse susceptibility for a $O(3)$-symmetric system a: Longitudinal susceptibility (light blue) and transverse susceptibilities (orange for y direction and green for z direction) as functions of the external magnetic field. **b**: Transverse VS longitudinal susceptibility, parametric in the external field h. The transverse susceptibility scales with a power law close to h^{-1}, as it is predicted by the Ward identity (2.22), while the longitudinal susceptibility scales with a power law close to $h^{-1/2}$ as it is predicted by eq. (2.50) with $\epsilon = 4 - d = 1$, because the system lives in a three-dimensional space $d = 3$. Simulation parameters: $J = 1$ and $T = 0.5$. The system is in a cubic box of size $10 \times 10 \times 10$.

2.3.3 Simulations for transverse and longitudinal susceptibilities

In order to see from simulations the relation 2.86 we performed MonteCarlo simulations of a spin system with the following microscopic $O(n)$-symmetric pseudo-Hamiltonian, perturbed by an external field,

$$H(\{\boldsymbol{\sigma}_i\}) = \frac{J}{2} \sum_{\langle i,j \rangle} (\boldsymbol{\sigma}_i - \boldsymbol{\sigma}_j)^2 + \sum_i (\sigma_i^2 - 1)^2 - \boldsymbol{h} \cdot \sum_i \boldsymbol{\sigma}_i \tag{2.87}$$

where the sum $\sum_{\langle i,j \rangle}$ is performed over all the couples of nearest neighbours on the lattice, the external space is three-dimensional $d = 3$ and also the spin space has three dimensions, with $n = 3$. Once the system is in the polarized phase, we measured the longitudinal and transverse susceptibilities as functions of the external magnetic field modulus $h = |\boldsymbol{h}|$. For this system they can be measured, using the fluctuation-dissipation relation [78],

$$\chi_\parallel = \frac{\beta}{N} \sum_{i,j} \left\langle \sigma_{\parallel i} \sigma_{\parallel j} \right\rangle - \left\langle \sigma_{\parallel i} \right\rangle \left\langle \sigma_{\parallel j} \right\rangle$$

$$\chi_\perp^{(\alpha)} = \frac{\beta}{N} \sum_{i,j} \left\langle \sigma_{\perp i}^{(\alpha)} \sigma_{\perp j}^{(\alpha)} \right\rangle - \left\langle \sigma_{\perp i}^{(\alpha)} \right\rangle \left\langle \sigma_{\perp j}^{(\alpha)} \right\rangle \tag{2.88}$$

where $\sigma_{\parallel i}$ is the component of the spin $\boldsymbol{\sigma}_i$ that is parallel to the external field $\boldsymbol{h}$ and $\sigma_{\perp i}^{(\alpha)}$ are the $n - 1 = 2$ components of the spin $\boldsymbol{\sigma}_i$ that are perpendicular to the

external field. In Fig. 2.4 we can see that the Ward identity 2.23 is verified, because the transverse susceptibility is compatible with the behaviour $\chi_\perp \sim h^{-1}$ and also the relation 2.86 is satisfied, because we can see from the figure that,

$$\chi_\| \sim \left[\chi_\perp^{(\alpha)}\right]^{1/2} \sim h^{-1/2} \tag{2.89}$$

We verified in a real finite-size system not only the well-known result of the Ward-Takahashi identity for the transverse susceptibility but also the highly non-trivial relation (2.86) that comes from a more detailed study of fluctuations in the symmetry-broken phase [17, 93].

   Regarding finite size effects in the simulations that we present in Fig. 2.4, we can use eq. (2.78) and eq. (2.80). If we are a bit more careful with numeric constants we see that (2.80) remains untouched, while (2.78) can be written more precisely as,

$$V \ll (n^2 + 2n)\frac{T\chi_\perp^2}{4m_0^2\chi_\|} \tag{2.90}$$

if we check the validity of the equation above and of eq. (2.80) for our simulations, we see that for small h they are simultaneously valid (we have an average magnetization $m_0 \simeq 0.9$), while for large h the above equation fails, while the (2.80) remains valid. This is reflected in the fact that in Fig. 2.4-**a**, for large h, the susceptibilities slightly depart from the predicted behaviour of eq. 2.57 and eq. (2.89).

2.3.4   Back to flocks # 2: a possible misunderstanding

We have no doubt now that with any classical $O(3)$ theory we could reproduce the full velocities' scale-free correlations of our experimental biological system (Fig. 1.6-**a**). It suffices to place the system in its broken-symmetry phase with high polarization, which is also compatible with the starling flocks state [24]. One may be tempted to identify the longitudinal fluctuations with the modulus fluctuations and justify in this way the speed's scale-free correlation of Fig. 1.6-**b**, but the calculations we have done in the previous sections state otherwise. One can see from Fig. 2.3 and equations (2.63)-(2.64) that longitudinal and transverse fluctuations, i.e. the Cartesian fluctuations, mix together the spherical fluctuations (phase and modulus). Moreover, to compute the divergence of the longitudinal susceptibility we have used eq. (2.61) (and checked its self-consistency) that clearly states that the modulus fluctuations are negligible with respect to the other degrees of freedom. This means that, even if we know that both the longitudinal and the transverse degree of freedom are scale-free correlated, we do not know yet which role has been played by the phase and modulus fluctuations. In the next section we will see what happens if we consider our system from the point of view of modulus and phase fluctuations, to discover if we can obtain speed scale-free correlations just with a standard $O(n)$ symmetric model.

2.4   Modulus and phase fluctuations

We can expand near the Landau minimum, in the spirit of eq. (2.25) and (2.26), but using modulus and phase fluctuations, instead of longitudinal and transverse

fluctuations [100]. We imagine that the equilibrium homogeneous field (that now we call ρ_0) points along the nth axis, hence we can write the generic field as,

$$\varphi_1 = [\rho_0 + \delta\rho(\boldsymbol{r})]\sin(\theta_1(\boldsymbol{r}))$$
$$\varphi_2 = [\rho_0 + \delta\rho(\boldsymbol{r})]\cos(\theta_1(\boldsymbol{r}))\sin(\theta_2(\boldsymbol{r}))$$
$$\varphi_3 = [\rho_0 + \delta\rho(\boldsymbol{r})]\cos(\theta_1(\boldsymbol{r}))\cos(\theta_2(\boldsymbol{r}))\sin(\theta_3(\boldsymbol{r}))$$
$$\ldots$$
$$\varphi_{n-1} = [\rho_0 + \delta\rho(\boldsymbol{r})]\cos(\theta_1(\boldsymbol{r}))\cos(\theta_2(\boldsymbol{r}))\ldots\cos(\theta_{n-2}(\boldsymbol{r}))\sin(\theta_{n-1}(\boldsymbol{r}))$$
$$\varphi_n = [\rho_0 + \delta\rho(\boldsymbol{r})]\cos(\theta_1(\boldsymbol{r}))\cos(\theta_2(\boldsymbol{r}))\ldots\cos(\theta_{n-2}(\boldsymbol{r}))\cos(\theta_{n-1}(\boldsymbol{r})) \qquad (2.91)$$

where $\delta\rho(\boldsymbol{r})$ is a generic space-dependent modulus fluctuation and $\theta_i(\boldsymbol{r})$ are the $n-1$ phase fluctuations possible in a n-dimensional space. Fluctuations are small, which means that $\delta\rho \ll \rho_0$ and $\theta_i \ll 1$ for every i. We substitute the above expression in the Hamiltonian (2.1) with zero external field $\boldsymbol{h}$. In order to obtain the fluctuations Hamiltonian, we have to compute the homogeneous part and the squared gradient of the field φ in eq. (2.1) as a function of the variables $\delta\rho$ and θ_i, defined in eq. (2.91). To simplify our notation we write,

$$\varphi_i = (\rho_0 + \delta\rho(\boldsymbol{r}))f_i(\{\theta_k(\boldsymbol{r})\}) \qquad (2.92)$$

where each function f_i is defined using eq. (2.91). The following relation descends from the definition,

$$\sum_{i=1}^{n} f_i^2 = 1 \qquad (2.93)$$

To verify the relation above it suffices to sum the various squared f_i, starting from the nth function and going backward, from n to 1, using $\sin^2(\theta_i) + \cos^2(\theta_i) = 1$ for every i. The homogeneous part of eq. (2.1) is easy to express in terms of modulus and phase fluctuations, we have,

$$\frac{t}{2}\varphi^2 = \frac{t}{2}\sum_{i=1}^{n}\varphi_i^2 = \frac{t}{2}\left(\rho_0 + \delta\rho(\boldsymbol{r})\right)^2\sum_{i=1}^{n}f_i^2 = \frac{t}{2}\left(\rho_0 + \delta\rho(\boldsymbol{r})\right)^2$$

$$= \text{const} + t\rho_0\delta\rho + \frac{t}{2}\delta\rho^2$$

$$u\varphi^4 = u\left(\varphi^2\right)^2 = u\left(\rho_0 + \delta\rho(\boldsymbol{r})\right)^4$$

$$= \text{const} + u\delta\rho^4 + 4u\rho_0\delta\rho^3 + 6u\rho_0^2\delta\rho^2 + 4u\rho_0^3\delta\rho \qquad (2.94)$$

For the gradient we have,

$$\frac{1}{2}\left(\nabla\varphi\right)^2 = \frac{1}{2}\sum_{i,\alpha}\left(\frac{\partial\varphi_i}{\partial x_\alpha}\right)^2 = \frac{1}{2}\sum_{i,\alpha}\left[(\rho_0 + \delta\rho)\frac{\partial f_i}{\partial x_\alpha} + \frac{\partial\delta\rho}{\partial x_\alpha}f_i\right]^2$$

$$= \frac{1}{2}(\rho + \delta\rho)^2\sum_{i,\alpha}\left(\frac{\partial f_i}{\partial x_\alpha}\right)^2 + \frac{1}{2}\sum_{\alpha}\left(\frac{\partial\delta\rho}{\partial x_\alpha}\right)^2$$

$$+ (\rho + \delta\rho)\sum_{\alpha}\frac{\partial\delta\rho}{\partial x_\alpha}\sum_{i}f_i\frac{\partial f_i}{\partial x_\alpha}$$

$$= \frac{1}{2} \left[(\rho + \delta\rho)^2 \, (\nabla f)^2 + (\nabla \delta\rho)^2 \right] \tag{2.95}$$

where i goes from 1 to n, α goes from 1 to d, we wrote $(\nabla f)^2 = \sum_{i,\alpha} \left(\frac{\partial f_i}{\partial x_\alpha} \right)^2$ and $(\nabla \delta\rho)^2 = \sum_\alpha \left(\frac{\partial \delta\rho}{\partial x_\alpha} \right)^2$. The third line of the above expression is equal to zero because we can write,

$$\sum_i f_i \frac{\partial f_i}{\partial x_\alpha} = \frac{1}{2} \frac{\partial}{\partial x_\alpha} \sum_i f_i^2 = 0 \tag{2.96}$$

using the (2.93). We can further simplify the expression of the gradient, computing the following,

$$
\begin{aligned}
(\nabla f)^2 &= \sum_{i,\alpha} \left(\frac{\partial f_i}{\partial x_\alpha} \right)^2 = \sum_{i,\alpha} \left(\sum_k \frac{\partial f_i}{\partial \theta_k} \frac{\partial \theta_k}{\partial x_\alpha} \right)^2 = \sum_{i,\alpha,k,q} \frac{\partial f_i}{\partial \theta_k} \frac{\partial \theta_k}{\partial x_\alpha} \frac{\partial f_i}{\partial \theta_q} \frac{\partial \theta_q}{\partial x_\alpha} \\
&= \sum_{\alpha,k,q} \frac{\partial \theta_k}{\partial x_\alpha} \frac{\partial \theta_q}{\partial x_\alpha} \sum_i \frac{\partial f_i}{\partial \theta_k} \frac{\partial f_i}{\partial \theta_q} = \sum_{\alpha,k,q} \frac{\partial \theta_k}{\partial x_\alpha} \frac{\partial \theta_q}{\partial x_\alpha} \delta_{kq} \prod_{l<k} \cos^2(\theta_l) \\
&\simeq \sum_{\alpha,k,q} \frac{\partial \theta_k}{\partial x_\alpha} \frac{\partial \theta_q}{\partial x_\alpha} \delta_{kq} = \sum_{\alpha,k} \left(\frac{\partial \theta_k}{\partial x_\alpha} \right)^2 \\
&= (\nabla \theta)^2 \tag{2.97}
\end{aligned}
$$

that plugged into eq. (2.95) gives some gradient-dependent terms. We made the approximation $\cos(\theta_l) \simeq 1$ because we are in the regime of small fluctuations. One could include higher power of the cosine expansion, but this does not change the final result of the analysis. In the above equation we used the relation,

$$\sum_i \frac{\partial f_i}{\partial \theta_k} \frac{\partial f_i}{\partial \theta_q} = \delta_{kq} \prod_{l<k} \cos^2(\theta_l) \tag{2.98}$$

To verify the above relation, one must use the definition (2.91). When $k = q$ we have,

$$\sum_i \left(\frac{\partial f_i}{\partial \theta_k} \right)^2 = \sum_{i \geq k} \left(\frac{\partial f_i}{\partial \theta_k} \right)^2 \tag{2.99}$$

because for $i < k$ the function f_i does not depend on θ_k. We can compute the above expression starting from the nth component in eq. (2.91) and then going backward up to the kth component. During the calculation we see that due to the property $\cos^2(\theta_i) + \sin^2(\theta_i) = 1$ we obtain,

$$
\begin{aligned}
\sum_{i \geq k} \left(\frac{\partial f_i}{\partial \theta_k} \right)^2 &= \left(\frac{\partial f_n}{\partial \theta_k} \right)^2 + \left(\frac{\partial f_{n-1}}{\partial \theta_k} \right)^2 + \cdots + \left(\frac{\partial f_k}{\partial \theta_k} \right)^2 \\
&= \cos_1^2 \cos_2^2 \ldots \sin_k^2 \ldots \cos_{n-2}^2 \cos_{n-1}^2 \\
&\quad + \cos_1^2 \cos_2^2 \ldots \sin_k^2 \ldots \cos_{n-2}^2 \sin_{n-1}^2 \\
&\quad + \cos_1^2 \cos_2^2 \ldots \sin_k^2 \ldots \sin_{n-2}^2
\end{aligned}
$$

$$\cdots$$
$$+ \cos_1^2 \cos_2^2 \ldots \cos_k^2$$
$$= \cos_1^2 \cos_2^2 \ldots \cos_{k-1}^2 = \prod_{l<k} \cos^2(\theta_l) \qquad (2.100)$$

where $\cos_i = \cos(\theta_i)$. When $k \neq q$ a similar mechanism bears a different result, we have,

$$\sum_{i \geq \max(k,q)} \frac{\partial f_i}{\partial \theta_k} \frac{\partial f_i}{\partial \theta_q} \qquad (2.101)$$

where once again we do not include the f_i for $i < \max(k,q)$ because they do not depend on θ_k or θ_q, if respectively $k > q$ or $k < q$. The above expression can be computed and it gives, if we consider $k > q$,

$$\sum_{i \geq \max(k,q)} \frac{\partial f_i}{\partial \theta_k} \frac{\partial f_i}{\partial \theta_q} = \frac{\partial f_n}{\partial \theta_k} \frac{\partial f_n}{\partial \theta_q} + \frac{\partial f_{n-1}}{\partial \theta_k} \frac{\partial f_{n-1}}{\partial \theta_q} + \cdots + \frac{\partial f_k}{\partial \theta_k} \frac{\partial f_k}{\partial \theta_q}$$
$$= \cos_1^2 \cos_2^2 \ldots (-\sin_q \cos_q) \ldots \cos_p^2 \ldots (-\sin_k \cos_k) \ldots \cos_{n-2}^2 \cos_{n-1}^2$$
$$+ \cos_1^2 \cos_2^2 \ldots (-\sin_q \cos_q) \ldots \cos_p^2 \ldots (-\sin_k \cos_k) \ldots \cos_{n-2}^2 \sin_{n-1}^2$$
$$+ \cos_1^2 \cos_2^2 \ldots (-\sin_q \cos_q) \ldots \cos_p^2 \ldots (-\sin_k \cos_k) \ldots \sin_{n-2}^2$$
$$\cdots$$
$$+ \cos_1^2 \cos_2^2 \ldots (-\sin_q \cos_q) \ldots \cos_p^2 \ldots (\sin_k \cos_k)$$
$$= 0 \qquad (2.102)$$

where $q < p < k$. Putting together the results (2.100) and (2.102) we obtain eq. (2.98). Finally, putting together the homogeneous contribution and the gradient expansion, the Hamiltonian of modulus and phase fluctuations can be written as a free part,

$$\mathcal{H}_0 = \frac{1}{2} \int \mathrm{d}^d r \ \left\{ (\nabla \delta\rho)^2 + \rho_0^2 \left(\nabla\theta\right)^2 + t\delta\rho^2 \right\} \qquad (2.103)$$

and an interaction,

$$\mathcal{H}_I = \int \mathrm{d}^d r \ \left\{ \frac{2\rho_0\delta\rho + \delta\rho^2}{2} (\nabla\theta)^2 + (t\rho_0 + 4u\rho_0)\,\delta\rho + 6u\rho_0\delta\rho^2 + 4u\rho_0\delta\rho^3 + u\delta\rho^4 \right\}$$

$$(2.104)$$

where $(\nabla \delta\rho)^2 = \sum_\alpha \left(\frac{\partial \delta\rho}{\partial x_\alpha}\right)^2$ and $(\nabla\theta)^2 = \sum_{i,\alpha} \left(\frac{\partial \theta_i}{\partial x_\alpha}\right)^2$. From the Hamiltonian (2.103) we see that, at tree level the modulus mode $\delta\rho$ has a mass, that is equal to t while the $n-1$ phase modes are massless (they are the Goldstone modes [52]). Moreover, if we look at the interacting part (2.104), we can see that we cannot produce corrections that involve a phase propagator at zero momentum to the modulus correlation function. The only term that mixes $\delta\rho$ and θ is $(2\rho_0\delta\rho + \delta\rho^2)(\nabla\theta)^2$, but it vanishes at zero momentum, thus it cannot give a contribution to

the modulus connected correlation function at $k = 0$. This means that, contrarily to the longitudinal fluctuations of eq. (2.59), the modulus fluctuations always remain massive i.e. short-range correlated. This is reflected in the free energy that, in the whole symmetry-broken phase, has a positive-curvature minimum in the modulus direction. Given this perspective we can say that the "true" representation of the Goldstone modes are the phase modes [100], while the modulus is the degree of freedom that remains untouched by any transformation belonging to the $O(n)$ group. In the previous setting of longitudinal and transverse fluctuations we find that at bare level the transverse fluctuations coincide with phase ones, but if we compute fluctuations at a more refined level, we find that longitudinal fluctuations too receive a contribution from the phase modes, hence the longitudinal susceptibility is divergent (2.86).

2.4.1 Back to flocks # 3: new physics is needed

Our task is to reproduce the phenomenology of starling flocks, with the simplest model possible. In this chapter we have reviewed the current knowledge about equilibrium models that describe polarized systems to find out if any existent model can achieve the goal.

Focusing on standard $O(n)$ models, we have found that the Goldstone modes (that are phase modes) are responsible for the divergence of longitudinal and transverse susceptibility. Through fluctuation-dissipation relations we can link these divergences with the diverging correlation length of phase fluctuations, hence the orientational scale-free correlations of Fig. 1.6-**a,c** can be reproduced with equilibrium Goldstone modes. We lack an explanation for the scale-free correlations of speed (modulus) fluctuations of Fig. 1.6-**b,d**. The scale-free longitudinal modes receive a contribution from modulus fluctuations, but they are not the cause of the longitudinal susceptibility divergence. In fact, to prove that the longitudinal susceptibility diverges in the symmetry-broken phase we resorted to the "principle of modulus conservation" [93], which tells us quite the opposite: in the symmetry-broken phase modulus fluctuations of a standard $O(n)$ theory are negligible with respect to transverse and longitudinal fluctuations. We also checked what happens to modulus fluctuations by directly computing the Hamiltonian of phase and modulus fluctuations around the Landau minimum and we have seen that the modulus mass term is not corrected by any interaction that involves a phase term. Hence, we conclude that an ordinary $O(n)$ theory cannot produce scale-free correlated modulus (i.e. speed) fluctuations as we have found in biological data of Fig. 1.6-**b,d**.

We must resort to a new idea in order to reproduce the experimental findings. In the next chapter we will introduce a novel model that is capable of doing so, and we will study its properties under different approximations.

2.A   Appendix: the susceptibility and the fluctuation-dissipation relation

In general the susceptibility is a matrix,

$$\chi_{\alpha\beta} = \frac{\partial m_\alpha}{\partial h_\beta} \tag{2.105}$$

that describes how the magnetization component α varies when an external small magnetic field is applied in the direction β. Definition 2.105 can be further generalized, for local magnetization and for a local external field [91] or for non-equilibrium dynamical systems [78], but for simplicity we will assume that the external field acting on our system does not vary in space and we will stick with the definition (2.105). Using the thermodynamic relations between the partition function Z, the Helmoltz free-energy $f(h)$ and the Gibbs free energy $g(m)$ we can write the susceptibility matrix also as [63],

$$\chi_{\alpha\beta} = -\frac{\partial^2 f}{\partial h_\alpha \partial h_\beta} = \left(\frac{\partial^2 g}{\partial m_\alpha \partial m_\beta} \right)^{-1} \tag{2.106}$$

From the definition (2.105) we can derive the fluctuation-dissipation theorem for the susceptibility, given that $m_\alpha = 1/V \int \mathrm{d}^d x \ \langle \varphi_\alpha(\boldsymbol{x}) \rangle$ and that our probability distribution is eq. (2.2) we have,

$$
\begin{aligned}
\chi_{\alpha\beta}\Big|_{h=0} &= \frac{1}{V}\frac{\partial}{\partial h_\beta}\left[\frac{1}{Z}\int \mathrm{D}\boldsymbol{\varphi} \left(\int \mathrm{d}^d x \ \varphi_\alpha(\boldsymbol{x}) \right) \ e^{-\beta\mathcal{H}[\varphi]} \right]\Bigg|_{h=0} \\
&= \frac{\beta}{V}\int \mathrm{d}^d x \ \mathrm{d}^d y \Big[\langle \varphi_\alpha(\boldsymbol{x})\varphi_\beta(\boldsymbol{y}) \rangle - \langle \varphi_\alpha(\boldsymbol{x}) \rangle \langle \varphi_\beta(\boldsymbol{y}) \rangle \Big]\Bigg|_{h=0} \\
&= \beta \int \mathrm{d}^d r \Big[\langle \varphi_\alpha(\boldsymbol{0})\varphi_\beta(\boldsymbol{r}) \rangle - \langle \varphi_\alpha(\boldsymbol{0}) \rangle \langle \varphi_\beta(\boldsymbol{r}) \rangle \Big]\Bigg|_{h=0}
\end{aligned}
\tag{2.107}
$$

where the last passage was possible because our system is homogeneous, hence the connected correlation function in square brackets only depends on the distance vector $\boldsymbol{r}$ between the observables. If the system is also isotropic the connected correlation function in square brackets can be computed using an appropriate adaptation of eq. (1.4), if possible phase averages can be used instead of space averages (see section 1.3.1). This relation links a response function (the susceptibility), in the limit of vanishing external field, with the correlation function of the same observable at zero field. At the critical point, in an infinite system, when the correlation length diverges, so does the susceptibility [91] and we can use the fluctuation-dissipation theorem to find the Fisher relation [14] between critical exponents $\gamma = \nu(2 - \eta)$. Applying these results to a finite-size system, we find that, when a system is scale-free, i.e. when the correlation length of a certain observable scales with the size of the system,

$$\xi \sim L \tag{2.108}$$

we have that the susceptibility of the same observable must scale,

$$\chi \sim \int_0^L \mathrm{d}r \; C(r) \sim \int_0^L \mathrm{d}r \; \frac{g(r/\xi)}{r^{d-2+\eta}} \sim L^{2-\eta} \tag{2.109}$$

where $C(r)$ is the connected correlation function of the analyzed observable, we can write it as a product of a scale-free power law $r^{-d+2-\eta}$ and a scale-dependent part $g(r/\xi)$.

Chapter 3

The Marginal model

In the previous chapters we have seen that natural starling flocks are polarized systems, with average speed around 12 m/s and they show scale-free correlations of full velocity vector fluctuations and of speed fluctuations. We also have revised the $O(n)$ model and we have seen that it can reproduce all the experimental features, except speed's scale-free correlations.

We present now two models: the "pseudo-Gaussian" model [12, 34], a first attempt to reproduce speed scale-free correlations, that has some shortcomings, and the Marginal model which, as we shall see in the next chapters, it will prove to be the solution of the problem [27, 34]. In this chapter I will present the theoretical analysis that I have made of these two model, namely the spin-wave analysis of the pseudo-Gaussian model and the mean-field analysis of the marginal model. We introduce these model using an equilibrium approach, hence we will use on-lattice n-dimensional spins $\boldsymbol{\sigma}_i$ instead of velocities $\boldsymbol{v}_i$. This approach is needed in order to simplify calculations and it is also justified because flocks have been proven to be in a state of local equilibrium [85].

In the next chapter we will promote the spins to velocities and introduce a set of dynamics equations for velocities and positions, then we will compare theoretical results with numerical off-equilibrium simulations and experimental findings. The agreement between off-equilibrium simulations, experiments and our theoretical predictions (see chapter 4) will confirm a posteriori that the equilibrium approximation of this chapter is valid.

3.1 Microscopic models for flocking

In the spirit of Heisenberg spin models [102] we define the Hamiltonian (or cost function) of the model we will present here as,

$$H\left(\{\boldsymbol{\sigma}_i\}\right) = \frac{J}{2} \sum_{i,j} n_{ij} \left(\boldsymbol{\sigma}_i - \boldsymbol{\sigma}_j\right)^2 + \sum_i V(\sigma_i) \tag{3.1}$$

where J is the alignment strength, i, j go from 1 to the number of spins in the system N and n_{ij} is the interaction matrix, which is defined as $n_{ij} = 1$ if i and j are nearest neighbours and $n_{ij} = 0$ otherwise. The nearest-neighbours alignment interaction is sensible, since it resembles the topological imitation mechanism that has been

observed in starling flocks [8]. We stress the fact that in the above Hamiltonian the modulus of every $\boldsymbol{\sigma}_i$ is not fixed, because we are interested in modulus' fluctuations. Each particle's modulus is bounded by a "potential" $V(\sigma_i)$ that acts independently on every particle and it is a function of the spin modulus $\sigma_i = |\boldsymbol{\sigma}_i|$. In this way, configurations with extremely large modulus values are energetically disfavored, just like in a real flock, where the speed of each bird cannot deviate too much from a reference value (for physiological and aerodynamical reasons). For simplicity's sake we consider a cubic lattice, then if we fix on a certain site i, its nearest neighbours will be the $2d$ spins that are directly connected to the site via the cubic lattice links. We define the side of the cubic lattice to be L, such that $N = L^3$.

If we were dealing with an active system, the matrix $n_{ij} = n_{ij}(t)$ would have depended on time, because in natural flocks individuals change their position in space hence nearest neighbours may vary during the time evolution of the system. However, it has been shown in [85] that, due to the large polarization of real flocks, the relaxation time scale of $n_{ij}(t)$ is significantly larger than that of the velocities, so that a quasi-equilibrium approach to the problem is reasonable and it is sound to consider a time-independent n_{ij}. The validity of this approach will be retrospectively confirmed by the remarkable agreement between the predictions of the approximate equilibrium theory derived here and the results from self-propelled particles simulations presented in the next chapter.

In this equilibrium setting, the probability distribution of the spins is the Boltzmann distribution [63],

$$P\left(\{\boldsymbol{\sigma}_i\}\right) = \frac{e^{-\beta H(\{\boldsymbol{\sigma}_i\})}}{Z(\beta)} \tag{3.2}$$

$$Z(\beta) = \int \prod_k \mathrm{d}^n\sigma_k \; e^{-\beta H(\{\boldsymbol{\sigma}_i\})} \tag{3.3}$$

where $\beta = 1/(k_B T)$; we set $k_B = 1$ and all the integrals in $\mathrm{d}^n\sigma_k$ span the whole n-dimensional real space. The interaction term we considered in eq. (3.1) is different from the Heisenberg model's (that is only $\sum_{i,j} n_{ij}\boldsymbol{\sigma}_i \cdot \boldsymbol{\sigma}_j$) because if the modulus fluctuates the correct way to take into account imitation of both orientation and modulus is to use the discrete Laplacian matrix, that is defined for a generic graph as,

$$\Lambda_{ik} = -n_{ik} + \delta_{ik} \sum_j n_{ij} \tag{3.4}$$

and gives,

$$\sum_{i,k} \Lambda_{ik}\boldsymbol{\sigma}_i \cdot \boldsymbol{\sigma}_k = \frac{1}{2} \sum_{i,k} n_{ik}(t)(\boldsymbol{\sigma}_i - \boldsymbol{\sigma}_k)^2 \tag{3.5}$$

in a model were the spins' moduli are fixed (e.g Ising, Heisenberg) the term above is equivalent to the classic interaction term, apart from an additive constant.

3.2 Pseudo-Gaussian model

The pseudo-Gaussian model is defined by the cost function 3.1 with the potential,

$$V(\sigma_i) = g(\sigma_i - 1)^2 \tag{3.6}$$

where the parameter g controls the stiffness of the potential. The Hamiltonian of this model was introduced in [12], where it was derived using a maximum entropy approach [67, 68]. I will now show some of the calculations that were contained in [12] with some new contributions. We will try to understand how the average modulus of the pseudo-Gaussian model changes as a function of the parameter g and as a function of the number of individuals in the system N. Similarly, we will study the modulus correlation length of this model, to capture its dependence on the parameter g, in order to understand when the system becomes scale-free. Our aim is always to reproduce the experimental findings of chapter 4.

3.2.1   Spin-wave approximation and modulus Hamiltonian

In this section I describe how to derive an approximation for the average modulus distribution and for the modulus correlation length. The approximation I am going to use was first applied in [12]. The starting point is the Hamiltonian 3.1 with the pseudo-Gaussian potential 3.6,

$$H(\{\boldsymbol{\sigma}_i\}) = \frac{J}{2} \sum_{i,j} n_{ij} (\boldsymbol{\sigma}_i - \boldsymbol{\sigma}_j)^2 + g \sum_i (\sigma_i - 1)^2 \qquad (3.7)$$

Our aim is to marginalize the (3.2) to get a probability distribution for the average modulus (notice that, although the confining potential is Gaussian, it is so in the *modulus*, hence the model is in fact not Gaussian). It is convenient to rewrite (3.7) in terms of the individual moduli $\sigma_i = |\boldsymbol{\sigma}_i|$ and flight directions $\hat{\boldsymbol{\sigma}}_i = \boldsymbol{\sigma}_i/\sigma_i$. In the deeply ordered phase, one can use the spin-wave approximation (SW) [41], as already done in previous analysis of starling flocks [12, 13]. When the polarization is large (enforced in our model by choosing $J \gg 1$), every spin is very close to the polarization vector. Hence:

$$\boldsymbol{\sigma}_i = \sigma_i \hat{\boldsymbol{\sigma}}_i \qquad \text{with} \quad |\hat{\boldsymbol{\sigma}}_i| = 1 \qquad (3.8)$$

$$\hat{\boldsymbol{\sigma}}_i \simeq \boldsymbol{n} \left(1 - \frac{\pi_i^2}{2} \right) + \boldsymbol{\pi}_i \qquad (3.9)$$

where $\boldsymbol{n}$ is the unit vector along the polarization vector $\boldsymbol{\Phi} = \frac{1}{N} \sum_i \hat{\boldsymbol{\sigma}}_i$, and the $\boldsymbol{\pi}_i$ are the fluctuations orthogonal to $\boldsymbol{n}$. The constraint $\sum_i \boldsymbol{\pi}_i = 0$ holds by construction and, in the high ordered regime, $\pi_i^2 \ll 1$ for every i. The Hamiltonian (3.7) then becomes, up to order π_i^2:

$$H(\{\sigma_i\}, \{\boldsymbol{\pi}_i\}) = J \sum_{i,j} \Lambda_{ij} \sigma_i \sigma_j + g \sum_i (\sigma_i - v_0)^2 + J \sum_{i,j} \tilde{\Lambda}_{ij}(\{\sigma_k\}) \boldsymbol{\pi}_i \cdot \boldsymbol{\pi}_j \ , \quad (3.10)$$

where we defined the matrices:

$$\Lambda_{ij} = -n_{ij} + \delta_{ij} \sum_k n_{ik} \qquad \text{(Discrete Laplacian)} \qquad (3.11)$$

$$\tilde{\Lambda}_{ij}(\{\sigma_k\}) = -n_{ij} \sigma_i \sigma_j + \delta_{ij} \sum_k n_{ik} \sigma_i \sigma_k \qquad (3.12)$$

In terms of the variables $\{\sigma_i\}$ and $\{\boldsymbol{\pi}_i\}$, the probability density (3.2) becomes,

$$P(\{\sigma_i\}, \{\boldsymbol{\pi}_i\}) = \frac{\delta\left(\sum_k \boldsymbol{\pi}_k\right) \prod_i \sigma_i^{n-1} e^{-\beta H}}{\int \mathrm{D}\sigma' \mathrm{D}\boldsymbol{\pi}' \delta\left(\sum_k \boldsymbol{\pi}'_k\right) e^{-\beta H} \prod_i \sigma_i'^{n-1}} \tag{3.13}$$

where $\mathrm{D}\sigma' \equiv \prod_k \mathrm{d}\sigma'_k$, $\mathrm{D}\boldsymbol{\pi}' \equiv \prod_k \mathrm{d}\boldsymbol{\pi}'_k$ and n is the dimension of the spin vector. We now need to integrate out the fluctuations $\boldsymbol{\pi}_i$, to obtain the marginalized distribution of the individual moduli σ_i. Let us define

$$\Omega(\{\sigma_i\}) \equiv \prod_j \sigma_j^{n-1} \int \mathrm{D}\boldsymbol{\pi} \exp\left[-\beta J \sum_{i,j} \tilde{\Lambda}_{ij}(\{v_k\})\boldsymbol{\pi}_i \cdot \boldsymbol{\pi}_j\right] \delta\left(\sum_k \boldsymbol{\pi}_k\right) \tag{3.14}$$

The integral can be easily performed upon a change of integration variables from the $\{\boldsymbol{\pi}_i\}$ to the eigenvectors $\{\tilde{\boldsymbol{\pi}}_\alpha\}$ of the matrix $\tilde{\Lambda}$. Both Λ and $\tilde{\Lambda}$ inherit the translational invariance of the original Hamiltonian and have a constant eigenvector corresponding to a zero mode, since $\sum_j \Lambda_{ij} = \sum_j \tilde{\Lambda}_{ij} = 0$. The constraint on the $\{\boldsymbol{\pi}_i\}$ becomes a constraint on the zero mode, i.e. $\delta(\tilde{\boldsymbol{\pi}}_0)$, making the integral finite and leaving out only $n-1$ eigenvalues. We get

$$\Omega(\{\sigma_i\}) = \left[\prod_j \sigma_j^{n-1}\right] \left[\prod_{\alpha \neq 0} \tilde{\lambda}_\alpha(\{\sigma_k\})\right]^{-\frac{n-1}{2}} \tag{3.15}$$

where the $\{\tilde{\lambda}_\alpha\}$ are the eigenvalues of $\tilde{\Lambda}$ and depend on the $\{\sigma_i\}$ in some complicated way. Since we are interested in the distribution of the average modulus $s = (1/N)\sum_i \sigma_i$, we will now estimate the behaviour of Ω to leading order in s. Once again, it is convenient to make a change of variables, going from real space to the space of the eingenvectors $\{\hat{\sigma}_a\}$ of the discrete Laplacian Λ. Each σ_i can be decomposed into its $\hat{\sigma}_a$ components using the formula $\sigma_i = \sum_a w_i^{(a)} \hat{\sigma}_a$, where $w_i^{(a)}$ is the change of basis matrix. As mentioned above, the zero-mode has constant coefficients $w_i^{(0)} = 1/\sqrt{N}$ and the zero-mode eigenvector is therefore proportional to the mean modulus, i.e. it is exactly $\sqrt{N}s = \left(1/\sqrt{N}\right)\sum_i \sigma_i$. This also implies that for each σ_i we have

$$\sigma_i = s + \delta\sigma_i = s + \sum_{a \neq 0} w_i^{(a)} \hat{\sigma}_a \ . \tag{3.16}$$

We can now express the function Ω, in terms of this new representation

$$\Omega \sim \frac{\prod_j \sigma_j^{n-1}}{\left[\prod_{\alpha \neq 0} \tilde{\lambda}_\alpha(\{\sigma_k\})\right]^{\frac{n-1}{2}}} = \frac{\prod_j \left[s + \sum_{a \neq 0} w_j^{(a)} \hat{\sigma}_a\right]^{n-1}}{f\left(\left\{s + \sum_{a \neq 0} w_k^{(a)} \hat{\sigma}_a\right\}\right)}$$

$$= s^{n-1} \frac{\prod_j \left[1 + \sum_{a \neq 0} \frac{w_j^{(a)} \hat{\sigma}_a}{s}\right]^{n-1}}{f\left(\left\{1 + \sum_{a \neq 0} \frac{w_k^{(a)} \hat{\sigma}_a}{s}\right\}\right)} = s^{n-1} h\left(\left\{1 + \sum_{a \neq 0} \frac{w_k^{(a)} \hat{\sigma}_a}{s}\right\}\right) \ . \tag{3.17}$$

Here h is a generic rational function of its argument. The function f is a generic polynomial of order $(N-1)(n-1)$ in its argument (from dimensional analysis), hence it is safe to extract a $s^{(N-1)(n-1)}$, because s is present in the expansion of every σ_k.

The term Ω describes the contribution to the measure coming from the integration of the directional fluctuations. Once we integrate the directional fluctuations, we have an Hamiltonian that only depends on the moduli $\{\sigma_i\}$. Also in this case, we can express everything in terms of s and the non-zero modes $\{\hat{\sigma}_a\}$ of Λ. Remembering that $\sum_i w_i^{(a)} w_i^{(b)} = \delta_{ab}$, we get:

$$H = J \sum_{i,j} \Lambda_{ij}\sigma_i\sigma_j + g \sum_i (\sigma_i - 1)^2 = \sum_{a=1}^{N}(J\lambda_a + g)\hat{\sigma}_a^2 + gN(s-1)^2 \qquad (3.18)$$

where, with a slight abuse of notation, we still indicate with H the marginalised Hamiltonian depending only on the moduli.

3.2.2 Average modulus distribution

After the manipulations above we obtain the distribution for the average modulus and all the other modes $\hat{\sigma}_a$,

$$P(\{s, \hat{\sigma}_a\}) = \frac{\Omega(\{s, \hat{\sigma}_a\})\ e^{-\beta H}}{\int \mathrm{d}s'\ \mathrm{D}\hat{\sigma}'\ \Omega(\{s', \hat{\sigma}'_b\})\ e^{-\beta H}} \qquad (3.19)$$

with $a \neq 0$ and $\mathrm{D}\hat{\sigma}' \equiv \prod_{b \neq 0} \mathrm{d}\hat{\sigma}'_b$. We can now derive the distribution of the mean modulus $s = \frac{1}{N}\sum_i \sigma_i$ by marginalizing over all the non-zero modes $\hat{\sigma}_a$. To this end, we note that since $\left|w_i^{(a)}\right| < 1$ for every i and a, we have $\hat{\sigma}_a = \sum_i w_i^{(a)}\sigma_i < \sum_i \sigma_i = Ns$. The domain of the variables appearing in (3.19) is therefore:

$$0 \leq s < \infty \qquad (3.20)$$
$$-Ns \leq \hat{\sigma}_a \leq Ns \qquad \text{for } a \neq 0 \qquad (3.21)$$

We then get

$$P(s) = \frac{1}{Z_s}\exp\left[-N\beta g(s-1)^2\right]\int_{-Ns}^{Ns}\mathrm{D}\hat{\sigma}\ \Omega(s, \{\hat{\sigma}_a\})\ \exp\left[-\beta\sum_{a=1}^{N}(J\lambda_a + g)\hat{\sigma}_a^2\right]$$

$$= \frac{1}{Z_s}s^{n-1}\exp\left[-N\beta g(s-1)^2\right] \times$$

$$\times \int_{-Ns}^{Ns}\mathrm{D}\hat{\sigma}\ h\left(\left\{1 + \sum_{a\neq 0}\frac{w_k^{(a)}\hat{\sigma}_a}{s}\right\}\right)\ \exp\left[-\beta\sum_{a=1}^{N}(J\lambda_a + g)\hat{\sigma}_a^2\right] \qquad (3.22)$$

where Z_s is the normalization of the distribution and the integral in $\mathrm{D}\hat{\sigma}$ is over all the non-zero modes. We omitted all the irrelevant constants that cancel out through simplification between the distribution and its normalization. In the approximation where the relative fluctuations of the individual moduli are small, we can expand the

function h appearing in the above expression and compute the remaining Gaussian integral for large values of N. We obtain, at leading order,

$$P(s) = \frac{1}{Z} s^{n-1} \exp\left[-\frac{Ng}{T}(s-1)^2\right] \tag{3.23}$$

which is the probability distribution for the modulus zero mode $s = \frac{1}{N}\sum|\boldsymbol{\sigma}_i|$. This is a *new* result that tells us an important information about the mean value of the spatial average of the modulus. The above distribution can be obtained in a simpler but less rigorous way, explained in appendix 3.A. We stress that the above approximation is quite reasonable in the deeply ordered phase. The quantity $\delta\sigma_i = \sum_{a\neq 0} w_i^{(a)} \hat{\sigma}_a$ indeed represents the fluctuation of the individual modulus with respect to the mean modulus of the system, s, and it must not be confused with the fluctuations of the mean modulus itself. At low noise, when mutual interaction is strong, spins efficiently coordinate both their orientation and modulus so that we expect small individual deviations of both orientation and modulus from their spatial average. On the other hand, if the value of g is small, i.e. the control on the individual moduli is loose, the $\{\sigma_i\}$ can remain coordinated and at the same time strongly fluctuate (e.g. every modulus increases), giving rise to large fluctuations of s, while keeping the relative deviations $\delta\sigma_i$ small.

To get an analytical estimate of the typical modulus, we can compute the maximum of the distribution. By imposing $\frac{\partial P}{\partial s} = 0$ for $n = 3$, we obtain the following equation:

$$s_{typical}^2 - s_{typical} - \frac{T}{Ng} = 0 \tag{3.24}$$

that gives us the expression for the maximum:

$$s_{typical} = \frac{1}{2} + \frac{1}{2}\sqrt{1 + \frac{4T}{Ng}} \tag{3.25}$$

This result shows that the typical modulus is substantially different from the reference value 1 for small N, if g is small. The same happens to the mean of the distribution,

$$\langle s \rangle = \frac{\int\limits_0^\infty \mathrm{d}s \; s^3 \exp\left[-\frac{Ng}{T}(s-1)^2\right]}{\int\limits_0^\infty \mathrm{d}s \; s^2 \exp\left[-\frac{Ng}{T}(s-1)^2\right]} \tag{3.26}$$

which we can see in Fig. 3.1. When N and g are small, the mean modulus $\langle s \rangle$ grows to large values that are very different from the minimum of the pseudo-Gaussian potential $s = 1$. This result makes us think that, if we want the typical (and mean) modulus to be close to 1 for every system, regardless to their size N, the parameter g must be large. This is a *crucial* condition that the pseudo-Gaussian theory must satisfy if we want it to describe real flocks, where for every N the average modulus is around the same value ($\sim 12m/s$), as it is shown in Fig. 1.2-**a**. We wish to draw the reader's attention on the fact that, despite the approximations we used to derive them (in particular the fixed network assumption), the analytical results of this
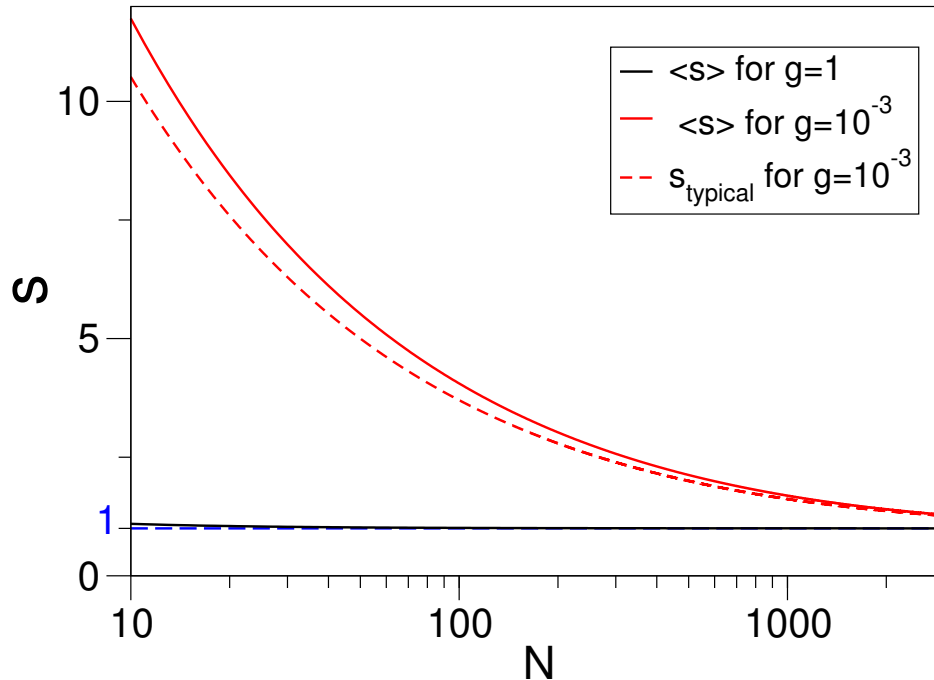
Figure 3.1. Mean and typical value of the modulus distribution. We present the mean value of the modulus distribution of eq. 3.26 (solid lines) for two values of the potential parameter g as functions of the system's number of spins N. We also plot the typical value of the modulus of eq. 3.25 (dashed line) only for the smallest g because, at this scale, for $g = 1$ the typical s is not distinguishable from $\langle s \rangle$. We can see that for small values of N and g the mean modulus and the typical modulus grow up to an order of magnitude above the reference value $s = 1$.

section are in perfect agreement with numerical simulations performed by using an actual self-propelled particle model (see Fig.4.2 of the next chapter). This is not surprising, considering that in the deeply ordered flocking phase the time scale to reshuffle the interaction network is much larger than the time of local relaxation [85].

3.2.3 Modulus correlation length

In the previous section we have computed the distribution of the average modulus; now we will se what condition is required in order to have scale-free correlations of the modulus fluctuations. Starting from the modulus Hamiltonian 3.18, disregarding couplings between moduli and phases and shifting every variable σ_i by 1 we obtain,

$$H = \sum_{i,j} \left[J\Lambda_{ij}\sigma_i\sigma_j + g\delta_{ij}\sigma_i\sigma_j \right] \tag{3.27}$$

In order to have an idea of the modulus correlation length's behaviour with the system's parameters, we imagine to take the limit of continuous space. If our system

lives on a cubic lattice the Hamiltonian then becomes,

$$\mathcal{H} = \int \mathrm{d}\boldsymbol{r} \left[\frac{J}{2} n_c \left(\nabla \sigma(\boldsymbol{r}) \right)^2 + g\sigma^2(\boldsymbol{r}) \right] \tag{3.28}$$

where n_c is the number of nearest neighbours of a spin (in the cubic lattice geometry $n_c = 2d$). If we compute the propagator in the infinite volume limit and then the correlation length we have,

$$G_{mod}(q) \sim \frac{1}{q^2 + \xi_{mod}^{-2}} \tag{3.29}$$

$$\xi_{mod} \sim \sqrt{\frac{Jn_c}{g}} \tag{3.30}$$

that is an approximation in the thermodynamic limit of the bulk modulus correlation length. If we want the system at finite size to display scale-free correlations, i.e. a correlation length that scales with the size of the system, the bulk correlation length must be much greater then the system's size, which means,

$$\xi_{mod} \gg L \tag{3.31}$$

that gives, using eq. 3.30,

$$g \ll \frac{1}{L^2} \tag{3.32}$$

Hence, if we want our system to have scale-free correlations of modulus fluctuations, we conclude that the parameter g must be small such that the bulk correlation length in eq. (3.30) is much greater than the linear size of the system.

3.2.4 Pros and cons of the pseudo-Gaussian model

The pseudo-Gaussian model (or Gaussian for short) can reproduce some key features that we find in experimental data. It has a symmetry-broken phase with scale-free orientational correlations (due to Goldstone modes, see [52, 53] and the previous chapter) and scale-free modulus correlations can be achieved if the stiffness g is small enough.

However, the pseudo-Gaussian model has some shortcomings that we will over-come with the marginal model. First of all, in the thermodynamic limit, the system is scale-free only when $g = 0$, i.e. when the potential vanishes and the energy of the system becomes unbounded. We would prefer a model that is well defined in every phase and that displays scale-free correlations in the infinite-volume limit without incurring into a singular limit like $g \to 0$. This is not a problem for starling flocks, since in those systems we never reach the thermodynamic limit, but if we want a theory that could be generalized to physical systems this is a reasonable requirement. Secondly and most importantly the results we have just shown from the spin-wave approximation for the typical modulus (eq. 3.25) and the modulus correlation length (eq. 3.30) pose an even bigger problem. We see that, in order to achieve a reasonable modulus for any system's size, g must be large enough; on the other hand the scale-free condition forces as to have a small g. Whether this two conflicting conditions can be simultaneously satisfied will be discussed in the next chapter, comparing the results of the pseudo-Gaussian model with experiments.

The $\lambda\phi^4$ model and the pseudo-Gaussian model

The Hamiltonian (3.7) is not analytical, since the potential depends on the modulus $\sigma = \sqrt{\sigma_x^2 + \sigma_y^2 + \sigma_z^2}$; this could be avoided by squaring the modulus and having a potential like,

$$V(\sigma) = (\sigma \cdot \sigma - 1)^2 \tag{3.33}$$

that is essentially the $\lambda\phi^4$ potential of classical Landau-Ginzburg field theory [91]. Several works that study collective behaviour with variable modulus indeed use this kind of potential [40, 42, 55, 88]. Although this may seem a potential genuinely different from the pseudo-Gaussian one that we considered in the previous section (after all, it generates a cubic, rather than linear, modulus-confining force), in fact it is not. In highly polarized and coherent systems individual modulus fluctuations are relatively mild, so that for $\sigma \sim 1$ we can rewrite the potential above as,

$$V(\sigma) = g(\sigma^2 - 1)^2 \simeq 2g(\sigma - 1)^2 + \ldots \tag{3.34}$$

which is nothing else than the harmonic potential that we already took into consideration. Hence, the $\lambda\phi^4$, or standard, theory is not suitable for our purposes, because it has a non-zero quadratic expansion around 1, which gives a non-zero curvature, leading to a saturation of the correlation length, and therefore to a violation of the scale-free phenomenology. Using the potential above we fall once again into the standard $O(n)$ phenomenology described in chapter 2. The only way to avoid this would be to put a vanishing amplitude (i.e. stiffness) g in front of the whole quartic potential; but this is exactly what we do in the pseudo-Gaussian case, and it would give us the same kind of conflicting constraints on g that we have just described. Incidentally, the fact that the pseudo-Gaussian or quadratic theory is essentially identical to the standard $O(n)$ model, shows that that theory is not Gaussian at all in the actual vectorial degrees of freedom, σ.

We have found that with a bounding potential that can be expanded quadratically, be it pseudo-Gaussian (eq. (3.6)) or standard $O(n)$ (eq. (3.33)), we have some difficulties in obtaining both scale-free modulus correlations and an average modulus that does not grow to implausible values for small systems. Hence we introduce in the next section the marginal model and we explain its main features, showing that it can potentially reproduce the phenomenology without any conflict.

3.3 The marginal Hamiltonian

We know that, when a theory has a renormalized potential with a flat direction, fluctuations with respect to the equilibrium value of the order parameter in that direction are scale-free. This phenomenon happens at the critical point for any theory for all the possible directions of the order parameter [14]. It also happens automatically in the symmetry-broken phase of a $O(n)$-symmetric theory [53], but only for the directions that are perpendicular to the equilibrium magnetization (see Fig. 3.2-**a**). In order to have a flat modulus direction in the symmetry-broken phase we can use a flat-minimum single-particle potential that, deep in the ordered phase where the entropy is negligible, is the main contribution to the renormalized
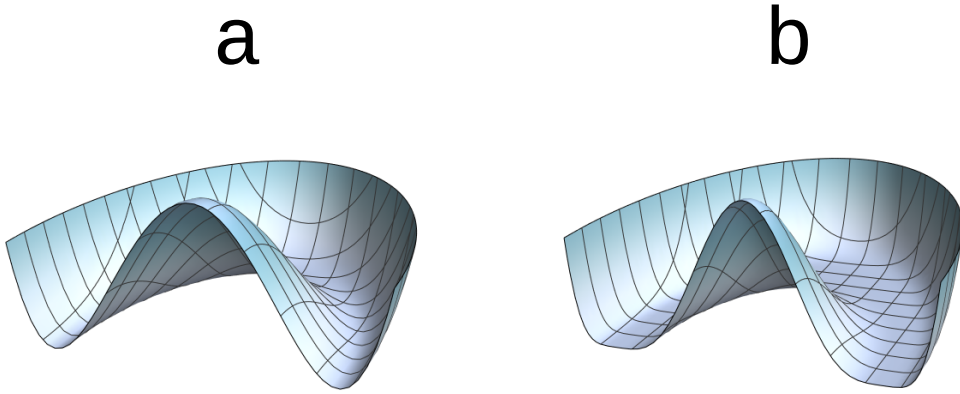
Figure 3.2. Potentials for $n = 2$**, in the polarized phase. a**: Standard $O(2)$ potential
with a flat angular direction and a non-vanishing mass in the modulus direction. **b**:
Marginal potential in $n = 2$, both modulus and phase directions are flat (or marginal).

potential (i.e. the free energy). With this choice, for $T \to 0$ (i.e. decreasing variance
of the noise), we obtain both high polarization and a flat-minimum free energy
that ensures scale-free modulus correlations (see Fig. 3.2-**b**). In order to select the
simplest flat-minimum potential we can guess its form by writing a generic analytic
$O(n)$-symmetric potential with a non-vanishing minimum value,

$$V(\sigma) = \left(\sigma^2 - 1\right)^p \tag{3.35}$$

where p is an even number, otherwise the potential does not have an absolute
minimum and it does not bound the modulus value. We immediately see that for
$p = 2$ we recover the standard $O(n)$ theory of eq. (3.33), with a potential shaped
as in Fig. 3.2-**a**. On the other hand, for $p = 4$ we have a $O(n)$-symmetric theory
that has a vanishing second (and third) derivative in its minimum, the first nonzero
contribution for a small displacement around the minimum is quartic, just what
we expect from a potential of the shape such as Fig. 3.2-**b**. Hence the microscopic
Hamiltonian of our model will be,

$$H(\{\boldsymbol{\sigma}_i\}) = \frac{J}{2} \sum_{i,j} n_{ij}(\boldsymbol{\sigma}_i - \boldsymbol{\sigma}_j)^2 + \lambda \sum_i (\sigma_i^2 - 1)^4 \tag{3.36}$$

where the parameter λ controls the strength of the potential. We call this model
"marginal" due to the fact that the minimum of its potential is marginal, in the sense
that it has a zero curvature minimum that is flat in every direction. For a different
derivation of the marginal potential, see appendix 3.B.

3.3.1   Mean-field approximation

In order to investigate whether marginal model's free energy, for vanishing tempera-
ture, resembles the flat-minimum shape of Fig. 3.2-**b** I performed the fully-connected
mean-field approximation of the marginal model. I will report here all the main
passages of the calculations I made for a generic model with an arbitrary number

of spin components n, while in [27] the results only for $n = 1$ are reported. We abandon the regular cubic lattice and we link every spin with all the other $N - 1$ spins in the system, i.e. $n_{ij} = 1$ for every i, j. The mean-field Hamiltonian is,

$$H\left(\{\boldsymbol{\sigma}_i\}\right) = \frac{J}{2N} \sum_{i,j} \left(\boldsymbol{\sigma}_i - \boldsymbol{\sigma}_j\right)^2 + \sum_i V(\sigma_i)$$

$$= -\frac{J}{N} \sum_{i,j} \boldsymbol{\sigma}_i \cdot \boldsymbol{\sigma}_j + \sum_i W(\sigma_i)$$

$$= -\frac{J}{N} \left(\sum_i \boldsymbol{\sigma}_i\right)^2 + \sum_i W(\sigma_i) \tag{3.37}$$

$$W(\sigma_i) \equiv J\sigma^2 + V(\sigma) \tag{3.38}$$

where we changed the interaction strength $J \to J/N$, in order to have an extensive Hamiltonian. We wrote a generic potential $V(\sigma)$ so that we can substitute in the end of the calculation the marginal expression 3.154 or any other potential, in order to make comparisons. To compute the Gibbs free energy we start from the partition function $Z(\beta)$,

$$Z(\beta) = \int \mathrm{D}\sigma \; e^{-\beta H} = \int \mathrm{D}\sigma \; e^{-\beta H} \int \mathrm{d}^n m \; \delta^n \left(\boldsymbol{m} - \frac{1}{N} \sum_i \boldsymbol{\sigma}_i\right)$$

$$= \int \mathrm{d}^n m \left[\int \mathrm{D}\sigma \; \delta^n \left(\boldsymbol{m} - \frac{1}{N} \sum_i \boldsymbol{\sigma}_i\right) e^{-\beta H}\right]$$

$$= \int \mathrm{d}^n m \; e^{-\beta N g(m)} \tag{3.39}$$

hence we have (disregarding irrelevant constants),

$$g(m) = -\frac{1}{\beta N} \log \int \mathrm{D}\sigma \; \delta^n \left(N\beta\boldsymbol{m} - \beta \sum_i \boldsymbol{\sigma}_i\right) e^{-\beta H} \tag{3.40}$$

where $\mathrm{D}\sigma = \prod_k \mathrm{d}^n \sigma_k$ and $g(m)$ is the intensive Gibbs free energy. Even if it is not evident from the equation above, we know that the Gibbs free energy depends only on the modulus of its variable $\boldsymbol{m}$, because the Hamiltonian (3.37) is $O(n)$-symmetric. If we plug into the above expression the mean-field Hamiltonian (3.37) we obtain (writing $m = |\boldsymbol{m}|$ and $\sigma_i = |\boldsymbol{\sigma}_i|$),

$$g(m) = -\frac{1}{\beta N} \log \int \mathrm{D}\sigma \; \delta^n \left(N\beta\boldsymbol{m} - \beta \sum_i \boldsymbol{\sigma}_i\right) \exp\left\{\frac{\beta J}{N} \left(\sum_i \boldsymbol{\sigma}_i\right)^2 - \beta \sum_i W(\sigma_i)\right\}$$

$$= -\frac{1}{\beta N} \log \left[e^{\beta N J m^2} \int \mathrm{D}\sigma \; \delta^n \left(N\beta\boldsymbol{m} - \beta \sum_i \boldsymbol{\sigma}_i\right) e^{-\beta \sum_i W(\sigma_i)}\right]$$

$$= -Jm^2 - \frac{1}{\beta N} \log \left[\int \mathrm{D}\sigma \int_{-i\infty}^{+i\infty} \mathrm{d}^n x \; \exp\left\{\beta N \boldsymbol{m} \cdot \boldsymbol{x} - \beta \boldsymbol{x} \cdot \sum_i \boldsymbol{\sigma}_i - \beta \sum_i W(\sigma_i)\right\}\right]$$

$$= -Jm^2 - \frac{1}{\beta N} \log \left[\int \mathrm{d}^n x \; e^{\beta N \boldsymbol{m} \cdot \boldsymbol{x}} \left(\int \mathrm{d}^n \sigma \exp\left\{-\beta \boldsymbol{\sigma} \cdot \boldsymbol{x} - \beta W(\sigma)\right\}\right)^N\right]$$

$$= -Jm^2 - \frac{1}{\beta N} \log\left[\int \mathrm{d}^n x\ e^{NS(\boldsymbol{x}, \boldsymbol{m})}\right] \tag{3.41}$$

$$S(\boldsymbol{x}, \boldsymbol{m}) = \beta \boldsymbol{m} \cdot \boldsymbol{x} + \log\left[\int \mathrm{d}^n \sigma e^{-\beta(\boldsymbol{\sigma} \cdot \boldsymbol{x} + W(\sigma))}\right] \tag{3.42}$$

where we express the δ-function using its integral form,

$$\delta^n(\boldsymbol{y}) \sim \int\limits_{-i\infty}^{+i\infty} \mathrm{d}^n x\ e^{-\boldsymbol{x} \cdot \boldsymbol{y}} \tag{3.43}$$

Since we want to investigate the critical properties of this theory, we perform the thermodynamic limit $N \to \infty$. This implies that we can solve the above integral in $\mathrm{d}^n x$ using the saddle point method, using N as a large parameter, disregarding corrections for finite N. The saddle point equation for the saddle point $\boldsymbol{x}_0$ is,

$$\left.\frac{\partial S}{\partial \boldsymbol{x}}\right|_{\boldsymbol{x} = \boldsymbol{x}_0} = 0 \tag{3.44}$$

which gives,

$$\boldsymbol{m} = \frac{\int \mathrm{d}^n \sigma \boldsymbol{\sigma} \exp\left\{-\beta(\boldsymbol{\sigma} \cdot \boldsymbol{x}_0 + W(\sigma))\right\}}{\int \mathrm{d}^n \sigma \exp\left\{-\beta(\boldsymbol{\sigma} \cdot \boldsymbol{x}_0 + W(\sigma))\right\}} \tag{3.45}$$

that is the equation that links the Gibbs free energy variable $\boldsymbol{m}$ with the saddle point value $\boldsymbol{x}_0$. Performing the integral in eq. (3.41) using the saddle point expression $S(\boldsymbol{x}_0, \boldsymbol{m})$ we can write the mean-field Gibbs free energy in the thermodynamic limit,

$$g(m) = -Jm^2 - \boldsymbol{m} \cdot \boldsymbol{x}_0 - \frac{1}{\beta} \log \int \mathrm{d}^n \sigma \exp\left\{-\beta(\boldsymbol{\sigma} \cdot \boldsymbol{x}_0 + W(\sigma))\right\} \tag{3.46}$$

We can compute numerically the above expression for any temperature (that is, any β) to have an idea of the free energy's shape when the temperature goes to zero. We can find the result for $n = 3$ in Fig. 3.3, where we compare the expression above with the free energy of a standard $O(n)$ model (we simply use a quadratic-minimum potential $V = (\sigma^2 - 1)^2$). As we can see from the figure, the marginal model exhibits a flat minimum both at the standard critical temperature T_c common to the $O(n)$ model, and for $T = 0$. On the other hand the standard $O(n)$ model has a positive curvature for vanishing T. If the Gibbs free energy's minimum is truly flat in the modulus direction (i.e. it has a zero second and third derivative), the model has scale-free correlations of all its degrees of freedom, both phase and modulus, thus reproducing the experimental findings in starling flocks.

3.3.2   Low-temperature expansion

In order to compute the curvature of the free energy's minimum of Fig. 3.3 we perform a low-temperature expansion of the Gibbs free energy of eq. (3.46). The expansion consists in evaluating the integrals in $\mathrm{d}^n \sigma$ of eq.s (3.45) and (3.46) using the saddle point method, for $\beta \to \infty$. This time, since we are interested in the behaviour for vanishing T we will not stop at leading order, but we will compute the
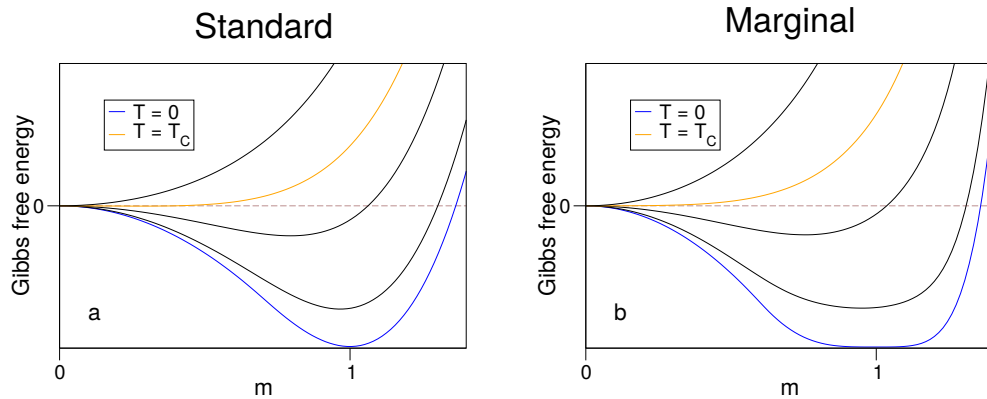
Figure 3.3. Mean-field Gibbs free energy for $n = 3$, as function of its variable m, for some temperature values. a: Standard $O(n)$ model with a bare potential $V = (\sigma^2 - 1)^2$. The Gibbs free energy becomes flat for a certain critical temperature T_c, when all the degrees of freedom of the order parameter become scale-free. For $T = 0$ the curvature in the minimum is finite. **b**: Marginal model with a bare potential $V = (\sigma^2 - 1)^4$. The Gibbs free energy becomes flat for a certain critical temperature T_c, when all the degrees of freedom of the order parameter become scale-free. For $T = 0$ too the curvature in the minimum becomes zero, suggesting the same phenomenology as the finite critical temperature.

corrections to the free energy up to T^2. The saddle point equation for the integrals of eq.s (3.45) and (3.46) is the same and it defines the saddle point value $\boldsymbol{\sigma}_0$,

$$\boldsymbol{x}_0 + \frac{\partial W}{\partial \boldsymbol{\sigma}}\bigg|_{\boldsymbol{\sigma} = \boldsymbol{\sigma}_0} = 0 \tag{3.47}$$

that links the value $\boldsymbol{x}_0$ from the previous saddle point for large N with the value of the saddle point for small temperature $\boldsymbol{\sigma}_0$.

Now we make use of the system's symmetries, in order to simplify our calculations; from eq. (3.46) we see that, due to the fact that the free energy depends only on the modulus of $\boldsymbol{m}$, $\boldsymbol{m}$ and $\boldsymbol{x}_0$ must be parallel. Furthermore, from eq. (3.45) we see that also $\boldsymbol{\sigma}_0$ must be parallel to $\boldsymbol{m}$, otherwise the integral on the numerator would vanish. Noticing these properties we can write, without loss of generality,

$$\boldsymbol{m} = m\hat{\boldsymbol{n}} \qquad \boldsymbol{\sigma}_0 = \sigma_0\hat{\boldsymbol{n}} \qquad \boldsymbol{x}_0 = x_0\hat{\boldsymbol{n}} \tag{3.48}$$

where $\hat{\boldsymbol{n}}$ is a unit vector. This simplification will help us reducing many relations between vectors into simpler scalar equations.

In order to have an explicit expression in m for the free energy of eq. (3.46) we have to expand eq. (3.45) and use eq. (3.47) in order to express both σ_0 and x_0 as functions of m; this procedure will be simplified by using eq. (3.48). Then we have to plug the expressions of $\sigma_0(m)$ and $x_0(m)$ into eq. (3.46) and solve the integral in $\mathrm{d}^n\sigma$. In the end we will obtain the $g(m)$ as an expansion with a term for $T = 0$ and corrections of order T and T^2. Expanding eq. (3.45) for large β, we expect to find an expression for σ_0 of this form,

$$\sigma_0 = m + TA_m + T^2B_m \tag{3.49}$$

where A_m and B_m are two functions of m that we will compute later. If we plug the above expression into eq. (3.47) we find for x_0,

$$x_0 = -W'_{\sigma_0} = -W'(m + TA_m + T^2 B_m)$$

$$\simeq -W'_m - TW''_m A_m - T^2 \left[W''_m B_m + \frac{1}{2} W'''_m A_m^2 \right] \tag{3.50}$$

where f' indicates the first derivative of the function f with respect to its argument and f_m indicates that the argument of the function is m. From now on we will indicate ordinary derivatives with superscripts f', f'', f''', etc. and the argument of functions either with subscripts f_m, f_{σ_0}, etc.. or with brackets $f(m), f(\sigma_0)$. Greek letters in subscripts will indicate derivation with respect to a certain component, i.e. $f_{\alpha\beta}(x) = \frac{\partial^2 f}{\partial x_\alpha \partial x_\beta}$. In order to find an expression for the Gibbs free energy we need to perform the integral of eq. (3.46), that will have a form like,

$$\int \mathrm{d}^n \sigma \exp \left\{ -\beta(\sigma_1 x_0 + W(\sigma)) \right\}$$

$$\simeq \exp \left\{ -\beta(\sigma_0 x_0 + W_{\sigma_0}) \right\} \left(\det W_{\mu\nu}(\sigma_0) \right)^{-1/2} (1 + TC_{\sigma_0}) \tag{3.51}$$

where we used the saddle point method to approximate the integral. $W_{\mu\nu}$ is the Hessian matrix of the function W and C is the first correction to the Gaussian approximation of the integral, which will be computed later. We now put together eq.s (3.49), (3.50) and (3.51) and we use them to expand eq. (3.46) as a function of m, up to order T^2,

$$g(m) \simeq -Jm^2 - x_0 m - T \log \left[\exp \left\{ -\beta(\sigma_0 x_0 + W_{\sigma_0}) \right\} \left(\det W_{\mu\nu}(\sigma_0) \right)^{-1/2} (1 + TC_{\sigma_0}) \right]$$

$$= -Jm^2 - x_0 m + W_{\sigma_0} + x_0 \sigma_0 + \frac{T}{2} \log \left[\det W_{\mu\nu}(\sigma_0) \right] - T \log \left(1 + TC_{\sigma_0} \right)$$

$$\simeq -Jm^2 - x_0 m + W(m + TA_m + T^2 B_m) + x_0 \cdot (m + TA_m + T^2 B_m) +$$

$$+ \frac{T}{2} \log \left[\det W_{\mu\nu}(m + TA_m) \right] - T \log(1 + TC_m)$$

$$\simeq -Jm^2 + W_m + TW'_m A_m + T^2 W'_m B_m + \frac{T^2}{2} W''_m A_m^2 - T(W'_m + TW'' A_m) \cdot$$

$$\cdot (A_m + TB_m) + \frac{T}{2} \log(\det W_{\mu\nu}(m)) + \frac{T^2}{2} \frac{A_m (\det W_{\mu\nu}(m))'}{\det W_{\mu\nu}(m)} - T^2 C_m$$

$$= \lambda V_m + \frac{T}{2} \log(\det W_{\mu\nu}(m)) + T^2 \left[\frac{A_m (\det W_{\mu\nu}(m))'}{2 \det W_{\mu\nu}(m)} - C_m - \frac{W''_m A_m^2}{2} \right] \tag{3.52}$$

From the equation above we see that we do not need to compute the term B_m from the expansion (3.49), since it disappears from the final expression of $g(m)$. Before computing the needed terms, we stress the fact that in the limit of $T \to 0$ the mean-field low-temperature free energy (3.52) simplifies to the bare potential, that in the case of the marginal model means $g(m) \simeq V_m = \lambda(m^2 - 1)^4$. This implies that even at mean field level, i.e. disregarding fluctuations, the marginal model's free energy develops a zero-curvature minimum in the modulus direction, when the temperature drops to zero. This result suggests that in a finite-dimensional system with short-ranged interactions, for low enough temperature, the modulus' fluctuations will develop scale-free correlations.

3.3.3 Expanding the integrals for low temperature

We now compute explicitly all the terms of the above expansion, in order to calculate the behaviour of the equilibrium magnetization and of susceptibilities as functions of the temperature. For practical purposes we fix the direction of the unit vector $\hat{n}$ to be along the first axis.

Determinant of $W_{\mu\nu}$ and its derivative

The Hessian matrix $W_{\mu\nu}(m)$ is,

$$
\begin{aligned}
W_{\mu\nu}(m) &= \frac{\partial^2 W}{\partial m_\mu \partial m_\nu} = \frac{\partial}{\partial m_\mu}\left(\frac{m_\nu}{m}W'\right) \\
&= \left(\delta_{\mu\nu} - \frac{m_\mu m_\nu}{m^2}\right)\frac{W'}{m} + \frac{m_\mu m_\nu}{m^2}W''
\end{aligned}
\tag{3.53}
$$

which means that $W_{\mu\nu}$ is diagonal and it gives W'' in the direction of $\hat{n}$ and W'/m in the other orthogonal directions. The determinant is easily computed,

$$
\det W_{\mu\nu} = W''\left(\frac{W'}{m}\right)^{n-1}
\tag{3.54}
$$

and also its derivative,

$$
(\det W_{\mu\nu})' = W'''\left(\frac{W'}{m}\right)^{n-1} + (n-1)\frac{(W'')^2(W')^{n-2}}{m^{n-1}} - (n-1)\frac{W''(W')^{n-1}}{m^n}
\tag{3.55}
$$

Using eq. (3.54) we can express the term of order T in eq. (3.52), that is,

$$
\begin{aligned}
\frac{T}{2}\log\left(\det W_{\mu\nu}\right) &= \frac{T}{2}\left[\log(W'') + (n-1)\log\left(\frac{W'}{m}\right)\right] \\
&= \frac{T}{2}\left[\log(2J + V'') + (n-1)\log\left(2J + \frac{V'}{m}\right)\right]
\end{aligned}
\tag{3.56}
$$

where we can see that the second term in square brackets vanishes for a scalar order parameter, i.e. when $n = 1$. The determinant derivative in eq. (3.55) will be useful for the order T^2 term in eq. (3.52), but first we need to compute the other terms from the expansion of the σ integrals in eq. (3.45) and (3.46).

A_m and C_m

From eq. (3.45) and (3.48) we have,

$$
m = \frac{\displaystyle\int d^n\sigma\, \sigma_1 \exp\left\{-\beta(\sigma_1 x_0 + W(\sigma))\right\}}{\displaystyle\int d^n\sigma \exp\left\{-\beta(\sigma_1 x_0 + W(\sigma))\right\}}
\tag{3.57}
$$

We will now expand the above equation using the saddle point method. We will expand up to order T (or β^{-1}) both the numerator and the denominator, because

the latter is none other than the integral in eq. (3.46) that also needs to be computed in order to obtain the term C_m. After defining the quantity $\delta\sigma_\mu = \sigma_m u - \sigma_{0\mu}$, we can expand the exponential's argument above,

$$
m \simeq \frac{\int d^n\sigma \ \sigma_1 \exp\left(-\beta\frac{W_{\mu\nu}}{2}\big|_{\sigma_o}\delta\sigma_\mu\delta\sigma_\nu - \beta\frac{W_{\mu\nu\alpha}}{6}\big|_{\sigma_o}\delta\sigma_\mu\delta\sigma_\nu\delta\sigma_\alpha - \beta\frac{W_{\mu\nu\alpha\gamma}}{24}\big|_{\sigma_o}\delta\sigma_\mu\delta\sigma_\nu\delta\sigma_\alpha\delta\sigma_\gamma + \dots\right)}{\int d^n\sigma \ \exp\left(-\beta\frac{W_{\mu\nu}}{2}\big|_{\sigma_o}\delta\sigma_\mu\delta\sigma_\nu - \beta\frac{W_{\mu\nu\alpha}}{6}\big|_{\sigma_o}\delta\sigma_\mu\delta\sigma_\nu\delta\sigma_\alpha - \beta\frac{W_{\mu\nu\alpha\gamma}}{24}\big|_{\sigma_o}\delta\sigma_\mu\delta\sigma_\nu\delta\sigma_\alpha\delta\sigma_\gamma + \dots\right)}
$$

$$(3.58)$$

where we are implying the sum over repeated indices. Performing the change of variable $y_\mu = \sqrt{\beta}\delta\sigma_\mu$ we obtain,

$$
m \simeq \frac{\int d^n y \ \left(\frac{y_1}{\sqrt{\beta}} + \sigma_0\right)\exp\left(-\frac{W_{\mu\nu}}{2}\big|_{\sigma_o}y_\mu y_\nu - \frac{W_{\mu\nu\alpha}}{6\beta^{1/2}}\big|_{\sigma_o}y_\mu y_\nu y_\alpha - \frac{W_{\mu\nu\alpha\gamma}}{24\beta}\big|_{\sigma_o}y_\mu y_\nu y_\alpha y_\gamma\right)}{\int d^n y \ \exp\left(-\frac{W_{\mu\nu}}{2}\big|_{\sigma_o}y_\mu y_\nu - \frac{W_{\mu\nu\alpha}}{6\beta^{1/2}}\big|_{\sigma_o}y_\mu y_\nu y_\alpha - \frac{W_{\mu\nu\alpha\gamma}}{24\beta}\big|_{\sigma_o}y_\mu y_\nu y_\alpha y_\gamma\right)}
$$

$$
\simeq \sigma_0 + T^{1/2}\frac{\int d^n y \ y_1 e^{-\frac{W_{\mu\nu}}{2}\big|_{\sigma_o}y_\mu y_\nu}\left[1 - T^{1/2}\frac{W_{\mu\nu\alpha}}{6}\big|_{\sigma_o}y_\mu y_\nu y_\alpha - T\frac{W_{\mu\nu\alpha\gamma}}{24}\big|_{\sigma_o}y_\mu y_\nu y_\alpha y_\gamma +\right.}{\int d^n y \ e^{-\frac{W_{\mu\nu}}{2}\big|_{\sigma_o}y_\mu y_\nu}\left[1 - T^{1/2}\frac{W_{\mu\nu\alpha}}{6}\big|_{\sigma_o}y_\mu y_\nu y_\alpha - T\frac{W_{\mu\nu\alpha\gamma}}{24}\big|_{\sigma_o}y_\mu y_\nu y_\alpha y_\gamma +\right.}
$$

$$
\frac{\left. +\frac{1}{2}\left(T^{1/2}\frac{W_{\mu\nu\alpha}}{6}\big|_{\sigma_o}y_\mu y_\nu y_\alpha + T\frac{W_{\mu\nu\alpha\gamma}}{24}\big|_{\sigma_o}y_\mu y_\nu y_\alpha y_\gamma\right)^2 + \dots\right]}{\left. +\frac{1}{2}\left(T^{1/2}\frac{W_{\mu\nu\alpha}}{6}\big|_{\sigma_o}y_\mu y_\nu y_\alpha + T\frac{W_{\mu\nu\alpha\gamma}}{24}\big|_{\sigma_o}y_\mu y_\nu y_\alpha y_\gamma\right)^2 + \dots\right]}
$$

$$
\simeq \sigma_0 + T\frac{-\frac{W_{\mu\nu\alpha}}{6}\big|_{\sigma_o}\langle y_1 y_\mu y_\nu y_\alpha\rangle_G + O(T)}{1 + T\left[\frac{W_{\mu\nu\alpha}W_{\mu'\nu'\alpha'}}{72}\big|_{\sigma_o}\langle y_\mu y_\nu y_\alpha y_{\mu'} y_{\nu'} y_{\alpha'}\rangle_G - \frac{W_{\mu\nu\alpha\gamma}}{24}\big|_{\sigma_o}\langle y_\mu y_\nu y_\alpha y_\gamma\rangle_G\right] + O(T^2)}
$$

$$(3.59)$$

where the Gaussian average $\langle\cdot\rangle_G$ is made with the measure $d^n y \ e^{-\frac{W_{\mu\nu}}{2}\big|_{\sigma_o}y_\mu y_\nu}$, which means that we have,

$$
\langle y_\mu\rangle_G = 0
$$
$$
\langle y_{\mu 1} y_{\mu 2} \dots y_{\mu p}\rangle_G = 0 \qquad \text{for } p \text{ odd}
$$
$$
\langle y_\mu y_\nu\rangle_G = [W_{\mu\nu}]^{-1}\big|_{\sigma_0} = \begin{cases} (W''_{\sigma_0})^{-1} & \text{for } \mu = \nu = 1 \\ \sigma_0/W'_{\sigma_0} & \text{for } \mu = \nu \neq 1 \\ 0 & \text{otherwise} \end{cases}
$$
$$
\langle y_{\mu 1} y_{\mu 2} \dots y_{\mu p}\rangle_G = \langle y_{\mu 1} y_{\mu 2}\rangle_G \dots \left\langle y_{\mu(p-1)} y_{\mu p}\right\rangle_G + \text{permutations} \qquad \text{for } p \text{ even}
$$

$$(3.60)$$

where we easily computed the inverse of the matrix $W_{\mu\nu}$ because it is diagonal (see eq. (3.53)) and we can compute any product of an even number of variables via Wick's theorem [121]. We remark that in eq. (3.59) we already omitted the averages

with an odd number of variables, due to the rules of (3.60). If we approximate eq. (3.59) up to order T we can compute the function A_m (defined in eq. (3.49)),

$$m \simeq \sigma_0 - T \frac{W_{\mu\nu\alpha}}{6} \bigg|_{\sigma_0} \langle y_1 y_\mu y_\nu y_\alpha \rangle_G$$

$$\sigma_0 \simeq m + T \frac{W_{\mu\nu\alpha}}{6} \bigg|_m \langle y_1 y_\mu y_\nu y_\alpha \rangle_G \, (\sigma_0 = m)$$

$$A_m = \frac{W_{\mu\nu\alpha}(m)}{6} \langle y_1 y_\mu y_\nu y_\alpha \rangle_G \, (m) \tag{3.61}$$

To compute the above expression we need to find the expression of $W_{\mu\nu\alpha}$, we do it taking the derivative of $W_{\mu\nu}$ of eq. (3.53),

$$W_{\mu\nu\alpha}(m) = \frac{\partial W_{\mu\nu}(m)}{\partial m_\alpha} = \frac{\partial}{\partial m_\alpha} \left[\left(\delta_{\mu\nu} - \frac{m_\mu m_\nu}{m^2} \right) \frac{W'_m}{m} + \frac{m_\mu m_\nu}{m^2} W''_m \right]$$

$$= (\delta_{\mu\nu} m_\alpha + \delta_{\mu\alpha} m_\nu + \delta_{\nu\alpha} m_\mu) \frac{1}{m^2} \left(V''_m - \frac{V'_m}{m} \right) +$$

$$+ \frac{m_\mu m_\nu m_\alpha}{m^3} \left(3 \frac{V'_m}{m^2} - 3 \frac{V''_m}{m} + V'''_m \right) \tag{3.62}$$

looking at eq. (3.61), the rules from (3.60) and the equation above we understand that only some combinations of indices give nonzero contribution to A_m. We have,

$$A_m = \frac{1}{6} \left[W_{111} \langle y_1 y_1 y_1 y_1 \rangle_G + 3 \sum_{\mu \neq 1} W_{\mu\mu 1} \langle y_1 y_1 y_\mu y_\mu \rangle_G \right]$$

$$= \frac{1}{2} \frac{V'''_m}{(2J + V''_m)^2} + (n-1) \frac{V''_m - V'_m/m}{2m(2J + V''_m)(2J + V'_m/m)} \tag{3.63}$$

that is a term needed for the order T^2 correction to the free energy in eq. (3.52). In order to compute the last part that we need, the term C_m, we notice that its definition from eq. (3.51) coincides with the denominator of eq. (3.57), hence using the denominator of (3.59) we can identify,

$$C_m = \frac{W_{\mu\nu\alpha} W_{\mu'\nu'\alpha'}}{72} \bigg|_m \langle y_\mu y_\nu y_\alpha y_{\mu'} y_{\nu'} y_{\alpha'} \rangle_G \, (m) - \frac{W_{\mu\nu\alpha\gamma}}{24} \bigg|_m \langle y_\mu y_\nu y_\alpha y_\gamma \rangle_G \, (m) \tag{3.64}$$

We can compute the first part of C_m using the expression (3.62), remembering the rules (3.60),

$$\frac{W_{\mu\nu\alpha} W_{\mu'\nu'\alpha'}}{72} \bigg|_m \langle y_\mu y_\nu y_\alpha y_{\mu'} y_{\nu'} y_{\alpha'} \rangle_G \, (m) = \frac{1}{72} \left[W_{111} W_{111} \langle y_1 y_1 y_1 y_1 y_1 y_1 \rangle_G + \right.$$

$$\left. + 6 W_{111} \sum_{\mu \neq 1} W_{\mu\mu 1} \langle y_1 y_1 y_1 y_1 y_\mu y_\mu \rangle_G + 9 \sum_{\mu \neq 1, \nu \neq 1} W_{\mu\mu 1} W_{\nu\nu 1} \langle y_1 y_1 y_\nu y_\nu y_\mu y_\mu \rangle_G \right]$$

$$= \frac{5}{24} \frac{(V'''_m)^2}{(2J + V''_m)^3} + \frac{n-1}{4} \frac{V'''_m (V''_m - V'_m/m)}{m(2J + V''_m)^2 (2J + V'_m/m)} +$$

$$+ \frac{(n-1)(n+2)}{8} \frac{(V_m'' - V_m'/m)^2}{m^2(2J + V_m'')(2J + V_m'/m)^2} \tag{3.65}$$

To this expression, we have to add the second term of the expression (3.64), hence we need to compute the fourth derivatives of W, using eq. (3.62),

$$W_{\mu\nu\alpha\gamma} = \frac{\partial W_{\mu\nu\alpha}}{\partial m_\gamma} = \frac{\partial}{\partial m_\gamma} \Bigg[(\delta_{\mu\nu} m_\alpha + \delta_{\mu\alpha} m_\nu + \delta_{\nu\alpha} m_\mu) \frac{1}{m^2} \left(V_m'' - \frac{V_m'}{m} \right) +$$

$$+ \frac{m_\mu m_\nu m_\alpha}{m^3} \left(3\frac{V_m'}{m^2} - 3\frac{V_m''}{m} + V_m''' \right) \Bigg]$$

$$= (\delta_{\mu\nu}\delta_{\alpha\gamma} + \delta_{\mu\alpha}\delta_{\nu\gamma} + \delta_{\mu\gamma}\delta_{\nu\alpha}) \frac{1}{m^2} \left(V_m'' - \frac{V_m'}{m} \right) + (\delta_{\mu\nu} m_\alpha m_\gamma + \delta_{\mu\alpha} m_\nu m_\gamma + \delta_{\mu\gamma} m_\nu m_\alpha +$$

$$+ \delta_{\nu\alpha} m_\mu m_\gamma + \delta_{\nu\gamma} m_\mu m_\alpha + \delta_{\alpha\gamma} m_\mu m_\nu) \frac{1}{m^3} \left(V_m''' - 3\frac{V_m''}{m} + 3\frac{V_m'}{m^2} \right) +$$

$$+ \frac{m_\mu m_\nu m_\alpha m_\gamma}{m^4} \left(V_m'''' - 6\frac{V_m'''}{m} + 15\frac{V_m''}{m^2} - 15\frac{V_m'}{m^3} \right) \tag{3.66}$$

which gives,

$$\frac{W_{\mu\nu\alpha\gamma}}{24} \bigg|_m \langle y_\mu y_\nu y_\alpha y_\gamma \rangle_G (m) = \frac{1}{24} \Bigg[W_{1111} \langle y_1 y_1 y_1 y_1 \rangle_G + 12 \sum_{\mu \neq 1} W_{\mu\mu 11} \langle y_\mu y_\mu y_1 y_1 \rangle_G +$$

$$+ \sum_{\mu \neq 1, \nu \neq 1} W_{\mu\mu\nu\nu} \langle y_\mu y_\mu y_\nu y_\nu \rangle_G \Bigg]$$

$$= \frac{1}{8} \frac{V_m''''}{(2J + V_m'')^2} + \frac{n-1}{2} \frac{V_m''' - 2V_m''/m + 2V_m'/m^2}{m(2J + V_m'')(2J + V_m'/m)} +$$

$$+ \frac{(n-1)(n+1)}{24} \frac{V_m'' - V_m'/m}{m^2(2J + V_m'/m)^2} \tag{3.67}$$

Now that we have computed A_m ((3.63)) and C_m ((3.64), (3.65) and (3.67)) we can write explicitly the term of order T^2 of the Gibbs free energy (3.52). We can do it for any n (see appendix 3.C); here we write the expression for $n = 1$,

$$T^2 \left[\frac{A_m (\det W_{\mu\nu}(m))'}{2 \det W_{\mu\nu}(m)} - C_m - \frac{W_m'' A_m^2}{2} \right]$$

$$= T^2 \left[\frac{1}{4} \frac{(V_m''')^2}{(2J + V_m'')^3} - \frac{5}{24} \frac{(V_m''')^2}{(2J + V_m'')^3} + \frac{1}{8} \frac{V''''}{(2J + V_m'')^2} - \frac{1}{8} \frac{(V_m''')^2}{(2J + V_m'')^3} \right]$$

$$= T^2 \left[\frac{1}{8} \frac{V_m''''}{(2J + V_m'')^2} - \frac{1}{12} \frac{(V_m''')^2}{(2J + V_m'')^3} \right] \tag{3.68}$$

where we used eq. (3.55) to express the determinant's derivative. We can see, confronting eq.s (3.52), (3.56) and (3.68), that the term above is the lowest-order term in T that contains the term V_m'''', the lowest derivative of V that does not vanish for $m = 1$.

3.4 Comparison between standard $O(n)$ model and marginal model

Now we use the explicit form of the mean-field Gibbs free energy, computed in the previous subsection, in order to study the critical behaviour of the marginal model for $T \to 0$. Since we express the free energy as a function of the potential V, we can use a standard $O(n)$-model potential,

$$V_m^{(std)} = \lambda(1 - m^2)^2 \tag{3.69}$$

to have a reference for the behaviour that a generic non-marginal model has for vanishing temperature. We point out that the above "standard" $O(n)$ potential can be expanded in the vicinity of $m = 1$ and it has the same form of the pseudo-Gaussian potential $V \sim (m - 1)^2$. If we had a pseudo-Gaussian potential in eq. (3.37), we would have encountered the same phenomenology of the standard $O(n)$ model, hence we will not report the exact results of the mean-field pseudo-Gaussian model here because they are a replica of the standard's.

3.4.1 Magnetization and longitudinal susceptibility

We compare the marginal and the standard $O(n)$ model by computing their equilibrium magnetization as an expansion for vanishing temperature,

$$m_{eq} = m_0 + T m_1 + T^2 m_2 + O\left(T^3\right) \tag{3.70}$$

using the Gibbs free energy's property [63],

$$\left.\frac{\mathrm{d}g}{\mathrm{d}m}\right|_{m=m_{eq}} = 0 \tag{3.71}$$

Then, we will compute the longitudinal susceptibility as an expansion for vanishing T, using [93],

$$\chi_{\parallel} = \frac{1}{4m_{eq}^2}\left(\left.\frac{\mathrm{d}^2 g}{\mathrm{d}m^2}\right|_{m=m_{eq}}\right)^{-1} \tag{3.72}$$

that can be recovered by using eq. (2.57) and (2.58) for $h = 0$.

Equilibrium magnetization

Using together eq.s (3.70), (3.71) and (3.52) we find that, for both models, , at zero order (which means $T = 0$),

$$V'(m_0) = 0 \tag{3.73}$$

$$4m_0(m_0^2 - 1) = 0 \qquad \text{standard}$$

$$8m_0(m_0^2 - 1)^3 = 0 \qquad \text{marginal}$$

$$\tag{3.74}$$

that means $m_0 = 1$, as we expect for the magnetization at zero temperature. Going to the first order in T we have,

$$\lambda V'(m_{eq}) + \frac{T}{2}\left[\frac{V'''(m_{eq})}{2J + V''(m_{eq})} + (n-1)\frac{V''(m_{eq})/m_{eq} - V'(m_{eq})/m_{eq}^2}{2J + \frac{V'(m_{eq})}{m_{eq}}}\right] = 0$$
(3.75)

$$Tm_1 V''(m_0) + \frac{T}{2}\left[\frac{V'''(m_0)}{2J + V''(m_0)} + (n-1)\frac{V''(m_0)}{2Jm_0}\right] = 0$$
(3.76)

where we expanded m_{eq} in order to have an equation of order T, to find the value of m_1. For the standard model we have,

$$\begin{aligned}
m_1^{(std)} &= -\frac{1}{2V''(m_0)}\left[\frac{V'''(m_0)}{2J + V''(m_0)} + (n-1)\frac{V''(m_0)}{2Jm_0}\right] \\
&= -\frac{1}{4}\left[\frac{3}{(J + 4\lambda)} + \frac{n-1}{J}\right]
\end{aligned}$$
(3.77)

that is sensible because it tells us that the average magnetization decreases when the temperature increases and that the deviation from 1 is smaller when the interaction strength J is larger. If we want to use the same procedure to find the value of $m_1^{(mrg)}$, for the marginal model, we cannot use eq. (3.76), because the left hand side identically vanishes. This happens due to the fact that the marginal potential is flat, hence $V'' = V''' = 0$ in the "bare" minimum m_0. For the marginal case, we must use the expression of the Gibbs free energy up to order T^2 in order to compute the correction m_1. The expression (3.75) then becomes,

$$V'(m_{eq}) + \frac{T}{2}\left[\frac{V'''(m_{eq})}{2J + V''(m_{eq})} + (n-1)\frac{V''(m_{eq})/m_{eq} - V'(m_{eq})/m_{eq}^2}{2J + \frac{V'(m_{eq})}{m_{eq}}}\right] +$$
$$+ T^2 D(m_{eq}) = 0$$
(3.78)

where the term $D(m_{eq})$ includes the corrections of order T^2 coming from the derivative with respect to m of eq. (3.52). To compute this contribution we have to include the terms C_m ((3.64)), A_m ((3.63)) and $(\det W_{\mu\nu})'$ ((3.55)). If we expand the above equation at order T^2 we can see that all the terms of order 1 and order T vanish and we remain with,

$$\frac{T^2}{2}\left[\frac{m_1 V''''(m_0)}{2J}\right] + T^2 D(m_0) = 0$$
(3.79)

that gives,

$$m_1^{(mrg)} = -\frac{4JD(m_0)}{V''''(m_0)} = -\frac{1}{2J}\left[\frac{5}{2} + (n-1)\right]$$
(3.80)

computations for $D(m_0)$ are in the appendix 3.C. In the end we have, using eq.s (3.70), (3.77) and (3.80),

$$m_{eq}^{(std)} \simeq 1 - \frac{T}{4J}\left[\frac{3}{(1 + 4\lambda/J)} + (n-1)\right]$$
(3.81)

$$m_{eq}^{(mrg)} \simeq 1 - \frac{T}{2J}\left[\frac{5}{2} + (n-1)\right] \tag{3.82}$$

where we can see that, for the two models we are comparing, the structure of the equilibrium magnetization is the same near zero temperature. In both cases we have a negative linear correction in T that decreases when the interaction strength J increases; the numerical coefficients are different but the qualitative behaviour of the equilibrium magnetization is the same. We see that, if we want to be in the polarized phase, we just have to choose a small temperature, as it is for standard ferromagnetic models [63].

Longitudinal susceptibility

We use now eq. (3.72) with eq.s (3.81) and (3.82) to find the longitudinal susceptibility for both the standard $O(n)$ model and the marginal model. Once again we use eq. (3.52) up to order T, plugging it into eq. (3.72),

$$
\begin{aligned}
\chi_\parallel &= \frac{1}{4m_{eq}^2}\Bigg\{V''(m_{eq}) + \frac{T}{2}\Bigg[\frac{V''''(m_{eq})}{(2J+V''(m_{eq}))} - \frac{(V'''(m_{eq}))^2}{(2J+V''(m_{eq}))^2} + \\
&\quad + (n-1)\frac{(V'''(m_{eq})/m_{eq} - 2V''(m_{eq})/m_{eq}^2 + 2V'(m_{eq})/m_{eq}^3)}{(2J+V'(m_{eq})/m_{eq})} + \\
&\quad - (n-1)\frac{(V''(m_{eq})/m_{eq} - V'(m_{eq})/m_{eq}^2)^2}{(2J+V'(m_{eq})/m_{eq})^2}\Bigg]\Bigg\}^{-1} \\
&\simeq \frac{1}{4m_0^2}(1+2Tm_1/m_0)^{-1}\Bigg\{V''(m_0) + Tm_1V'''(m_0) + \\
&\quad + \frac{T}{2}\Bigg[\frac{V''''(m_0)}{(2J+V''(m_0))} - \frac{(V'''(m_0))^2}{(2J+V''(m_0))^2} + \\
&\quad + \frac{(n-1)}{2J}\left(V'''(m_0)/m_0 - 2V''(m_0)/m_0^2\right) - \frac{(n-1)}{4J^2}\left(V''(m_0)/m_0\right)^2\Bigg]\Bigg\}^{-1} \\
&\simeq \frac{1}{4m_0^2}\Bigg\{V''(m_0) + 2T\frac{V''(m_0)m_1}{m_0} + Tm_1V'''(m_0) + \\
&\quad + \frac{T}{2}\Bigg[\frac{V''''(m_0)}{(2J+V''(m_0))} - \frac{(V'''(m_0))^2}{(2J+V''(m_0))^2} + \\
&\quad + \frac{(n-1)}{2J}\left(V'''(m_0)/m_0 - 2V''(m_0)/m_0^2\right) - \frac{(n-1)}{4J^2}\left(V''(m_0)/m_0\right)^2\Bigg]\Bigg\}^{-1}
\end{aligned}
\tag{3.83}
$$

If we plug in the expressions (3.81) and (3.82) and the models' potentials (3.69) and (3.154) we find,

$$\chi_\parallel^{(std)} \simeq \frac{1}{4m_0^2 V''^{(std)}(m_0)} + O(T) = \frac{1}{32} + O(T) \tag{3.84}$$

$$\chi_{\parallel}^{(mrg)} \simeq \frac{J}{Tm_0^2 V''''^{(mrg)}(m_0)} + \text{const} = \frac{1}{T}\frac{J}{384} + \text{const} \tag{3.85}$$

Hence we have that, following the mean-field approximation, for the standard $O(n)$-model the longitudinal susceptibility is constant in the limit of vanishing temperature, while for the marginal model the longitudinal susceptibility diverges for $T \to 0$. The first result is not unexpected, we already know from the Landau approximation of a generic $O(n)$-model (see chapter 2) that the longitudinal susceptibility at tree level (that is equivalent to mean.field) stays finite in the whole symmetry-broken phase (eq. (2.30)), because this kind of approximation is unable to capture phase modes' divergent contribution to the longitudinal susceptibility. The result about the marginal model is, on the other hand, promising. Even at mean-field level the marginal longitudinal susceptibility diverges for vanishing temperature. Since this divergence cannot be caused by phase fluctuations, because the mean-field approximation cannot capture the contribution of phase fluctuations to the longitudinal degree of freedom, another effect must be present. The other degree of freedom that is involved in longitudinal fluctuations is the modulus hence, as we will see in the next section, the contribution of modulus fluctuations in this theory plays a crucial role for $T \to 0$.

3.4.2   The modulus susceptibility

We show now that, at mean field level, the longitudinal susceptibility captures the collective behaviour of moduli correlations. From the fluctuation-dissipation relation (2.107) applied on a lattice we can write the longitudinal susceptibility as,

$$\chi_{\parallel} = \frac{\beta}{N} \sum_{i,j} \left[\left\langle \sigma_{\parallel i} \sigma_{\parallel j} \right\rangle - \left\langle \sigma_{\parallel i} \right\rangle \left\langle \sigma_{\parallel j} \right\rangle \right] \tag{3.86}$$

where $\sigma_{\parallel i}$ is the component of the spin $\boldsymbol{\sigma}$ at lattice site i that is parallel to the equlibrium magnetization. Given this definition we have that $\left\langle \sigma_{\parallel i} \right\rangle = m$. If we define θ_i as the angle between σ_i and m, we can write the above equation as,

$$\chi_{\parallel} = \frac{\beta}{N} \sum_{i,j} \left[\left\langle \sigma_i \sigma_j \cos\theta_i \cos\theta_j \right\rangle - \left\langle \sigma_i \cos\theta_i \right\rangle \left\langle \sigma_j \cos\theta_j \right\rangle \right] \tag{3.87}$$

If we assume that modulus fluctuations are decoupled from phase fluctuations (that is reasonable given our generic results of chapter 2, that apply to any $O(n)$-symmetric system), we can simplify the above expression,

$$
\begin{aligned}
\chi_{\parallel} &= \frac{\beta}{N} \sum_{i,j} \left[\left\langle \sigma_i \sigma_j \right\rangle \left\langle \cos\theta_i \cos\theta_j \right\rangle - \left\langle \sigma_i \right\rangle \left\langle \cos\theta_i \right\rangle \left\langle \sigma_j \right\rangle \left\langle \cos\theta_j \right\rangle \right] \\
&= \frac{\beta}{N} \sum_{i,j} \Bigg[\left\langle \sigma_i \sigma_j \right\rangle \left\langle \cos\theta_i \cos\theta_j \right\rangle - \left\langle \sigma_i \right\rangle \left\langle \sigma_j \right\rangle \left\langle \cos\theta_i \cos\theta_j \right\rangle + \\
&\quad + \left\langle \sigma_i \right\rangle \left\langle \sigma_j \right\rangle \left\langle \cos\theta_i \cos\theta_j \right\rangle - \left\langle \sigma_i \right\rangle \left\langle \cos\theta_i \right\rangle \left\langle \sigma_j \right\rangle \left\langle \cos\theta_j \right\rangle \Bigg]
\end{aligned}
$$

$$\simeq \frac{\beta}{N} \sum_{i,j} \left[\left(\langle \sigma_i \sigma_j \rangle - \langle \sigma_i \rangle \langle \sigma_j \rangle \right) \left(1 - \langle \theta_i^2 \rangle + \frac{1}{4} \langle \theta_i^2 \theta_j^2 \rangle + \dots \right) + \right.$$

$$\left. + \langle \sigma_i \rangle \langle \sigma_j \rangle \frac{1}{4} \left(\langle \theta_i^2 \theta_j^2 \rangle - \langle \theta_i^2 \rangle \langle \theta_j^2 \rangle + \dots \right) \right]$$

$$= \frac{\beta}{N} \sum_{i,j} \left[\left(\langle \sigma_i \sigma_j \rangle - \sigma^2 \right) \left(1 - v_\theta + \frac{1}{4} \langle \theta_i^2 \theta_j^2 \rangle + \dots \right) + \sigma^2 \frac{1}{4} \left(\langle \theta_i^2 \theta_j^2 \rangle - v_\theta^2 + \dots \right) \right] \tag{3.88}$$

where $\sigma = \langle \sigma_i \rangle$ and $v_\theta = \langle \theta_i^2 \rangle$. From the equation above we see that in general the longitudinal susceptibility is a complex combination of modulus and phase fluctuations of various orders. In a standard $O(n)$ theory modulus fluctuations are massive (see section 2.4) and the leading contribution that makes the longitudinal susceptibility diverge for vanishing external field, in the symmetry-broken phase, comes from phase fluctuations. The results of eq.s (3.84) and (3.85)], however, are computed in the mean field approximation scheme and cannot take into account the second order phase fluctuations that are present in the above equation. Moreover, if the temperature is low enough, the amplitude of phase fluctuations is small, hence we can also disregard v_θ. In the end we can assume that, in mean-field we can write,

$$\chi_\parallel^{(MF)} \simeq \frac{\beta}{N} \sum_{i,j} \left[\langle \sigma_i \sigma_j \rangle - \sigma^2 \right] \equiv \chi_\sigma \tag{3.89}$$

where χ_σ is the modulus susceptibility, that can be computed with the formula above or adding a term in the Hamiltonian like,

$$h_\sigma \sum_i |\boldsymbol{\sigma}_i| \tag{3.90}$$

and computing,

$$\chi_\sigma \bigg|_{h_\sigma = 0} = \frac{\partial \sigma}{\partial h_\sigma} \bigg|_{h_\sigma = 0} \tag{3.91}$$

with $\sigma = 1/N \sum_i \langle \sigma_i \rangle = \langle \sigma_i \rangle$ as we defined before. Finally, if we put together the result of eq. (3.89) with the mean-field approximations (3.84) and (3.85) we can have an idea of what happens, at least at mean-field level, at the modulus degree of freedom in both the standard $O(n)$ model and the marginal model, for vanishing temperature. To sum up the results we have,

$$\chi_\sigma^{(std)} \sim \text{const} \tag{3.92}$$

$$\chi_\sigma^{(mrg)} \sim \frac{1}{T} \tag{3.93}$$

The first relation tells an information that was already discovered in section 2.4: in a standard $O(n)$ model the modulus does not develop scale-free correlations for vanishing temperature, and given the result of section 2.4 this property holds for any temperature below the critical one T_c. On the other hand, we see from the second

relation that the marginal modulus susceptibility, within the mean-field approximation and in the thermodynamic limit, diverges for vanishing temperature. Given the fluctuation-dissipation relation (3.89), this implies that the modulus connected correlation function of the marginal model is scale-free when the temperature drops to zero at mean field level; the exponent may be corrected in finite dimension, but hopefully the divergence is robust. If that was the case, it would imply that, for a sufficiently low temperature, any finite-size system would have a modulus correlation length that is proportional to the size of the system. The marginal model would be capable of reproducing then the experimental findings of Fig. 1.6, just lowering enough the temperature parameter. In the nest chapter we will show the results of numerical simulations to see if the predicted mean-field behaviour implies scale-free correlations of modulus (speed) fluctuations.

3.5   Spin-wave modulus distribution

Let us now consider what happens to the marginal model average modulus distribution. We can follow a similar procedure as the one used for the pseudo-Gaussian model, i.e. we apply the SW approximation to deal with directional fluctuations and we decompose in normal modes for the modulus fluctuations. We end up with a distribution with the same structure as the one of (3.19) with

$$H = \sum_{a=1}^{N} J\lambda_a \hat{\sigma}_a^2 + \lambda \sum_i \left(\sum_{a,b} w_i^{(a)} w_i^{(b)} \hat{\sigma}_a \hat{\sigma}_b - 1 \right)^4 \tag{3.94}$$

Integration over the non-zero modes with this effective Hamiltonian is clearly a hard task, due to the non-Gaussian contributions. However, in the approximation where the relative modulus fluctuations are small, things simplify: we can easily extract the zero mode contribution $\simeq N\lambda(s^2 - 1)^4$ in the exponent, while at leading order the integration over the remaining modes (which is non Gaussian in this case) will produce a constant integral. The distribution for the average modulus s will then be:

$$P(s) = \frac{1}{Z} s^{d-1} \exp\left\{ \left[-\frac{N\lambda}{T}(s^2 - 1)^4 \right] \right\} \tag{3.95}$$

The agreement between theory and simulations is less accurate than in the pseudo-Gaussian case, but we still have a satisfying match between the predicted average mean modulus and the value measured from numerical simulations (Fig.4.3 of the next chapter). Once again we can compute the maximum of the distribution to estimate the typical mean modulus. For $d = 3$ we get:

$$1 - \frac{4N\lambda}{T} \left(s_{typical} \right)^2 \left(\left(s_{typical} \right)^2 - 1 \right)^3 = 0 \tag{3.96}$$

Since we are interested in the behaviour of $s_{typical}$ in N at fixed T and λ, we can solve this equation in the two limits of big N and small N, obtaining:

$$s_{typical} \simeq \begin{cases} 1 + \left(\frac{T}{32N\lambda} \right)^{1/3} & \text{for } N \gg \frac{T}{\lambda} \\ \left(\frac{T}{4N\lambda} \right)^{1/8} & \text{for } N \ll \frac{T}{\lambda} \end{cases} \tag{3.97}$$

Here we can see that, in order to obtain a typical modulus close to the reference value $s = 1$ we just need to choose a small enough temperature T, that is the same requirement for the system to have scale-free correlations (see section above). While with the Gaussian model we had two conflicting conditions over the parameter g, here we have just to choose a small enough T and then adjust the value of λ in order to obtain the right polarization, according to experimental data and we gain both an average modulus close to a reference value (in this case $s = 1$) for every system's size N and scale-free modulus correlations for every system's linear size L.

3.6 The amplitude of the correlation function

From the expression of the modulus susceptibility (3.93) and its derivation of the previous sections it may not be clear whether the divergence for vanishing T is a trivial effect of the prefactor β in eq. (3.89) or it really comes from a divergent correlation length, hence from a critical phenomenon. Here I address this problem by computing the contribution to modulus susceptibility that comes from the trivial correlation amplitude and the prefactor β. We can analyze the modulus susceptibility of eq. (3.89) to separate the contribution from the correlation function's amplitude and the actual correlation range. If we define $\delta\sigma_i = \sigma_i - \sigma$, with $\sigma = 1/N \left\langle \sum_i \sigma_i \right\rangle$ and ,we have,

$$\chi_\sigma = \frac{\beta}{N} \sum_{ij} \langle \delta\sigma_i \delta\sigma_j \rangle = \frac{\beta}{N} \left(\sum_i \left\langle \delta\sigma_i^2 \right\rangle + \sum_{i \neq j} \langle \delta\sigma_i \delta\sigma_j \rangle \right) \tag{3.98}$$

We define the single particle fluctuation (or variance),

$$C_0 \equiv 1/N \sum_i \left\langle \delta\sigma_i^2 \right\rangle \tag{3.99}$$

hence we have,

$$\chi_\sigma = \beta C_0 \left(1 + \frac{\sum_{i \neq j} \langle \delta\sigma_i \delta\sigma_j \rangle}{N C_0} \right) \tag{3.100}$$

For a common critical point at a certain finite T_c, β and C_0 separately go to constant values and the only source of divergence for the susceptibility (in the thermodynamic limit) is the sum of the connected correlations between different spins, $\sum_{i \neq j} \langle \delta\sigma_i \delta\sigma_j \rangle$.

Let us see what happens for $T \to 0$ ($\beta \to \infty$). There might be two sources of divergences, the factor βC_0 and the term $\frac{\sum_{i \neq j} \langle \delta\sigma_i \delta\sigma_j \rangle}{N C_0}$. One might be tempted to say that all the divergence is contained in the denominator $C_0 = 1/N \sum_i \langle \delta\sigma_i^2 \rangle$, because the modulus fluctuations of the single spin go to zero for $T \to 0$, but the connected correlations between different spins also do so. Furthermore, using the following inequality,

$$\left\langle (\delta\sigma_i - \delta\sigma_j)^2 \right\rangle \geq 0 \tag{3.101}$$

one obtains,

$$\left\langle \delta\sigma_i^2 \right\rangle + \left\langle \delta\sigma_j^2 \right\rangle \geq 2 \langle \delta\sigma_i \delta\sigma_j \rangle \tag{3.102}$$

due to translational invariance one has $\left\langle \delta\sigma_i^2 \right\rangle = \left\langle \delta\sigma_j^2 \right\rangle$, in the end we have,

$$\left\langle \delta\sigma_i^2 \right\rangle \geq \langle \delta\sigma_i \delta\sigma_j \rangle \tag{3.103}$$

$$C_0 = \frac{1}{N} \sum_i \left\langle \delta\sigma_i^2 \right\rangle \geq \langle \delta\sigma_i \delta\sigma_j \rangle \tag{3.104}$$

So we define the "normalized" connected correlation functions between different spins' moduli as,

$$\langle \delta\sigma_i \delta\sigma_j \rangle_{\mathcal{N}} = \frac{\langle \delta\sigma_i \delta\sigma_j \rangle}{C_0} \leq 1 \tag{3.105}$$

where, because of the (3.104), we are assured that, for each $i \neq j$ and for any T it is true that $\langle \delta\sigma_i \delta\sigma_j \rangle_{\mathcal{N}} < 1$. There is no problem with C_0 in the denominator, indeed we can write the susceptibility as,

$$\chi_\sigma = \beta C_0 \left(1 + \frac{1}{N} \sum_{i \neq j} \langle \delta\sigma_i \delta\sigma_j \rangle_{\mathcal{N}} \right) \tag{3.106}$$

Now it is clear that the divergence of χ_σ can come either from βC_0, where C_0 is the correlation function amplitude, or from the infinite sum (in the thermodynamic limit) of all the "normalized" connected correlation functions between different spins' moduli; in this sum each term $\langle \delta s_i \delta s_j \rangle_{\mathcal{N}}$ is finite and smaller than 1 but, of course, if $N \to \infty$, the sum might diverge, that is the case of the marginal model, for $T \to 0$. The sum can diverge if the correlation function is long-ranged, and this happens close to a critical point, where the correlation length diverges. Now we will show that in the marginal model the quantity βC_0 is finite in the thermodynamic limit, hence the divergence of the modulus susceptibility comes exclusively from the correlation length divergence.

We write the generic form of C_0, both for the standard model and for the marginal model, using the mean-field approximation. In the end we will see that, for both models, the contribution of βC_0 does not change the behaviour of the susceptibility for vanishing temperature. To compute C_0 (3.99) we need to know the average spin modulus, that is,

$$s \equiv \langle \sigma_j \rangle = \frac{\int \prod_k \mathrm{d}\boldsymbol{\sigma}_k \ \sigma_j e^{-\beta H}}{\int \prod_k \mathrm{d}\boldsymbol{\sigma}_k \ e^{-\beta H}} \tag{3.107}$$

where the Hamiltonian H is the mean-field Hamiltonian (3.37). This time we decouple the interaction term of the Hamiltonian through the Hubbard-Stratonovich transformation [121],

$$e^{\frac{\beta J}{N}\left(\sum_i \boldsymbol{\sigma}_i\right)^2} = \left(\frac{\beta N}{4\pi J}\right)^{n/2} \int \mathrm{d}\boldsymbol{x} \, e^{-\frac{\beta N}{4J}x^2 + \beta\boldsymbol{x}\cdot\left(\sum_i \boldsymbol{\sigma}_i\right)} \tag{3.108}$$

that gives us the following expression for the average spin modulus,

$$s = \frac{\int \prod_k \mathrm{d}\boldsymbol{\sigma}_k \ \sigma_j \int \mathrm{d}\boldsymbol{x} \ e^{-\beta\sum_i\left[J\sigma_i^2 + V(\sigma_i^2) - \boldsymbol{x}\cdot\boldsymbol{\sigma}_i\right] - \frac{\beta N}{4J}x^2}}{\int \prod_k \mathrm{d}\boldsymbol{\sigma}_k \ \int \mathrm{d}\boldsymbol{x} \ e^{-\beta\sum_i\left[J\sigma_i^2 + V(\sigma_i^2) - \boldsymbol{x}\cdot\boldsymbol{\sigma}_i\right] - \frac{\beta N}{4J}x^2}} \tag{3.109}$$

Now we use the notation,

$$[...]_{\sigma,x} \equiv \left[J\sigma^2 + V\left(\sigma^2\right) - \boldsymbol{x} \cdot \boldsymbol{\sigma} \right] \tag{3.110}$$

to lighten the notation. In the numerator of eq. (3.109) we can group together $N-1$ integrals in $\boldsymbol{\sigma}_k$ and in the denominator we can do the same for N integrals,

$$s = \frac{\int \mathrm{d}\boldsymbol{\sigma}_j \; \sigma_j \int \mathrm{d}\boldsymbol{x} \; e^{-\beta[...]_{\sigma_j,x} - \frac{\beta N}{4J}x^2} \left(\int \mathrm{d}\boldsymbol{\sigma} \; e^{-\beta[...]_{\sigma,x}} \right)^{N-1}}{\int \mathrm{d}\boldsymbol{x} \; e^{-\frac{\beta N}{4J}x^2} \left(\int \mathrm{d}\boldsymbol{\sigma} \; e^{-\beta[...]_{\sigma,x}} \right)^N} \tag{3.111}$$

$$= \frac{\int \mathrm{d}\boldsymbol{\sigma}_j \; \sigma_j \int \mathrm{d}\boldsymbol{x} \; e^{-\beta[...]_{\sigma_j,x}} \left(\int \mathrm{d}\boldsymbol{\sigma} \; e^{-\beta[...]_{\sigma,x}} \right)^{-1} \exp\left(N\left\{ -\frac{\beta}{4J}x^2 + \log\left(\int \mathrm{d}\boldsymbol{\sigma} \; e^{-\beta[...]_{\sigma,x}} \right) \right\} \right)}{\int \mathrm{d}\boldsymbol{x} \; \exp\left(N\left\{ -\frac{\beta}{4J}x^2 + \log\left(\int \mathrm{d}\boldsymbol{\sigma} \; e^{-\beta[...]_{\sigma,x}} \right) \right\} \right)} \tag{3.112}$$

Now we perform the x integral with the saddle point method, with the condition $N \to \infty$ (i.e. the thermodynamic limit), keeping only the term of the lowest order. The saddle point value of the variable $\boldsymbol{x}$ is $\boldsymbol{x}_0$ and it is defined by the equation that maximizes the exponent of $\exp\left(N\{...\}\right)$:

$$\frac{\boldsymbol{x}_0}{2J} = \frac{\int \mathrm{d}\boldsymbol{\sigma} \; \boldsymbol{\sigma} e^{-\beta[...]_{\sigma,x_0}}}{\int \mathrm{d}\boldsymbol{\sigma} \; e^{-\beta[...]_{\sigma,x_0}}} \tag{3.113}$$

Plugging the saddle point value into the equation for s (and dropping the index j) we finally have:

$$s = \frac{\int \mathrm{d}\boldsymbol{\sigma} \; \sigma e^{-\beta[...]_{\sigma,x_0}}}{\int \mathrm{d}\boldsymbol{\sigma} \; e^{-\beta[...]_{\sigma,x_0}}} \tag{3.114}$$

That we want to solve in the limit $\beta \to \infty$ that leads to another equation for a saddle point value for $\boldsymbol{\sigma}$ that we call $\boldsymbol{\sigma}_0$:

$$\frac{\partial}{\partial \boldsymbol{\sigma}} [...]_{\sigma,x_0} \bigg|_{\boldsymbol{\sigma}=\boldsymbol{\sigma}_0} = 0 \tag{3.115}$$

$$2J\boldsymbol{\sigma}_0 + 2\boldsymbol{\sigma}_0 V'\left(\sigma_0^2\right) = \boldsymbol{x}_0 \tag{3.116}$$

Now we have (in a similar way of eq. (3.52)) three variables to determine s, $\boldsymbol{x_0}$, $\boldsymbol{\sigma_0}$ and three equations to obtain them, (3.113), (3.114) and (3.116). The last two variables are vectors so we have $2n+1$ scalar variables and scalar equations. Here we can make the same observation that we used for the computation of the Gibbs free energy and notice at that, given the form of eq. (3.113) and (3.116), $\boldsymbol{x}_0$ and $\boldsymbol{\sigma}_0$ are parallel, furthermore there is no constraint on the direction of the two vectors, it is not fixed by the two equations just mentioned. Once again, giving the arbitrariness of $\boldsymbol{x}_0$'s direction we fix it to be along the x-axis (one of the n possible axes), i.e.:

$$\boldsymbol{x_0} = (x_0, 0, ..., 0) \tag{3.117}$$

hence eq. 3.116 gives:

$$x_0 = 2J\sigma_{0x} + 2\sigma_{0x}V'(|\boldsymbol{\sigma}_0|^2) \tag{3.118}$$

$$0 = 2J\sigma_{0j} + 2\sigma_{0j}V'(|\boldsymbol{\sigma}_0|^2) \qquad \text{for } j \neq x \tag{3.119}$$

which implies for $\boldsymbol{\sigma}_0$:

$$\boldsymbol{\sigma_0} = (\sigma_{0x}, 0, ..., 0) \equiv (\sigma_0, 0, ..., 0) \tag{3.120}$$

Indeed $\boldsymbol{x_0}$ and $\boldsymbol{\sigma}_0$ are parallel, just like magnetization and external field. Hence our equations are:

$$x_0 = 2J\sigma_0 + 2\sigma_0 V'(\sigma_0^2) \tag{3.121}$$

$$\frac{x_0}{2J} = \frac{\int \mathrm{d}\boldsymbol{\sigma} \ \sigma_x \ e^{-\beta\left[J\sigma^2 + V\left(\sigma^2\right) - x_0\sigma_x\right]}}{\int \mathrm{d}\boldsymbol{\sigma} \ e^{-\beta\left[J\sigma^2 + V\left(\sigma^2\right) - x_0\sigma_x\right]}} \tag{3.122}$$

$$s \equiv \langle \sigma \rangle = \frac{\int \mathrm{d}\boldsymbol{\sigma} \ \sigma \ e^{-\beta\left[J\sigma^2 + V\left(\sigma^2\right) - x_0\sigma_x\right]}}{\int \mathrm{d}\boldsymbol{\sigma} \ e^{-\beta\left[J\sigma^2 + V\left(\sigma^2\right) - x_0\sigma_x\right]}} \tag{3.123}$$

$$v \equiv \left\langle \sigma^2 \right\rangle = \frac{\int \mathrm{d}\boldsymbol{\sigma} \ \sigma^2 e^{-\beta\left[J\sigma^2 + V\left(\sigma^2\right) - x_0\sigma_x\right]}}{\int \mathrm{d}\boldsymbol{\sigma} \ e^{-\beta\left[J\sigma^2 + V\left(\sigma^2\right) - x_0\sigma_x\right]}} \tag{3.124}$$

Notice that in the case with generic n we have $s \neq \langle \sigma_x \rangle$. Hence we have to compute the relation between the two, it suffices to do that up to order T. Since we will use the saddle point method for $\beta \to \infty$ we shall expand the modulus σ near the saddle point σ_0 up to quadratic order, to have corrections up to $O(T)$ (remember: we always do the substitution $y = \beta^{1/2}\left(\sigma - \sigma_0\right)$). Given that we obtain:

$$\sigma = (\boldsymbol{\sigma} \cdot \boldsymbol{\sigma})^{1/2} = \{[\boldsymbol{\sigma}_0 + (\boldsymbol{\sigma} - \boldsymbol{\sigma}_0)] \cdot [\boldsymbol{\sigma}_0 + (\boldsymbol{\sigma} - \boldsymbol{\sigma}_0)]\}^{1/2} \tag{3.125}$$

$$= \sigma_0 \left[1 + 2\frac{\sigma_0\left(\sigma_x - \sigma_0\right)}{\sigma_0^2} + \frac{(\boldsymbol{\sigma} - \boldsymbol{\sigma}_0)^2}{\sigma_0^2}\right]^{1/2} \tag{3.126}$$

$$\simeq \sigma_0 \left[1 + \frac{\sigma_0\left(\sigma_x - \sigma_0\right)}{\sigma_0^2} + \frac{(\boldsymbol{\sigma} - \boldsymbol{\sigma}_0)^2}{2\sigma_0^2} - \frac{\sigma_0^2\left(\sigma_x - \sigma_0\right)^2}{2\sigma_0^4}\right] \tag{3.127}$$

$$= \sigma_x + \frac{\sigma_{n-1}^2}{2\sigma_0} \tag{3.128}$$

$$\sigma_{n-1}^2 \equiv \sum_{i \neq x} \sigma_i^2 \tag{3.129}$$

Plugging this expression into eq. 3.123 and looking at eq. 3.122 we discover:

$$s \simeq \frac{x_0}{2J} + \frac{1}{2\sigma_0}\frac{\int \mathrm{d}\boldsymbol{\sigma} \ \sigma_{n-1}^2 \ e^{-\beta\left[J\sigma^2 + V\left(\sigma^2\right) - x_0\sigma_x\right]}}{\int \mathrm{d}\boldsymbol{\sigma} \ e^{-\beta\left[J\sigma^2 + V\left(\sigma^2\right) - x_0\sigma_x\right]}} \tag{3.130}$$

$$= \frac{x_0}{2J} + \frac{n-1}{2\sigma_0}\frac{\int \mathrm{d}\boldsymbol{\sigma} \ \sigma_\alpha^2 \ e^{-\beta\left[J\sigma^2 + V\left(\sigma^2\right) - x_0\sigma_x\right]}}{\int \mathrm{d}\boldsymbol{\sigma} \ e^{-\beta\left[J\sigma^2 + V\left(\sigma^2\right) - x_0\sigma_x\right]}} \qquad \text{with } \alpha \neq x \tag{3.131}$$

Using a similar procedure we can compute $v \equiv \langle \sigma^2 \rangle$ up to order T, indeed, expanding σ^2 near $\boldsymbol{\sigma}_0$:

$$\sigma^2 = (\boldsymbol{\sigma} \cdot \boldsymbol{\sigma}) = [\boldsymbol{\sigma}_0 + (\boldsymbol{\sigma} - \boldsymbol{\sigma}_0)] \cdot [\boldsymbol{\sigma}_0 + (\boldsymbol{\sigma} - \boldsymbol{\sigma}_0)] \tag{3.132}$$

$$= \sigma_0^2 + 2\sigma_0\left(\sigma_x - \sigma_0\right) + (\boldsymbol{\sigma} - \boldsymbol{\sigma}_0)^2 \tag{3.133}$$

$$= \sigma_0^2 + 2\sigma_0 \left(\sigma_x - \sigma_0 \right) + \left(\sigma_x - \sigma_0 \right)^2 + \sigma_{n-1}^2 \tag{3.134}$$

Plugging it into eq. 3.124 and looking at eq. 3.122 we have:

$$v = \sigma_0^2 + 2\sigma_0 \left(\frac{x_0}{2J} - \sigma_0 \right) + \frac{\int \mathrm{d}\boldsymbol{\sigma} \ (\sigma_x - \sigma_0)^2 \ e^{-\beta \left[J\sigma^2 + V(\sigma^2) - x_0 \sigma_x \right]}}{\int \mathrm{d}\boldsymbol{\sigma} \ e^{-\beta \left[J\sigma^2 + V(\sigma^2) - x_0 \sigma_x \right]}} +$$
$$+ \frac{\int \mathrm{d}\boldsymbol{\sigma} \ \sigma_{n-1}^2 \ e^{-\beta \left[J\sigma^2 + V(\sigma^2) - x_0 \sigma_x \right]}}{\int \mathrm{d}\boldsymbol{\sigma} \ e^{-\beta \left[J\sigma^2 + V(\sigma^2) - x_0 \sigma_x \right]}} \tag{3.135}$$

For the computation of all the previous multi-dimensional integrals (eq.s (3.122), (3.131) and (3.135)) with the saddle point approximation, see appendix 3.D. We will go on with the calculations assuming the saddle-point integrals to be done. Hence our set of equations becomes:

$$\begin{cases} x_0 = 2J\sigma_0 + V'(\sigma_0) \\ s \simeq \frac{x_0}{2J} + \frac{(n-1)}{2(2J\sigma_0 + V'(\sigma_0))} T \\ \frac{x_0}{2J} \simeq \sigma_0 - T A_n(\sigma_0) - T^2 B_n(\sigma_0) \\ v \simeq \sigma_0^2 + 2\sigma_0 \left(\frac{x_0}{2J} - \sigma_0 \right) + \frac{T}{2J + V''(\sigma_0)} + \frac{n-1}{2J} T \end{cases} \tag{3.136}$$

$$A_n(\sigma_0) \equiv \frac{1}{2} \left[\frac{V_0'''}{(2J + V_0'')^2} + \frac{(n-1)(\sigma_0 V_0'' - V_0')}{\sigma_0 (2J\sigma_0 + V_0')(2J + V_0'')} \right] \tag{3.137}$$

$$B_n(\sigma_0) \equiv \frac{1}{8} \left[\frac{V_0'''''}{(2J + V_0'')^3} + \frac{2(n-1)V_0''''}{(2J\sigma_0 + V_0')(2J + V_0'')^2} + \text{terms in} V_0', V_0'', V_0''' \right] \tag{3.138}$$

where we didn't write the terms in V_0', V_0'', V_0''' inside $B_n(\sigma_0)$ because they will not contribute to the expansion; they vanish at $\sigma_0 = 1$. First of all, we can compute C_0, that is, up to order T, using the equations of 3.136:

$$C_0 = \left\langle \sigma^2 \right\rangle - \left\langle \sigma \right\rangle^2 = v - s^2$$

$$\simeq \sigma_0^2 + 2\sigma_0 \left(\frac{x_0}{2J} - \sigma_0 \right) + \frac{T}{2J + V''(\sigma_0)} + \frac{n-1}{2J} T - \left[\frac{x_0}{2J} + \frac{(n-1)}{2(2J\sigma_0 + V'(\sigma_0))} T \right]^2$$

$$\simeq \sigma_0^2 + 2\sigma_0 \left(-T A_n(\sigma_0) \right) + \frac{T}{2J + V''(\sigma_0)} + \frac{n-1}{2J} T - \left[\sigma_0 - T A_n(\sigma_0) + \right.$$

$$\left. + \frac{(n-1)}{2(2J\sigma_0 + V'(\sigma_0))} T \right]^2 \tag{3.139}$$

$$\simeq \frac{T}{2J + V''(\sigma_0)} + \frac{n-1}{2J} T - \frac{(n-1)\sigma_0}{2J\sigma_0 + V'(\sigma_0)} T \tag{3.140}$$

Now we write σ_0 as $1 - aT$ (calculations for a in appendix 3.D) with $a > 0$ and we obtain, always up to order T for C_0:

$$\beta C_0 = \beta \left[\frac{T}{2J + V''(1)} + \frac{n-1}{2J} T - \frac{(n-1)}{2J + V'(1)} T + O(T^2) \right] \tag{3.141}$$
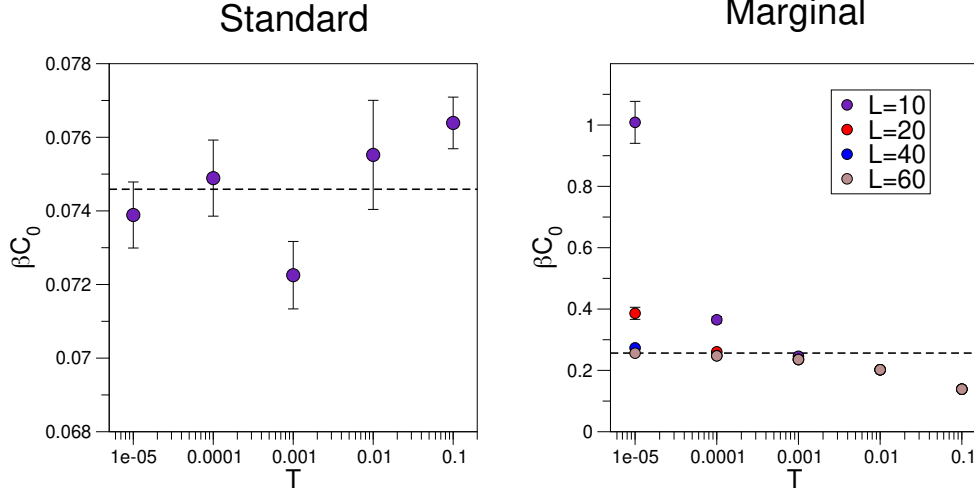
Figure 3.4. βC_0 **for vanishing temperature. Nearest neighbours interaction on a cubic lattice. Standard**: Monte Carlo simulations for the standard $O(n)$ model with a bare potential $V = (\sigma^2 - 1)^2$. The factor βC_0 goes to a constant value, in the limit of vanishing temperature. Results for a box of size $L = 10$, at bigger sizes the result is the same. Simulation parameters: $J = \lambda = 1$. **Marginal**: Monte Carlo simulations for the marginal model with a bare potential $V = (\sigma^2 - 1)^4$. The factor βC_0 moderately grows for vanishing temperature but the growth is suppressed as the size of the system increases. Simulation parameters: $J = \lambda = 1$. Error bars have been computed using the blocking procedure described in [1], together with the Jackknife method. To ensure thermalization for the whole range of temperatures and for both models that we analyzed we performed 20000 Monte Carlo steps without measuring and then we measured the quantities of interest on a thermalized simulation of 10^6 steps. The soundness of the thermalization was checked by looking at the energy and the average modulus as functions of the Monte Carlo step (an example of the thermalization for a system at low temperature can be found in the appendix 3.E).

$$= \frac{1}{2J + V''(1)} + O(T) \tag{3.142}$$

We can say, looking at the formula above, that the value of βC_0 in mean field, at the first relevant order, is n-independent and finite for vanishing temperature. Computing it for the standard and the marginal model we finally have,

$$\beta C_0^{(std)} \simeq \frac{1}{2J + 8\lambda} \tag{3.143}$$

$$\beta C_0^{(mrg)} \simeq \frac{1}{2J} \tag{3.144}$$

where we see that the factors βC_0 go asymptotically to a constant value. In Fig. 3.4 we can see both systems' βC_0s computed from a simulation on a cubic lattice, with nearest neighbours interaction. We can see from the figure that our mean field prediction is, at least qualitatively, correct. For vanishing temperature βC_0 goes to a constant value; for the marginal model we can see that the factor grows for the smallest sizes, but this effect vanishes as the size increases. The finite-size effect on

βC_0 can be computed at mean field, expanding the saddle-point integral in N up to first order corrections, one can find for the marginal model,

$$\beta C_0^{mrg} \simeq \frac{1}{2J} + AT + \frac{B}{TN} + \frac{C}{N} + \dots \tag{3.145}$$

where A,B and C are three numeric constants that depend on n,J and λ. We can see that the third contribution $B/(TN)$ vanishes in the thermodynamic limit but when the number of particles is not strictly infinite, it gives a divergent contribution for $T \to 0$. This fact does not change the result of (3.144), which tells us that the divergence of the modulus susceptibility (3.93) (which can happen only in the thermodynamic limit) is *not* a trivial effect of the factor β in the definition of the susceptibility. However, if we wanted to measure the critical exponents of our theory (as we will do in chapter 5) using the finite-size scaling of the modulus susceptibility, the finite-size divergence in eq. (3.145) could be problematic. The scaling with the temperature of the modulus susceptibility at finite size could be modified by the contribution of the divergent part of the amplitude of correlation functions (3.145). Nonetheless, we see from Fig. 3.4 that the divergence of βC_0 in the realistic case of nearest neighbours interaction is way weaker than $\sim 1/T$ and almost non-existent as the system's size is bigger than $L = 20$, hence the measurements on the susceptibility (see Fig. 5.1 of last chapter) will not be affected by it. Furthermore, for what concerns comparison between the marginal model and data, we do not need to compute the susceptibility, we measure only the correlation length defined by eq. (1.10), which is not affected at all by the amplitude of the correlation function, since it appears both in the numerator and in the denominator, hence it does not contribute to our estimate of the correlation length.

In the end we can say that the divergence in the marginal model's modulus susceptibility, computed in the mean-field approximation (3.93), is not determined by the prefactor β in the definition (3.89), because the prefactor's divergence is tamed by the vanishing correlation amplitude C_0. Hence we believe that the presence of a "marginal critical point" for $T \to 0$ is a bone-fide collective effect and it explains the divergence of the modulus susceptibility. This property suggests that, for a finite size system with short range interaction, the marginal model will show scale-free modulus correlations, just like the experimental data. In the next chapter we will compare our theoretical results and expectations with the appropriate off-equilibrium simulations and with experimental data, to see what our theory can add to the state-of-the-art flocking models.

3.A Appendix: mean-field argument for the average modulus distribution

We can also find the average modulus' distribution 3.23 using a quick mean-field argument. We claim that, due to the high polarization of the system, we can write every individual spin as:

$$\boldsymbol{\sigma}_i = \boldsymbol{\sigma} + \boldsymbol{\epsilon}_i \tag{3.146}$$

where $\boldsymbol{\sigma}$ is the average spin $\boldsymbol{\sigma} = 1/N \sum_i \boldsymbol{\sigma}_i$, and $\boldsymbol{\epsilon}_i$ is the deviation of each individual spin from the average, with $|\boldsymbol{\epsilon}_i| \ll |\boldsymbol{\sigma}|$. By definition we have $\sum_i \boldsymbol{\epsilon}_i = 0$. We plug (3.146) into the Hamiltonian 3.7, disregarding $\boldsymbol{\epsilon}_i$ (hence enforcing a mean-field spin for every particle) and we obtain,

$$\mathcal{H}(\{\boldsymbol{\sigma}_i\}) = g \sum_i (1 - \sigma)^2 = Ng(1 - \sigma)^2 \tag{3.147}$$

To compute the distribution of the collective variable $\boldsymbol{\sigma}$, we need to change variable from $\{\boldsymbol{\sigma}_i\}$ to $\{\{\boldsymbol{\epsilon}_i\}, \boldsymbol{\sigma}\}$ (enforcing the constraint $\delta\left(\sum_i \boldsymbol{\epsilon}_i\right)$). This computation produces a constant that will cancel with the normalization of the probability distribution; in the end we have,

$$P(\{\boldsymbol{\epsilon}_i\}, \boldsymbol{\sigma}) = \frac{e^{-\frac{Ng}{T}(1-\sigma)^2}}{\int d\boldsymbol{\sigma} \prod_i d\boldsymbol{\epsilon}_i \delta\left(\sum_i \boldsymbol{\epsilon}_i\right) e^{-\frac{Ng}{T}(1-\sigma)^2}} \tag{3.148}$$

We integrate over the $\{\boldsymbol{\epsilon}_i\}$ and then we change variable from $d\boldsymbol{\sigma} = d\sigma_x d\sigma_y d\sigma_z$ to $d\sigma d\phi d\theta$, gaining the jacobian σ^2. After integrating over the angular variables we have the probability distribution for σ:

$$P(\sigma) = \frac{\sigma^2 e^{-\frac{Ng}{T}(1-\sigma)^2}}{\int d\sigma \, \sigma^2 \, e^{-\frac{Ng}{T}(1-\sigma)^2}} \tag{3.149}$$

the variable σ, if we use its definition from (3.146), is $\sigma = |\boldsymbol{\sigma}_i - \boldsymbol{\epsilon}_i|$. Since we decided to completely ignore fluctuations, we conclude that $\sigma = \sigma_i$ and therefore $\sigma = 1/N \sum_i \sigma_i = \sigma$. After the identification of s and σ, the equation above coincides with the SW-approximation distribution 3.23.

3.B Appendix: an alternative derivation for the marginal potential

We derive now the form of the marginal potential in a more careful way, assuming only that it must be a polynomial. The potential must also have only even powers of the modulus of $\boldsymbol{\sigma}$, otherwise the Hamiltonian would not be analytic ($\sigma = |\boldsymbol{\sigma}| = \sqrt{\boldsymbol{\sigma} \cdot \boldsymbol{\sigma}}$). Other constraints on the potential's form are on its derivatives in the minimum,

$$\left.\frac{\partial V}{\partial \sigma}\right|_{\sigma=1} = 0 \qquad \left.\frac{\partial^2 V}{\partial \sigma^2}\right|_{\sigma=1} = 0 \qquad \left.\frac{\partial^3 V}{\partial \sigma^3}\right|_{\sigma=1} = 0 \tag{3.150}$$

$$\left.\frac{\partial^4 V}{\partial \sigma^4}\right|_{\sigma=1} > 0 \qquad \text{minimum condition} \qquad (3.151)$$

One has three equations from (3.150) and one inequality from (3.151), so the potential shall have four parameters to be determined,

$$V(\sigma) = A + B\sigma^2 + C\sigma^4 + D\sigma^6 + \lambda\sigma^8 \qquad (3.152)$$

where A is an additional arbitrary constant term of no relevance. If we plug the potential (3.152) into (3.150) and (3.151) we obtain,

$$\begin{cases} B + 2C + 3D + 4\lambda = 0 \\ B + 6C + 15D + 28\lambda = 0 \\ C + 5D + 14\lambda = 0 \\ C + 15D + 70\lambda > 0 \end{cases}$$

that gives,

$$B = -4\lambda \quad C = 6\lambda \quad D = -4\lambda \quad \lambda > 0 \qquad (3.153)$$

Plugging this result into the (3.152) and fixing the arbitrary constants $A = \lambda$ one has,

$$V(\sigma) = \lambda\left(1 - 4\sigma^2 + 6\sigma^4 - 4\sigma^6 + \sigma^8\right) = \lambda\left(\sigma^2 - 1\right)^4 \qquad (3.154)$$

The inequality $\lambda > 0$, coming from the minimum condition, is also consistent with the fact that, for $\sigma^2 \to \infty$, the potential must diverge to $+\infty$, in order to bound the energy of the system. In principle, any potential of the form (3.35) with $p = 2q$ and $q \geq 2$ satisfies eq.s (3.150) and (3.151), but the result of eq. (3.154) is the simplest one, which involves the lowest powers of σ^2.

3.C Appendix: terms of order T^2 of the Gibbs free energy

The generic (i.e for any n) term of order T^2 of the free energy (3.52), for the marginal model that has $V(m) = (1 - m^2)^4$, is,

$$T^2\left[\frac{A_m(\det W_{\mu\nu}(m))'}{2\det W_{\mu\nu}(m)} - C_m - \frac{W_m'' A_m^2}{2}\right]$$

$$= \frac{T^2\lambda}{2}\left\{6J^2\lambda\left(m^2 - 1\right)^2\left[m^6\left(14n^2 + 564n - 487\right) - 6m^4\left(5n^2 + 128n - 85\right) + \right.\right.$$

$$\left. + 3m^2\left(6n^2 + 76n - 37\right) - 2\left(n^2 + 12n - 4\right)\right] + J^3\left[m^4\left(n^2 + 60n + 44\right) + \right.$$

$$\left. - 2m^2\left(n^2 + 36n + 8\right) + n^2 + 12n - 4\right] + 48J\lambda^2\left(m^2 - 1\right)^5 \cdot$$

$$\cdot\left[7m^6\left(7n^2 + 144n - 153\right) + m^4\left(-63n^2 - 564n + 534\right) + \right.$$

$$+ 3m^2 \left(5n^2 + 48n - 41\right) - n^2 - 12n + 4\Big] + 32\lambda^3 \left(m^2 - 1\right)^8 \cdot$$

$$\cdot \left[49m^6 \left(14n^2 + 12n - 29\right) - 42m^4 \left(7n^2 + 32n - 37\right) + \right.$$

$$\left. + m^2 \left(42n^2 + 348n - 381\right) - 2 \left(n^2 + 12n - 4\right)\right]\Big\}/$$

$$/\left\{ \left[J + 4\lambda \left(m^2 - 1\right)^3\right]^2 \left[J + 4\lambda \left(7m^2 - 1\right) \left(m^2 - 1\right)^2\right]^3 \right\} \tag{3.155}$$

where we used the expressions for A_m, C_m and $\det W_{\mu\nu}$ that we computed in the section 3.3.3 and we plugged them into Mathematica. If we take the derivative with respect to m of the above expression (without the T^2), we obtain the term $D(m)$ of eq. (3.78),

$$D(m) = -2\lambda m \Big\{ - 16J^2\lambda^3 \left(m^2 - 1\right)^6 \Big[7m^8 \left(448n^2 - 20316n + 16967\right) + $$

$$+ m^6 \left(-2464n^2 + 169236n - 89273\right) - 3m^4 \left(352n^2 + 19308n - 2251\right) + $$

$$+ m^2 \left(416n^2 + 11100n + 2725\right) - 2 \left(16n^2 + 468n + 479\right)\Big] - 4J^3\lambda^2 \left(m^2 - 1\right)^3 \cdot$$

$$\cdot \Big[m^8 \left(952n^2 - 11604n - 17047\right) + m^6 \left(-1984n^2 + 20412n + 50605\right) + $$

$$+ 3m^4 \left(368n^2 - 3204n - 12323\right) + m^2 \left(-64n^2 + 948n + 9703\right) + $$

$$- 4 \left(2n^2 + 36n + 133\right)\Big] - J^4\lambda \left(m^2 - 1\right) \Big[m^6 \left(104n^2 + 2100n - 11969\right) + $$

$$- 3m^4 \left(72n^2 + 1316n - 4533\right) + 3m^2 \left(40n^2 + 724n - 1297\right) - 8n^2 - 324n + 53\Big] + $$

$$+ J^5 \left[-m^2 \left(n^2 + 60n + 44\right) + n^2 + 36n + 8\right] + 64J\lambda^4 \left(m^2 - 1\right)^9 \cdot$$

$$\cdot \Big[49m^8 \left(28n^2 + 5820n - 5875\right) - 7m^6 \left(1456n^2 + 27324n - 24223\right) + $$

$$+ m^4 \left(4200n^2 + 68292n - 51333\right) + m^2 \left(-592n^2 - 12732n + 6523\right) + $$

$$+ 28n^2 + 864n + 692\Big] + 256\lambda^5 \left(m^2 - 1\right)^{12} \Big[1372m^8 \left(14n^2 + 12n - 29\right) + $$

$$- 49m^6 \left(224n^2 + 972n - 1139\right) + 21m^4 \left(112n^2 + 1188n - 1225\right) + $$

$$+ m^2 \left(-224n^2 - 4404n + 3761\right) + 8n^2 + 252n + 181\Big]\Big\}/$$

$$/\left\{ \left[J + 4\lambda \left(m^2 - 1\right)^3\right]^3 \left[J + 4\lambda \left(7m^2 - 1\right) \left(m^2 - 1\right)^2\right]^4 \right\} \tag{3.156}$$

once we compute it at $m = m_0 = 1$ we have,

$$D(m_0) = D(1) = \frac{\lambda}{J^2}[120 + 48(n - 1)] \tag{3.157}$$

that appears in eq. (3.80).

3.D Appendix: computation of the correlation amplitude

We compute all the saddle point integrals we use to have the equations in the system 3.136. We start from the 3.122 and we expand everything near the saddle point $\boldsymbol{\sigma_0} = (\sigma_0, 0, ..., 0)$:

$$\sigma_x = \sigma_0 + (\sigma_x - \sigma_0) \tag{3.158}$$

$$f(\boldsymbol{\sigma}) \equiv J\sigma^2 + V(\sigma^2) - x_0\sigma_x \tag{3.159}$$

$$f(\boldsymbol{\sigma}) \simeq f(\boldsymbol{\sigma_0}) + \frac{f_{ij}}{2}(\sigma_i - \sigma_{0i})(\sigma_j - \sigma_{0j}) + \frac{f_{ijk}}{6}(\sigma_i - \sigma_{0i})(\sigma_j - \sigma_{0j})(\sigma_k - \sigma_{0k}) +$$
$$+ ... + \frac{f_{ijklm}}{5!}(\sigma_i - \sigma_{0i})(\sigma_j - \sigma_{0j})(\sigma_k - \sigma_{0k})(\sigma_l - \sigma_{0l})(\sigma_m - \sigma_{0m}) + ... \tag{3.160}$$

where $f_{ij...k} = \frac{\partial}{\partial \sigma_i}\frac{\partial}{\partial \sigma_j}...\frac{\partial}{\partial \sigma_k}f\Big|_{\boldsymbol{\sigma}=\boldsymbol{\sigma_0}}$ and we are using the Einstein summation convention. Hence we make into the integral of the 3.122 the expansion near $\boldsymbol{\sigma_0}$, followed by the substitution $\boldsymbol{z} = \beta^{1/2}(\boldsymbol{\sigma} - \boldsymbol{\sigma_0})$:

$$\frac{x_0}{2J} = \sigma_0 + \tag{3.161}$$

$$+ \beta^{-1/2} \frac{\int \mathrm{d}\boldsymbol{z} \ z_x e^{-\frac{f_{ij}}{2}z_i z_j} \left[1 - \left(\beta^{-1/2}\frac{f_{ijk}}{6}z_i z_j z_k + ... + \beta^{-3/2}\frac{f_{ijklm}}{5!}z_i z_j z_k z_l z_m + ...\right) + \frac{1}{2}(...)^2 + ...\right]}{\int \mathrm{d}\boldsymbol{z} \ e^{-\frac{f_{ij}}{2}z_i z_j} \left[1 - \left(\beta^{-1/2}\frac{f_{ijk}}{6}z_i z_j z_k + ... + \beta^{-3/2}\frac{f_{ijklm}}{5!}z_i z_j z_k z_l z_m + ...\right) + \frac{1}{2}(...)^2 + ...\right]} \tag{3.162}$$

From now on we will not write some terms, mainly because they do not contribute for symmetry reasons in the integral or because they vanish once calculated in the marginal case (e.g. $V''(\sigma_0 = 1)$). Expanding x_0 up to T^2 order we have,

$$\frac{x_0}{2J} \simeq \sigma_0 - T\frac{1}{6}\sum_{ijk} f_{ijk} \langle z_x z_i z_j z_k \rangle_0 - T^2\frac{1}{5!}\left(\sum_{ijklm} f_{ijklm} \langle z_x z_i z_j z_k z_l z_m \rangle_0 + \text{"irrelevant" terms}\right) \tag{3.163}$$

where,

$$\langle (...) \rangle_0 = \frac{\int \mathrm{d}\boldsymbol{z} \ (...) e^{-\frac{f_{ij}}{2}z_i z_j}}{\int \mathrm{d}\boldsymbol{z} \ e^{-\frac{f_{ij}}{2}z_i z_j}} \tag{3.164}$$

To compute the Gaussian averages we will use Wick's theorem, hence we need to know the Gaussian average $\langle y_a y_b \rangle_0 = (f^{-1})_{ab}$, where f^{-1} is the inverse of the matrix of the second derivatives of the function $f(\boldsymbol{\sigma})$, evaluated for $\boldsymbol{\sigma} = \boldsymbol{\sigma}_0$. We will discover that the matrix is diagonal, hence $(f^{-1})_{ab} = (f_{ab})^{-1}$. We start computing f_{ab},

$$f_{ab} = \frac{\partial^2 f(\boldsymbol{\sigma})}{\partial \sigma_a \partial \sigma_b}\Big|_{\boldsymbol{\sigma}=\boldsymbol{\sigma}_0} = \frac{\partial}{\partial \sigma_a}\frac{\partial}{\partial \sigma_b}\left[J\sigma^2 + V(\sigma) - x_0\sigma_x\right]\Big|_{\boldsymbol{\sigma}=\boldsymbol{\sigma}_0} \tag{3.165}$$

$$= \frac{\partial}{\partial \sigma_a} \left[2J\sigma_b + \frac{\sigma_b}{\sigma} V'(\sigma) - x_0 \delta_{bx} \right] \Bigg|_{\boldsymbol{\sigma}=\boldsymbol{\sigma}_0} \tag{3.166}$$

$$= 2J\delta_{ab} + \delta_{ab} \frac{V'(\sigma_0)}{\sigma_0} - \delta_{ax}\delta_{bx} \frac{V'(\sigma_0)}{\sigma_0} + \delta_{ax}\delta_{bx} V''(\sigma_0) \tag{3.167}$$

the only non-zero terms of the matrix are on the diagonal,

$$f_{xx} = 2J + V_0'' \equiv M_x^{-1} \tag{3.168}$$

$$f_{jj} = \frac{2J\sigma_0 + V_0'}{\sigma_0} \equiv M_j^{-1} \qquad \text{for } j \neq x \tag{3.169}$$

Hence we have,

$$\langle y_a y_b \rangle_0 = (f^{-1})_{ab} = \delta_{ab} M_a \tag{3.170}$$

Now we can start to compute the corrections in T and T^2 from the 3.163. The term of the first order in T (we called it before $A_n(\sigma_0)$, see 3.136) according to Wick's theorem and the calculation we just performed reads,

$$A_n(\sigma_0) = \frac{1}{6} \sum_{ijk} f_{ijk} \langle z_x z_i z_j z_k \rangle_0 = \frac{1}{6} \sum_{ijk} f_{ijk} \left(\langle z_x z_i \rangle \langle z_j z_k \rangle_0 + \text{all the other contractions} \right) \tag{3.171}$$

$$= \frac{1}{6} \sum_{ijk} f_{ijk} \left(\delta_{ix} \delta_{jk} M_x M_j + \text{all the other contractions} \right) \tag{3.172}$$

looking at the 3.169 we notice that the term is constant in j so, by a simple renaming of indices, we can simplify further the previous expression,

$$A_n(\sigma_0) = \frac{1}{2} \sum_{ijk} f_{ijk} \delta_{ix} \delta_{jk} M_x M_j = \frac{1}{2} \sum_j f_{xjj} M_x M_j \tag{3.173}$$

To obtain our result we need to compute f_{xjj} (we can start from the previous computation with two derivatives),

$$f_{xjj} = \frac{\partial}{\partial \sigma_x} \frac{\partial}{\partial \sigma_j} \frac{\partial}{\partial \sigma_j} f(\boldsymbol{\sigma}) \Bigg|_{\boldsymbol{\sigma}=\boldsymbol{\sigma}_0} = \frac{\partial}{\partial \sigma_x} \left(2J + \frac{V'(\sigma)}{\sigma} - \frac{\sigma_j^2 V'(\sigma)}{\sigma^3} + \frac{\sigma_j^2 V''(\sigma)}{\sigma^2} \right) \Bigg|_{\boldsymbol{\sigma}=\boldsymbol{\sigma}_0} \tag{3.174}$$

$$= \left[-\frac{V_0'}{\sigma_0^2} + \frac{V_0''}{\sigma_0} + \frac{\delta_{jx} V_0'}{\sigma_0^2} - \frac{\delta_{jx} V_0''}{\sigma_0} + \delta_{jx} V_0''' \right] \tag{3.175}$$

Here too we have two possibilities,

$$f_{xxx} = V_0''' \tag{3.176}$$

$$f_{xjj} = \left[\frac{V_0''}{\sigma_0} - \frac{V_0'}{\sigma_0^2} \right] \qquad \text{for } j \neq x \tag{3.177}$$

where the term f_{xjj} does not depend on j, hence our order T correction is,

$$A_n(\sigma_0) = \frac{1}{2} \sum_j f_{xjj} M_x M_j = \frac{1}{2} \left[f_{xxx} M_x^2 + (n-1) f_{xjj} M_x M_j \right] \tag{3.178}$$

$$= \frac{1}{2}\left[\frac{V_0'''}{(2J+V_0'')^2} + \frac{(n-1)(\sigma_0 V_0'' - V_0')}{\sigma_0(2J\sigma_0 + V_0')(2J+V_0'')}\right] \tag{3.179}$$

as stated before.

For the second order the correction coefficient is, without unnecessary terms,

$$B_n(\sigma_0) = \frac{1}{5!}\sum_{ijklm} f_{ijklm}\langle z_x z_i z_j z_k z_l z_m\rangle_0 = \frac{1}{5!}\sum_{ijklm} f_{ijklm}\left(\langle z_x z_i\rangle\langle z_j z_k\rangle\langle z_l z_m\rangle_0 + \text{all cont.}\right) \tag{3.180}$$

$$= \frac{5!!}{5!}\sum_{ijklm} f_{ijklm}\delta_{ix}M_x\delta_{jk}M_j\delta_{lm}M_l = \frac{1}{8}\sum_{ij} f_{xiijj}M_x M_i M_j \tag{3.181}$$

$$= \frac{1}{8}[f_{xxxxx}M_x^3 + 2(n-1)f_{xxxjj}M_x^2 M_j + $$
$$+ (n-1)(n-2)f_{xiijj}M_x M_i M_j + (n-1)f_{xiiii}M_x M_i^2] \tag{3.182}$$

we did the last passage because we know for sure that each term with some indices i or j different from x it's i(or j)-independent. We know it because the i(or j) dependence can only be expressed through σ_{0j}s and they are all zero if $j \neq x$. Of course in the previous formula it is always $i \neq x$ and $j \neq x$ and in the third term also $i \neq j$. To figure out which terms we do really need and to avoid computing too many derivatives we should keep in mind the fact just stated before that $\sigma_{oj} = 0$ for any $j \neq x$ and the fact that $B_n(\sigma_0)$ will be needed only for the marginal model, at $\sigma_0 = 1$, hence we can completely disregard all terms with $V'(\sigma_0)$, $V''(\sigma_0)$ and $V'''(\sigma_0)$. Guided by these ideas we can compute only the terms,

$$f_{xxxxx} = V_0''''' \tag{3.183}$$

$$f_{xxxjj} = \frac{V_0''''}{\sigma_0} + \text{other terms vanishing at } \sigma_0 = 1 \tag{3.184}$$

$$f_{xiijj} = 0 + \text{other terms} \tag{3.185}$$

$$f_{xiiii} = 0 + \text{other terms} \tag{3.186}$$

$$\tag{3.187}$$

Hence we remain only with,

$$B_n(\sigma_0) = \frac{1}{8}\left[f_{xxxxx}M_x^3 + 2(n-1)f_{xxxjj}M_x^2 M_j\right] \tag{3.188}$$

$$= \frac{1}{8}\left[\frac{V_0'''''}{(2J+V_0'')^3} + \frac{2(n-1)V_0''''}{(2J\sigma_0 + V_0')(2J+V_0'')^2}\right] \tag{3.189}$$

that is what we used in 3.136.

In the end we compute the corrections for s and v, they appeared in eq. 3.131 and 3.135, here we can stop at order T. They are very easy to compute, the first one is:

$$C_1 \equiv \frac{\int d\boldsymbol{\sigma} \ \sigma_{n-1}^2 \ e^{-\beta[J\sigma^2 + V(\sigma^2) - x_0\sigma_x]}}{\int d\boldsymbol{\sigma} \ e^{-\beta[J\sigma^2 + V(\sigma^2) - x_0\sigma_x]}} \tag{3.190}$$

$$= (n-1)\frac{\int \mathrm{d}\boldsymbol{\sigma} \ \sigma_{k\neq x}^2 \ e^{-\beta\left[J\sigma^2+V(\sigma^2)-x_0\sigma_x\right]}}{\int \mathrm{d}\boldsymbol{\sigma} \ e^{-\beta\left[J\sigma^2+V(\sigma^2)-x_0\sigma_x\right]}} \tag{3.191}$$

$$\simeq (n-1)T\frac{\int \mathrm{d}\boldsymbol{z} \ z_{k\neq x}^2 \ e^{-\frac{f_{ij}}{2}z_i z_j}}{\int \mathrm{d}\boldsymbol{z} \ e^{-\frac{f_{ij}}{2}z_i z_j}} \tag{3.192}$$

$$= (n-1)T\left\langle z_{k\neq x}^2\right\rangle_0 = (n-1)TM_{k\neq x} = \frac{(n-1)\sigma_0}{2J\sigma_0+V_0'}T \tag{3.193}$$

and the other, that we find only in the 3.135 is:

$$C_2 \equiv \frac{\int \mathrm{d}\boldsymbol{\sigma} \ (\sigma_x-\sigma_0)^2 \ e^{-\beta\left[J\sigma^2+V(\sigma^2)-x_0\sigma_x\right]}}{\int \mathrm{d}\boldsymbol{\sigma} \ e^{-\beta\left[J\sigma^2+V(\sigma^2)-x_0\sigma_x\right]}} \tag{3.194}$$

$$\simeq T\frac{\int \mathrm{d}\boldsymbol{z} \ z_x^2 \ e^{-\frac{f_{ij}}{2}z_i z_j}}{\int \mathrm{d}\boldsymbol{z} \ e^{-\frac{f_{ij}}{2}z_i z_j}} \tag{3.195}$$

$$= T\left\langle z_x^2\right\rangle_0 = TM_x = \frac{T}{2J+V_0''} \tag{3.196}$$

We start from the standard model, hence we can consider from the start only terms up to order T, using the first and the third equation of the system 3.136 we have an equation for σ_0:

$$V'(\sigma_0) = -2JTA_n(\sigma_0) \tag{3.197}$$

If $\sigma_0 \simeq 1 - aT$ we have:

$$aT^\delta V''(1) = 2JTA_n(1) \tag{3.198}$$

hence we have:

$$\sigma_0 \simeq 1 - \frac{2JA_n(1)}{V''(1)}T \tag{3.199}$$

Using again the equations of 3.136 we can compute s and $\frac{x_0}{2J}$. Notice that, if we look at eq. 3.113 we can say that $\frac{x_0}{2J} = \langle \boldsymbol{\sigma} \rangle$ i.e. the magnetization vector. Given the arbitrary choice we made for the direction of $\boldsymbol{x}_0$ in the beginning, also the magnetization has only the x component different from zero and equal to $\frac{x_0}{2J}$, as one can see in eq. 3.122. Only in the $n=1$ case the average of the spin modulus and the spin average (if one chooses $x_0 > 0$) are the same, indeed in the mono-dimensional case $s = \frac{x_0}{2J}$. For generic n they are different and they are expressed as functions of σ_0 in the equations of 3.136. From there we have, up to order T:

$$\langle \sigma_x \rangle = \frac{x_0}{2J} \simeq \sigma_0 - TA_n(\sigma_0) \simeq 1 - \frac{2JA_n(1)}{V''(1)}T - TA_n(1) \tag{3.200}$$

$$= 1 - \left(\frac{3}{4(J+4\lambda)} + \frac{n-1}{4J}\right)T \tag{3.201}$$

Hence the magnetization depends on n, at first order in T. On the other hand, if we compute $s = \langle |\boldsymbol{\sigma}| \rangle$ at the same order, the n dependent term is exactly canceled:

$$s = \langle |\boldsymbol{\sigma}| \rangle \simeq \frac{x_0}{2J} + \frac{(n-1)}{2(2J\sigma_0+V'(\sigma_0))}T \tag{3.202}$$

$$\simeq 1 - \frac{2JA_n(1)}{V''(1)}T - A_n(1)T + \frac{(n-1)}{4J}T \tag{3.203}$$

$$= 1 - \frac{3}{4(J+4\lambda)}T \tag{3.204}$$

The value of s is the same for all ns, up to order T, in the standard model.

The results for the marginal model will be similar, always using the first and the third equation from 3.136, this time keeping terms up to order T^2, we obtain:

$$\frac{V'(\sigma_0)}{2J} = -TA_n(\sigma_0) - T^2 B_n(\sigma_0) \tag{3.205}$$

Remembering that in the marginal case $V'(1) = V''(1) = V'''(1) = A_n(1) = 0$ and using the usual $\sigma_0 \simeq 1 - aT$:

$$0 = -aT^2 A'_n(1) - T^2 B_n(1) \tag{3.206}$$

that gives $a = B_n(1)/A'_n(1)$. In the $n = 1$ case we discovered that, up to order T we had $\sigma_0 \simeq \frac{x_0}{2J}$, here is exactly the same, just use the equation liking x_0 and σ_0 from the system 3.136. Hence if we want to compute the quantities of interest, up to order T we have:

$$\langle \sigma_x \rangle = \frac{x_0}{2J} \simeq \sigma_0 \simeq 1 - \frac{B_n(1)}{A'_n(1)}T \tag{3.207}$$

$$= 1 - \left(\frac{V'''''(1)}{8JV''''(1)} + \frac{n-1}{4J} \right) T \tag{3.208}$$

$$= 1 - \frac{n+4}{4J}T \tag{3.209}$$

again, it is n-dependent, while the average modulus:

$$\langle |\boldsymbol{\sigma}| \rangle = s \simeq \frac{x_0}{2J} + \frac{(n-1)}{2(2J\sigma_0 + V'(\sigma_0))}T \tag{3.210}$$

$$\simeq 1 - \frac{B_n(1)}{A'_n(1)}T + \frac{n-1}{4J}T \tag{3.211}$$

$$= 1 - \frac{5}{4J}T \tag{3.212}$$

does not depend on n.

3.E   Appendix: thermalization at low temperature

We show in Fig. 3.5 the thermalization at low temperature of the simulation that we used for the results in Fig. 3.4. We see that if we start from a cold configuration, i.e. a configuration with all parallel spins of modulus 1, the thermalization is almost instantaneous. Given that, we started all our simulations in a cold configuration and we discarded for precaution the first 20000 Monte Carlo steps. In this way we are sure that our system has thermalized, even at the lowest temperatures. In these simulation we used a standard Monte Carlo simulation with the Metropolis algorithm [9].
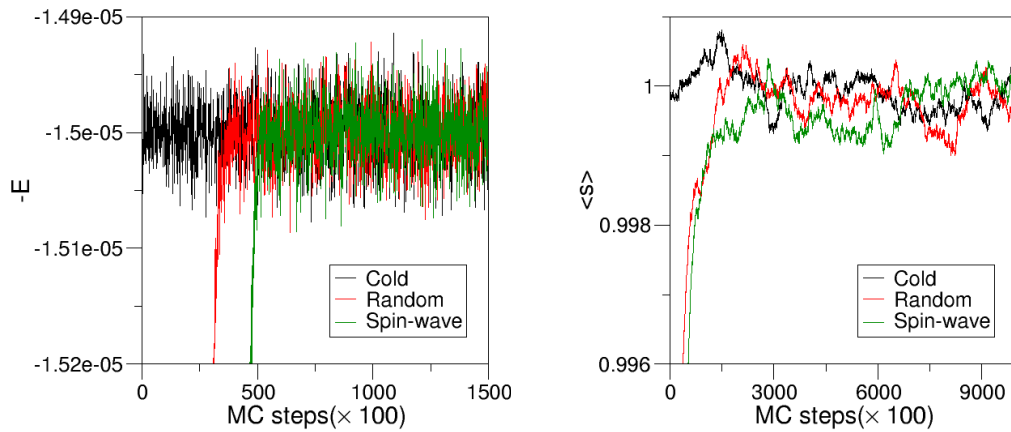
Figure 3.5. Thermalization at low temperature. We show minus the energy and the average spin modulus during a simulation. Size is $L = 60$ and $T = 10^{-5}$ while $J = \lambda = 1$. We initialize the system with all parallel spins of modulus 1 (black), with random spins of modulus 1, such that the average magnetization is 0, (red) and in a spin-wave configuration, i.e. $\sigma_i = (\cos(2\pi n_x/L), \sin(2\pi n_y/L), 0)$ where n_x and n_y are the (x, y) coordinates in the cubic lattice and go from 0 to $L-1$ (green). We can see that if we start from a cold configuration (black) the thermalization is almost instantaneous.

Chapter 4

Experimental and numerical validation of the marginal model

In the previous chapters we presented the main findings in flocks experimental data about scale-free correlations in a polarized phase. We described the properties of ferromagnetic models that are able to reproduce a part of flocks' phenomenology, pointing out that scale-free modulus correlations cannot be explained using standard equilibrium models; a new idea was needed. In the last chapter we described a first attempt in reproducing modulus (that in starling flock is the speed) scale-free correlations, the pseudo-Gaussian model and the marginal model. In this chapter, via the direct comparison between theory, simulations and experimental data, we will show that the marginal model retains all the positive aspects of the pseudo-Gaussian model, yet none of its problems and thus it is the most suitable model for describing starling flocks scale-free speed correlations.

In order to carry out this comparison we adopt the following validation strategy. We perform numerical simulations of self-propelled particles (SPP), using an appropriate dynamics, of both the pseudo-Gaussian model and the marginal model. In this way we can compare directly the models with the experimental data and see what theory is best. Doing SPP simulations is of course more appropriate than just relying on equilibrium results, since all biological systems are out-of-equilibrium. It is also an opportunity to confirm the validity of the local equilibrium approach [85] for a SPP system in its polarized phase. Hence, we need to find a suitable set of dynamics' equations that can include all the marginal model's properties that we described in the previous chapter. We have to promote spins $\boldsymbol{\sigma}_i$ to velocities $\boldsymbol{v}_i$ and find a way to describe the off-equilibrium dynamics of starlings. In order to do so, we will take inspiration from the most influential model of flocking behaviour, i.e. the Vicsek model [49, 110, 111], that will be briefly presented. Secondly we will introduce the pseudo-Gaussian SPP model [12, 34] and finally we will develop an SPP version of the marginal model. The SPP pseudo-Gaussian and marginal models will be compared with experimental data to see if they are capable of reproducing scale-free correlations of speed fluctuations in a regime where the average speed and polarization are compatible with the experimental ones.

The results that we will find in the SPP framework will be similar to the equilibrium ones that we discussed in the previous chapters, even if the interaction

between individuals is time-dependent.

4.1   A paradigm: the Vicsek model

The Vicsek model was introduced in [110], a review of the model and of some of its most recent upgrades can be found in [49]. The model describes a group of N self-propelled particles that move according to a discrete-time dynamics into a volume V. The main mechanism of this model is the alignment of velocities, each particle tends to align its velocity with the velocity of a group of neighbours, which can be defined in many ways, as we shall see later. The dynamics of this system is synchronous, i.e. all particles' positions and velocities are updated at the same time. To better understand the bulk properties of this system, periodic boundary condition are commonly used in simulations. The evolution equations for the particle i with coordinate $\boldsymbol{r}_i$ and velocity $\boldsymbol{v}_i$ is,

$$\boldsymbol{r}_i(t + \Delta t) = \boldsymbol{r}_i(t) + \Delta t \boldsymbol{v}_i(t + \Delta t)$$

$$\boldsymbol{v}_i(t + \Delta t) = v_0 \mathcal{R}_\eta \left[\frac{\sum_k n_{ik}(t)\boldsymbol{v}_k}{|\sum_k n_{ik}(t)\boldsymbol{v}_k|} \right] \tag{4.1}$$

where $\mathcal{R}_\eta$ is an operator that rotates the argument of a random solid angle extracted from a uniform distribution of amplitude $4\pi\eta$, Δt is the time step of the system and v_0 is the fixed value of every velocity modulus. η is a tunable parameter of the system and it goes from 0, when the system is purely deterministic, to 1, when the noise completely dominates the system, thus giving a set of independent random walkers. $n_{ik}(t)$ is the connectivity matrix, determining the interactions between neighbours. It is defined by,

$$n_{ik}(t) = \begin{cases} 1 & \text{if } |\boldsymbol{r}_i(t) - \boldsymbol{r}_k(t)| < r_{int} \\ 0 & \text{if } |\boldsymbol{r}_i(t) - \boldsymbol{r}_k(t)| > r_{int} \end{cases} \tag{4.2}$$

where r_{int} is the radius of interaction of the particles. We can see that the connectivity matrix is time dependent, which means that this is an off-equilibrium model. However, if the modulus of the velocity v_0 is not too big the reshuffling time is much larger than the equilibration time [85]. This means that for suitable time scales this model can be approximated by an equilibrium model with a fixed connectivity matrix. Vicsek model's dynamics is represented in Fig. 4.1, at each time step, every individual computes the average velocity of its neighbours $\boldsymbol{v}_{avg}$ (the individuals in the sphere of radius r_{int}), then its next step's velocity will be $\boldsymbol{v}_{avg}$ normalized in order to have modulus v_0 and rotated of a random solid angle extracted from a uniform distribution. This process mimics the imitation mechanism that is thought to be happening in real flocks, where each bird tries to align its velocity with its neighbours'; the biological mechanism is not perfect, hence the presence of the random rotation.

After fixing arbitrarily time and space units (for example $r_{int} = \Delta t = 1$), one must figure out the control parameters to determine the behaviour of the system. For the Vicsek model the control parameters are the particles speed (velocity modulus) v_0, the density of particles into the volume $\rho_0 = N/V$ and the noise magnitude η. Tuning these parameters, one can explore this system's phases. The Vicsek model
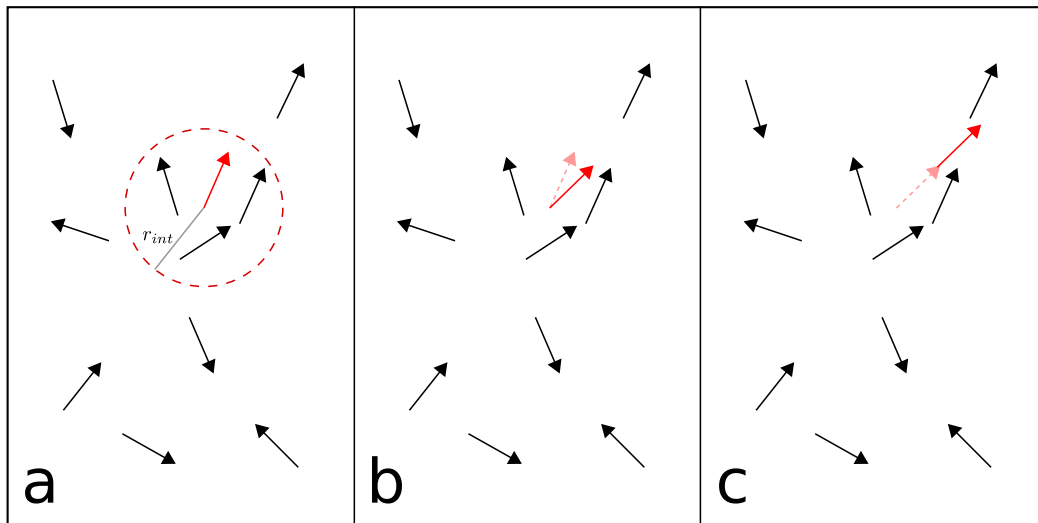
Figure 4.1. Picture of the Vicsek dynamics. Each particle tends to uniform its velocity
with the average of the velocities within its radius of interaction (its own previous velocity
included). This operation cannot happen perfectly, due to the noise enforced in eq. (4.1)
through the random rotation $\mathcal{R}_\eta$. **a**: Each particle computes its new velocity (red arrow)
as the normalized average of all the particles' velocities within the interaction radius
r_{int}. **b**: Then, the new velocity is rotated by a random quantity defined by the noise
magnitude η. **c**: Finally, the particle moves in the direction of the new velocity with a
displacement $v_0 \Delta t$.

possesses various phases, and a spontaneous symmetry-breaking takes place for
specific combinations of its parameters [111]. In particular, if the noise amplitude
is low enough, the system develops a global orientation, i.e. the polarization (1.3)
becomes non-zero [49].

The ordered phase of the Vicsek model, studied by Toner and Tu [106, 108, 109]
is a symmetry-broken phase of a system with a continuous symmetry. This means
that in this phase the system orientational degree of freedom has scale-free connected
correlations functions due to massless Goldstone modes [52]. The reasons of this
feature is explained in chapter 2 for generic continuous symmetry systems. The
peculiarity of this Toner and Tu phase is also the presence of scale-free correlations
in density fluctuations, but this feature has not been detected by analysing the flocks'
spatial fluctuations [23].

The Vicsek model, as it has just been pointed out, can accurately reproduce
the high polarization and the scale-free correlations of the orientational degree of
freedom. Of course, by construction, it cannot show speed fluctuations, so a different
model must be used to describe this phenomenon.

4.1.1   Topological interaction

Among the many possible versions of the Vicsek model [50], we mention the topologi-
cal Vicsek model, in which the interaction rule described in eq. (4.2) is abandoned in
favor of a topological interaction rule. This means that each individual interacts with
a fixed number of neighbours, regardless to their distance from the focal bird. This

choice for the interaction rule is more consistent with the actual mechanism found in starling flocks [8] and other groups of animals [48]. However, in the deeply polarized phase (the Toner-Tu phase [106, 107]), at fixed density, the phenomenology of the topological Vicsek model (i.e. the emergence of Goldstone modes and giant density fluctuations) is very similar to the metric version of the model [49]. Substantial differences are observed when the model undergoes a phase transition from the symmetrical disordered state to the symmetry-broken ordered one, but this regime is not useful to describe starling flocks, that live in the ordered phase, with very high polarization (see chapter 1).

4.1.2 Continuous time Vicsek model

The first formulation of the Vicsek model [110] was crucial to understand the fundamental properties of active particles and collective motion. It is also easy to perform numerical simulation with the original form of the Vicsek model, due to its discrete time. However, a continuous time version is more suitable to perform analytical calculations and to generalize the model to include speed fluctuations. A possible continuous version of the Vicsek model is defined by the differential equations,

$$
\begin{aligned}
\frac{\mathrm{d}\boldsymbol{r}_i}{\mathrm{d}t} &= \boldsymbol{v}_i \\
\frac{1}{\gamma}\frac{\mathrm{d}\boldsymbol{v}_i}{\mathrm{d}t} &= \frac{J}{v_0^2}\sum_k n_{ik}(t)\boldsymbol{v}_k + \lambda_i\boldsymbol{v}_i + \boldsymbol{\eta}_i
\end{aligned}
\tag{4.3}
$$

where the term γ fixes the timescale of the system's dynamical update, the constant J is the interaction strength (that was not present in the discrete time model), the term $\sum_k n_{ik}(t)\boldsymbol{v}_k$ is the short-range interaction term with the matrix $n_{ik}(t)$ defined by eq. 4.2, λ_i is a Lagrange multiplier that enforces the constraint $|\boldsymbol{v}_i| = v_0$ for every i and $\boldsymbol{\eta}_i$ is a Gaussian white noise with zero mean and variance,

$$
\langle \eta_{i\alpha}(t)\eta_{j\beta}(t') \rangle = \frac{2T}{\gamma}\delta_{ij}\delta_{\alpha\beta}\delta(t - t')
\tag{4.4}
$$

where α, β are $\boldsymbol{\eta}$'s dimensions. While in the discrete case we quantified the noise variance with the scalar η, here we use the temperature T. We can express the velocity equation of 4.3 as,

$$
\frac{1}{\gamma}\frac{\mathrm{d}\boldsymbol{v}_i}{\mathrm{d}t} = -\frac{\mathrm{d}H}{\mathrm{d}\boldsymbol{v}_i} + \lambda_i\boldsymbol{v}_i + \boldsymbol{\eta}_i
\tag{4.5}
$$

thus introducing the pseudo-Hamlitonian,

$$
H = -\frac{J}{v_0^2}\sum_{i,k} n_{ik}(t)\boldsymbol{v}_i \cdot \boldsymbol{v}_k
\tag{4.6}
$$

that resembles the pseudo-Hamiltonian of a spin model [63].

4.2   Fluctuating speed SPP models

Following the idea of equations 4.5 and 4.6 we can think of a model that contains the Vicsek nearest-neighbours interaction and that allows fluctuating speed [12, 34]. The evolution equations will be,

$$\frac{\mathrm{d}\boldsymbol{r}_i}{\mathrm{d}t} = \boldsymbol{v}_i$$
$$\frac{1}{\gamma}\frac{\mathrm{d}\boldsymbol{v}_i}{\mathrm{d}t} = -\frac{\mathrm{d}H}{\mathrm{d}\boldsymbol{v}_i} + \boldsymbol{\eta}_i \tag{4.7}$$

that are simply eq.s 4.5 without the Lagrangian multiplier to fix the speed. The noise $\boldsymbol{\eta}$ is a Gaussian white noise with the same variance as the Vicsek model (see eq. 4.4). The Hamiltonian H, that now must contain an interaction term and a speed-buonding potential, can be chosen between the pseudo-Gaussian Hamiltonian (3.7) and the marginal Hamiltonian (3.36). If we convert spins into velocities and we introduce a reference value v_0 for the speed we have,

$$H_{Gauss}(\{\boldsymbol{v}_i\}) = \frac{J}{2v_0^2}\sum_{i,j} n_{ij}(t)(\boldsymbol{v}_i - \boldsymbol{v}_j)^2 + \frac{g}{v_0^2}\sum_i (v_i - v_0)^2 \tag{4.8}$$

$$H_{Mrg}(\{\boldsymbol{v}_i\}) = \frac{J}{2v_0^2}\sum_{i,j} n_{ij}(t)(\boldsymbol{v}_i - \boldsymbol{v}_j)^2 + \frac{\lambda}{v_0^8}\sum_i \left(v_i^2 - v_0^2\right)^4 \tag{4.9}$$

We point out that the interaction matrix depends on time $n_{ij} = n_{ij}(t)$, this is the main feature that keeps the system out-of-equilbrium. There is a continuous reshuffling of the individuals inside the interaction radius that defines the matrix, following eq. 4.2. For a more detailed connection between the stochastic equations (4.7) and the equilibrium distribution (3.2) presented in the previous chapter, see appendix 4.A. In appendix 4.B we will present a more complex version of the Gaussian model, the StarDisplay model, introduced in [59, 60]. The StarDisplay model makes use of a different approach to biological system's modeling, but it is nevertheless based on some common ideas.

In order to check the theoretical results of the previous section and to compare our models with data, we performed numerical simulations using the Euler scheme [97] on the system of differential equations 4.7, our discretized equations are,

$$\boldsymbol{r}_i(t + \Delta t) = \boldsymbol{r}_i(t) + \boldsymbol{v}_i(t)\Delta t$$
$$\boldsymbol{v}_i(t + \Delta t) = \boldsymbol{v}_i(t) + \boldsymbol{F}_i\Delta t + \delta\boldsymbol{\eta}_i \tag{4.10}$$

where we set $\gamma = 1$ through a rescaling of time and the force is the derivative of the pseudo-Hamiltonians eq. 4.8 and 4.9,

$$\boldsymbol{F}_i^{Gauss} = -\frac{\mathrm{d}H_{Gauss}}{\mathrm{d}\boldsymbol{v}_i} = -\frac{J}{v_0^2}\sum_k n_{ik}(\boldsymbol{v}_i - \boldsymbol{v}_k) + \frac{2g}{v_0^2}\frac{\boldsymbol{v}_i}{|\boldsymbol{v}_i|}(v_0 - |\boldsymbol{v}_i|) \tag{4.11}$$

$$\boldsymbol{F}_i^{Mrg} = -\frac{\mathrm{d}H_{Mrg}}{\mathrm{d}\boldsymbol{v}_i} = -\frac{J}{v_0^2}\sum_k n_{ik}(\boldsymbol{v}_i - \boldsymbol{v}_k) + \frac{8\lambda}{v_0^8}\boldsymbol{v}_i\left(v_0^2 - \boldsymbol{v}_i^2\right)^3 \tag{4.12}$$

and the noise $\delta\boldsymbol{\eta}_i$ is a random gaussian variable with zero mean and variance,

$$\sigma_\eta^2 = 2dT\Delta t \tag{4.13}$$

often in literature one can find references to the single-particle part of eq. 4.11 as "linear speed control", even if the actual form of this term is not linear. This name refers to the fact that the potential is pseudo-quadratic (or pseudo-Gaussian), hence the force is "pseudo-linear" that becomes, for brevity, "linear". Using the equations 4.10 we simulated the pseudo-Gaussian model and the marginal model. Both models where simulated for various sizes and for the Gaussian model we report the results for some values of the parameter g. All the other parameters (see appendix 4.C for further explanation) were kept fixed.

4.3   Gaussian incompatibility

Adapting the equilibrium results of eq. (3.23) we can predict the form of the distribution of the average speed $s = 1/N \sum_i v_i$,

$$P(s) = \frac{1}{Z} s^{d-1} \exp\left\{\left[-\frac{Ng}{Tv_0^2}(s - v_0)^2\right]\right\} \tag{4.14}$$

We stress that the above approximation is reasonable even in our out-of-equilibrium simulations, as we can see from the match between coloured points and solid lines in Fig (4.2-**b**). This means that all the approximations in the previous chapter remain legitimate. Given that, the typical speed is (adapting eq. (3.25)),

$$s_{typical} = v_0\left[\frac{1}{2} + \frac{1}{2}\sqrt{1 + \frac{4T}{Ng}}\right] \tag{4.15}$$

This result shows that the typical speed is substantially different from v_0 for small N, if g is too small, the same happens for the mean speed as it is clearly shown in Fig. (4.2). This result makes us think that, if we want the typical (and mean) speed to be close to the reference value v_0 for every flock, regardless to their size N, the parameter g must be big. From the equation above we can say,

$$g \gg \frac{1}{N} \tag{4.16}$$

We do not bother with the value of T, because if we look at the structure of the model, both the Hamiltonian and the evolution equations and we stay within the quasi-equilibrium approximation, we can see that actually the group of parameters T, J and g is redundant and can be simplified by fixing $T = 1$ while moving only J and g.

   We wish to draw the reader's attention on the fact that, despite the approximations we used to derive them (in particular the fixed network assumption), the analytical results above in perfect agreement with numerical simulations performed by using an actual self-propelled particle model (Fig. (4.2)). This is not surprising, considering that in the deeply ordered flocking phase the time scale to reshuffle the interaction network is much larger than the time of local relaxation [85]. For what concerns the speed correlation length, we adapt the equilibrium result of eq. (3.30),
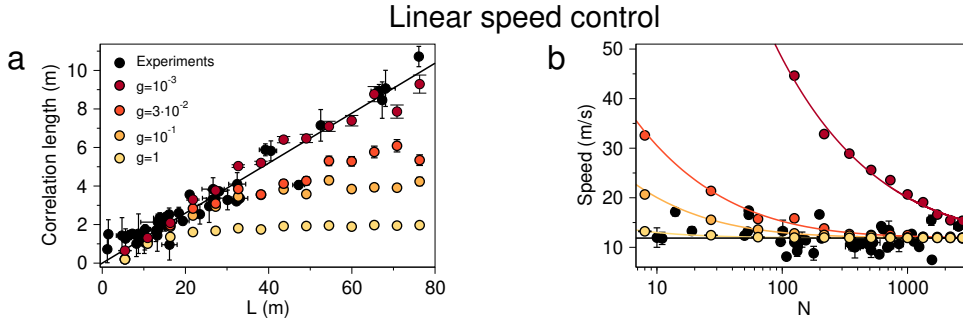
$$\xi_{speed} \sim r_c\sqrt{\frac{Jn_c}{g}} \tag{4.17}$$

Figure 4.2. Gaussian model simulations and experimental data. a: Natural flocks show a clear scale-free behaviour of the speed correlation length, ξ_{sp}, which scales linearly with L (Pearson coefficient $r_P = 0.97$, $p < 10^{-9}$). SPP simulations with linear speed control yields scale-free correlations over the entire range of L only at the *smallest* value of the stiffness g (dark red). **b**: Natural flocks show no detectable dependence of their mean speed on the number of birds in the flock (Spearman coefficient $r_S = -0.13$, $p = 0.21$; the black line is the average over all flocks). SPP simulations with linear control give a near-constant speed compatible with experiments only at the *largest* value of the stiffness g (light yellow); coloured lines represent the theoretical prediction, computed using the distribution (4.14). Linear speed control is therefore unable to reproduce both experimental traits at the same time.

where r_c is the average nearest neighbour distance. Once again, if the system at finite size shows scale-free correlations, i.e. a correlation length that scales with the size of the system, the bulk correlation length must be much greater then the system's size, which means,

$$\xi_{speed} \gg L \tag{4.18}$$

that gives a constraint on the parameter g,

$$g \ll L^{-2} \tag{4.19}$$

the relation above is only asymptotic, we are not including all the other constants that appear in eq. (4.17) because they are fixed by experimental data. This means that n_c and r_c can be directly matched, while J can be determined by matching the model's polarization with the experimental value. If we compare the result of the typical speed eq. (4.16) and the above relation (4.19) we have that g must satisfy simultaneously,

$$N^{-1} \ll g \ll L^{-2} \tag{4.20}$$

if for simplicity we imagine that our system is isotropically distributed in the 3D space we have $N \sim L^3$ and thus,

$$L^{-3} \ll g \ll L^{-2} \tag{4.21}$$

The relation above makes very hard for a single value of g to suit our needs for every value of L. To see if it is still manageable with this model to achieve simultaneously an average speed value coherent with experimental results while having scale-free speed correlations, we perform numerical simulations and we directly compare them with experimental data from starling flocks.

4.3.1   Pseudo-Gaussian model and data

The comparison between data and the Gaussian model is shown in Fig. (4.2), where experimental points are in black, simulations points are colored and the theoretical prediction of the average speed is represented by solid colored lines. Looking at panel **a** of the figure we can immediately see that, when g is small enough (dark red points), the model reproduces the scale-free behaviour of experimental data, for every size L in the accessible experimental range, just as we expected from the theoretical prediction of eq. (4.19). On the other hand, if g is too small (orange points and yellow points), from a certain size $\bar{L}$ the system's correlation length saturates to its bulk value and stays almost constant for every $L > \bar{L}$. Looking at panel **b**, however, gives us exactly the opposite problem; when g is large enough (yellow points) the speed stays almost constant for every number of individuals N and it is compatible with the experimental data while if g is too small (orange and dark red points) the average speed grows to unrealistically large values for the smaller Ns. This means that the pseudo-Gaussian model (or linear speed control model [34]) is not capable of reproducing with a single set of parameters the scale-free behaviour of the speed correlation length together with the constant value of the speed over all the flocks available.

A possible solution is to use a different value of g for every flock in order to ensure that each single system possesses this two properties simultaneously. This idea assumes the existence of a tuning mechanism such that the speed stiffness g depends on the size L of the flock, in a way to satisfy the condition,

$$\frac{1}{L^3} \ll g(L) \ll \frac{1}{L^2} \tag{4.22}$$

This is a rather narrow strip for $g(L)$ to live in, so that a biological mechanism fulfilling (4.22) would require some very tricky size-dependent fine-tuning. But in fact, even that could be insufficient: the two inequalities in (4.22) are asymptotic, namely they require the stiffness g to stay well clear of both boundaries, $1/L^3$ and $1/L^2$, not just between them; for medium-small values of L this becomes harder and harder to achieve. We can think of condition (4.22) as a wedge on the (g, L) plane, a wedge that closes rapidly when L decreases; the only way to keep this wedge open also for small values of L would be to tune also all other parameters, r_1, J, n_c, v_0 etc, beside tuning the stiffness g. Such a grandiose tuning seems unlikely, if not impossible, to achieve. We believe it is more realistic to turn to some other, tuning-free, control mechanism.

Given this problems with the pseudo-Gaussian model, a novel approach is needed in order to reproduce a constant average speed over all the observed system's sizes and scale-free correlations too. From the previous chapters 2 and 3 and the Gaussian model's results we can learn that, if we want to obtain scale-free speed correlations, we must have a free energy that is flat in the direction of the speed fluctuations. This is achievable for the Gaussian model, but at the cost of decreasing the stiffness of the whole bounding potential, eventually arriving at the singular limit $g \to 0$, where the energy is unbounded and the system is ill-defined. In the next section we will overcome this problem using the marginal model in its SPP version.
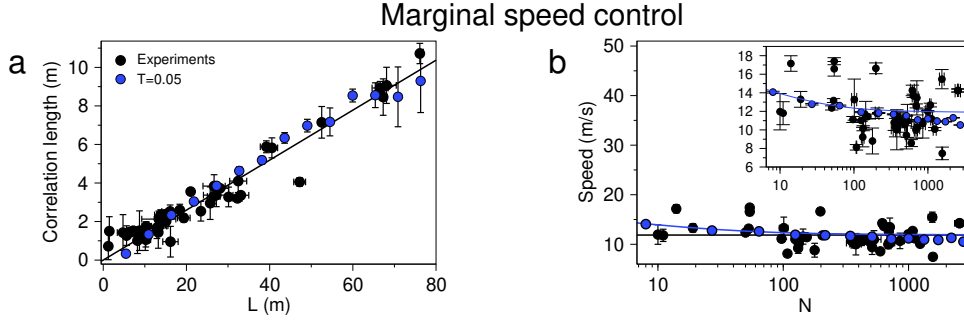
Figure 4.3. Marginal model simulations and experimental data. a: The correlation length in SPP simulations with marginal speed control scales linearly with L over the full range, provided that the temperature/noise T is low enough to have a polarization equal to the experimental one. **b**: At the *same* value of the parameters as in panel a, SPP simulations with marginal control give mean group's speed very weakly dependent on N, fully compatible with the experimental data; the blue line represents the theoretical prediction of (4.23). Inset: same data over a smaller range to appreciate the agreement between theory and simulations.

4.4 Marginal SPP model

From the equilibrium analysis of the marginal model of chapter 3 we see that, at least at mean field level, the marginal model presents a critical regime for $T \to 0$, where we expect for the speed degree of freedom to be scale-free. This phenomenon happens without the need to lower the potential stiffness, we only need to select a temperature low enough for the largest system to be scale-free. Let us see if this property is preserved when we transform the equilibrium spins of the previous chapter into velocities of self-propelled particles. We substitute the pseudo-Gaussian Hamiltonian with the marginal one. Hence the evolution equations will be the same, i.e. eq. (4.7), with the white noise variance of eq. (4.4) and the marginal Hamiltonian of eq. (4.9). Following the idea that the marginal model should presents scale-free speed correlations in the polarized phase just lowering enough the temperature T, we proceed to compute the approximate speed distribution via the spin-wave approximation [41] to see what happens for the marginal case. We performed numerical integration over the system of differential equations of the marginal SPP model, using the same Euler scheme of eq. (4.10), but this time the force is the marginal one, defined in eq. (4.12). Our theoretical prediction for the probability distribution of the average speed will be (adapting eq. (3.95)),

$$P(s) = \frac{1}{Z} s^{d-1} \exp\left\{ \left[-\frac{N\lambda}{Tv_0^8}(s^2 - v_0^2)^4 \right] \right\} \tag{4.23}$$

which gives a typical speed (from (3.97)),

$$s_{typical} \simeq v_0 \begin{cases} 1 + \left(\frac{T}{32N\lambda}\right)^{1/3} & \text{for } N \gg \frac{T}{\lambda} \\ \left(\frac{T}{4N\lambda}\right)^{1/8} & \text{for } N \ll \frac{T}{\lambda} \end{cases} \tag{4.24}$$

Simulation and theoretical results, compared with experimental data, are shown in Fig. (4.3). We can see that, with a single set of parameters, the marginal SPP

model is capable of reproducing, for the whole range of experimental data, both scale-free speed correlations (panel **a**) and almost constant speed for every N (panel **b** and inset). Once again we can also see from panel **b** that the theoretical prediction (solid blue line) is accurate with respect to the simulation results (blue points), thus confirming the validity of the quasi-equilibrium approximation [85].

Another evidence that confirms the strength of the marginal model, is that individual speed distributions have a good match with experimental ones. In Fig. (4.4) we can see that, once we choose for the Gaussian model a low enough g such that the correlation length scales with the size if the system, the individual speed distribution does not resemble at all the experimental individual speed distribution. On the other hand, the marginal model can reproduce effectively, with the same parameter choice that guarantees scale-free correlations, the experimental individual speed distributions.

One could expect that the single-individual speed distribution of the marginal model would have a vanishing second derivative in its maximum, just like the bare marginal potential's minimum or the Gibbs free energy minimum (in Fig. 3.3 we see its mean-field approximation) in the vanishing temperature limit. In fact, our expectations are different, we know that if we put our system exactly at $T = 0$, our marginal model is built in order to produce a system in its lowest energy state, where all the velocities are parallel with a modulus equal to v_0, hence the speed probability distribution of a single-individual for zero temperature is a delta function $P(s_i) = \delta(s_i - v_0)$. This limit distribution does not have a flat maximum, its curvature in the maximum goes to $-\infty$ while we decrease the temperature. Given that, our system should not have a finite temperature at which the probability distribution has a flat maximum, the "flatness" of the Gibbs free energy does not come from the single individual's probability distributions but it is linked to the divergence of the modulus susceptibility, a collective quantity that is not captured by any single-individual observable. We think that this point is quite solid but it could be strengthened by calculations and simulations.

We have achieved our goal; with the marginal model we can reproduce all the relevant phenomenology that is encountered in experimental data, with a single set of a small number of parameters (details about simulations in appendix 4.C). Using this model, we have a low-temperature phase where the polarization is high, the speed is around the reference value v_0 and the modulus fluctuations are scale-free correlated. We do not need any kind of fine-tuning, a single set of parameters is valid for all the sizes we analyzed in experimental data because the "critical" temperature of reference is $T = 0$. This means that, if we were to extend the model to bigger sizes, we would not need to tune the parameters to a particular finite value, we only need to lower the temperature and then adjust the other parameters to obtain the right polarization. This idea is simpler from a biological point of view and can be reversed in the following way: each individual from a flock has the same T, which measures the noise of the procedure of alignment with its neighbours and of its own speed control, the largest flock that can be formed is then the largest flock that has scale-free correlations with that given magnitude of noise T. We stress once again that all the main flocking phenomenology that we described in the first chapter is achieved by the marginal theory by doing just one very sensible thing, namely pushing the system into the ordered phase real flocks naturally belong to.
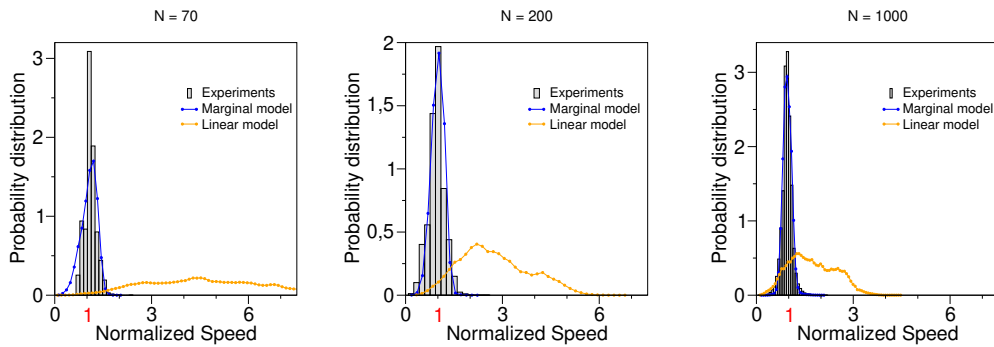
Figure 4.4. Individual speed distributions for some sizes. Histograms of individual speed distributions for experimental data (grey bars) superimposed with the result from marginal SPP simulations (blue line and points) and Gaussian (or linear) model simulations with $g = 10^{-3}$ in order to match the scale-free beahviour (orange line and points). The experimental speeds have been normalized by the total average speed ($v_{bio} \simeq 11.9m/s$) while the simulations speed have been normalized by the reference value v_0. We show the results for three sizes, 70 individuals (panel **a**) 200 individuals (panel **b**) and 1000 individuals (panel **c**). It is evident that the marginal model matches the experimental data while the Gaussian model is not compatible, both for the mean value and for the variance. One may ask if we expect to see the single-individual distribution to be flat in the maximum, mimicking the marginal potential minimum. In fact this is not the case as we explain in the main text.

The entropy-triggered conflict between scale-free correlation and moderate group speed that hinders linear control is therefore resolved by the marginal theory without any fuss. One could say that the choice of the theory's potential, i.e. the marginal potential, is itself a sort of fine-tuning, since every power of v_i^2 in the explicit form of the potential must be exactly that precise number, in order to obtain a zero-curvature minimum. This is true, but we stress the fact that any kind of soft potential with a vanishing second derivative in its minimum (which must be different from zero) can give the same result, since this is the most important ingredient of the model. Hence, we have potentially an infinite space of valid potentials which should bear the same result of our marginal theory, we could think also of non-polynomial potentials and other different kind of functions. Moreover, what we really think is a "weaker" fine-tuning is to define a set of parameters, which is anyway small, that define a theory that is capable of reproducing *all* the observed experimental systems without any size-dependent adjusting. We cannot say the same for the pseudo-Gaussian model that does not posses this same property, and requires a size-dependent choice of the parameters in order to reproduce the experimental results.

4.A   Appendix: Fokker-Planck equation for the SPP model

In order to clarify the link between the stochastic equations (4.7) with the equilibrium models we described in the previous chapter, we will now derive, under a reasonable approximation, the Fokker-Planck equation for the probability distribution of the $\boldsymbol{v}_i$ and we will see that the invariant probability distribution coincides with the Botzmann distribution 3.2, given the identification $\boldsymbol{\sigma}_i \equiv \boldsymbol{v}_i/v_0$. The main approximation we need to use is the "fixed network" approximation, i.e. the interaction matrix does not depend on time $n_{ij}(t) = n_{ij}$. This approximation is reasonable since in the state of the system we want to investigate the typical reshuffling time of the interaction network is greater than the equilibration time [85]. Given this approximation the Hamiltonian ((4.8) or (4.9)) does not depend anymore on the particles' positions, hence, if we want to study the velocities distribution, we can ignore the first equation of (4.7) and we are left with the velocity equation that we write in its discrete-time form (4.10),

$$\boldsymbol{v}_i(t+\Delta t) = \boldsymbol{v}_i(t) + -\frac{\mathrm{d}H(\{\boldsymbol{v}_k\})}{\mathrm{d}\boldsymbol{v}_i}\Delta t + \delta\boldsymbol{\eta}_i(t) \tag{4.25}$$

with the noise distribution that is,

$$P_\eta\left(\delta\boldsymbol{\eta}(t)_i\right) = \frac{e^{-\frac{\delta\eta_i^2}{4T\Delta t}}}{\sqrt{4\pi T\Delta t}} \tag{4.26}$$

and since the noise is uncorrelated we have that $P(\delta\boldsymbol{\eta}(t)_i, \delta\boldsymbol{\eta}(t')_j) = P(\delta\boldsymbol{\eta}(t)_i)P(\delta\boldsymbol{\eta}(t')_j)$. To find an evolution equation for the probability distribution of the $\boldsymbol{v}_i$ trajectories we can use the Chapman-Kolmogorov equation [123],

$$P(\boldsymbol{v}_i, t+\Delta t) = \int_{\mathbb{R}^n} \mathrm{d}^n v_i' \; P(\boldsymbol{v}_i', t)W(\boldsymbol{v}_i, \boldsymbol{v}_i', \Delta t) \tag{4.27}$$

where $P(\boldsymbol{v}_i, t)$ is the probability distribution for the velocity $\boldsymbol{v}_i$ at time t and $W(\boldsymbol{v}_i, \boldsymbol{v}_i', \Delta t)$ is the transition probability from a velocity $\boldsymbol{v}_i'$ to a velocity $\boldsymbol{v}_i$ in a time Δt. Given the noise distribution (4.26) we conclude that,

$$W(\boldsymbol{v}_i, \boldsymbol{v}_i', \Delta t) = P_\eta\left(\delta\boldsymbol{\eta}_i = \boldsymbol{v}_i - \boldsymbol{v}_i' + \frac{\mathrm{d}H(\{\boldsymbol{v}_k'\})}{\mathrm{d}\boldsymbol{v}_i'}\Delta t\right) = \frac{e^{-\frac{\left(\boldsymbol{v}_i - \boldsymbol{v}_i' + \frac{\mathrm{d}H(\{\boldsymbol{v}_k'\})}{\mathrm{d}\boldsymbol{v}_i'}\Delta t\right)^2}{4T\Delta t}}}{\sqrt{4\pi T\Delta t}} \tag{4.28}$$

Now we plug the equation above into the Chapman-Kolmogorov equation (4.27) and we expand the equation for small Δt, up to the first order. After some passages we obtain,

$$\frac{\partial P(\boldsymbol{v}_i, t)}{\partial t} = \frac{\partial}{\partial \boldsymbol{v}_i} \cdot \left[\frac{\mathrm{d}H}{\mathrm{d}\boldsymbol{v}_i}P(\boldsymbol{v}_i, t)\right] + T\Delta_{v_i}P(\boldsymbol{v}_i, t) \tag{4.29}$$

hence if we want the invariant distribution we have to solve the equation,

$$\frac{\partial P(\boldsymbol{v}_i, t)}{\partial t} = 0 = \frac{\partial}{\partial \boldsymbol{v}_i} \cdot \left[\frac{\mathrm{d}H}{\mathrm{d}\boldsymbol{v}_i} P_{inv}(\boldsymbol{v}_i) + T \frac{\partial}{\partial \boldsymbol{v}_i} P_{inv}(\boldsymbol{v}_i) \right] \tag{4.30}$$

which gives,

$$P_{inv} = \frac{1}{Z} e^{-\beta H(\{\boldsymbol{v}_i\})} \tag{4.31}$$

where Z is determined by the normalization. The equation above is equivalent to the equilibrium Boltzmann distribution 3.2, given that we used the fixed network approximation to decouple the velocity equation from the positions equation (4.7) that otherwise would have been too difficult to manipulate.

4.B Appendix: the StarDisplay model

Another possible approach to model scale-free speed correlations is presented in [59, 60], where the StarDisplay model is presented and studied. The core of the model is still a pseudo-Gaussian potential on the speeds and a short range interaction term but a lot of other terms have been added in the equations of motion in order to reproduce in great detail the flocking dynamics. While the purpose of the original pseudo-Gaussian model [12, 34] and of the marginal model [27, 34] is to capture the most important features of the flocking phenomenon while using the minimum number of parameter possible, in order to understand the fundamental mechanisms behind the studied biological system, for the StarDisplay model the final purpose is to reproduce the phenomenon in the most accurate way, matching the largest number of details, regardless to the number of parameters needed to do it. The model is defined in discrete time via the equations,

$$\boldsymbol{r}_i(t + \Delta t) = \boldsymbol{r}_i(t) + \boldsymbol{v}_i(t + \Delta t)\Delta t$$
$$\boldsymbol{v}_i(t + \Delta t) = \boldsymbol{v}_i(t) + \frac{1}{m} \left[F_i^{Steering}(t) + F_i^{Flight}(t) \right] \Delta t \tag{4.32}$$

the two forces in the evolution equation of the velocity can be decomposed in,

$$F_i^{Flight} = \boldsymbol{L}_i + \boldsymbol{D}_i + \boldsymbol{T}_0 + m\boldsymbol{g} \tag{4.33}$$
$$F_i^{Steering} = \boldsymbol{F}_i^{Social} + \boldsymbol{f}_i^\tau + \boldsymbol{f}_i^{Roost} + \boldsymbol{f}_i^\zeta \tag{4.34}$$

The first force, the "flight" force F_i^{Flight} is composed by the contributions coming from the standard modeling of fixed wing aerodynamics that are the lift $\boldsymbol{L}_i$, the drag $\boldsymbol{D}_i$, the thrust $\boldsymbol{T}_0$ and the gravity force $m\boldsymbol{g}$. Precise definitions of these forces can be found in [59], each force contains details about the wing length, density of air and other coefficients related to flight dynamics [59]. The steering force $F_i^{Steering}$ is composed by many different contributions. The social force $\boldsymbol{F}_i^{Social}$ contains a term that pushes each individual away from its neighbours, in order to avoid collisions; a term that aligns the velocity of a bird with its neighbours' (the same of the Vicsek model eq. 4.1 without the random rotation) and a cohesion force to prevent the flock from breaking apart. Then we have the force $\boldsymbol{f}_i^\tau$ that is the linear speed control

(just like the Gaussian model), the roosting force $\boldsymbol{f}_i^{Roost}$ that changes the velocity of each individual to point on a precise "roosting site", both horizontally and vertically and the random force $\boldsymbol{f}_i^{\zeta}$ that is a Gaussian white noise. Every force that is present in the steering term has its own parameter that is tuned to an appropriate value to reproduce flocking dynamics [59]. In [60] is shown the same result of [12] and of Fig. 4.2-**a** (dark red points), for a small enough speed control parameter the system is scale-free correlated both in the speed and in the orientation, hence this model is able to reproduce the key features of experimental data. However, we do not know if the StarDisplay model encounters the same problem of the Gaussian model for what concerns average speed value for small systems (i.e red point in Fig. 4.2-**b**). It would be interesting to know if the other terms that are present in this model are able to maintain a reasonable speed for every system's size, even when the speed control is very small.

4.C   Appendix: simulations details

Every SPP simulation has been made with a program made by Tomás S. Grigera adapted by me and my colleague Giulia Pisegna to the Gaussian and the marginal model. The evolution of the system has been performed in a cubic box with periodic boundary conditions, the starting configuration of each simulation was a simple cubic configuration, where each individual was placed at a distance of 1 simulation units from its nearest neighbours, with all the velocities pointing in the same direction. The sizes of the boxes' side goes from $L = 2$ up to $L = 70$ (in simulation units), with a number of individuals going from $N = L^3 = 8$ to $N = 343000$. After eliminating the initial steps of equilibration, measures were made every 1000 steps of integration for a total number of measurement of at least 1000 for every simulation.

Now we will explain the choice of the parameters for our SPP simulations for both the Gaussian and the marginal model. We will also point out the methodology we followed in order to compare simulations' results with experimental ones, especially regarding the systems' linear sizes and number of individuals.

The values of the main parameters we used in both Gaussian and marginal model's simulations are listed in Tab. 4.1, the other parameters we used are listed in the table's caption. As we already partially explained in the main sections of the chapter, the parameters J and v_0 for the Gaussian model and the parameters λ and v_0 for the marginal model are chosen in order to match the experimental value of the polarization 1.3 that is between $\phi \simeq 0.89$ and $\phi \simeq 0.99$. For the Gaussian case g is chosen in order to have either scale-free correlations or average speed close to v_0, for the marginal model T is chosen in order to be in the scale-free regime. Due to the redundancy of the parameters, for the Gaussian model the temperature is fixed to $T = 1$ while for the marginal model we fixed $J = 1$.

For all the simulations we used a metric interaction rule like eq. 4.2, with $r_{int} = 1.2$, such that each bird interacts, in its starting configuration, with its first 6 nearest neighbours because from experimental evidence the average number of interacting birds is close to 6 [8]. When working at fixed average density and in the very low temperature region where density fluctuations are small, there is not great

Speed control	g	λ	T	J
Linear	0.001	-	1	10
	0.03	-	1	10
	0.1	-	1	10
	1.0	-	1	10
Marginal	-	0.001	0.05	1

Table 4.1. Parameters of simulations. In this table we report the values of relevant parameters used in the numerical SPP simulations. The other parameters are the interaction radius $r_{int} = 1.2$, the speed reference value $v_0 = 1$ and the integration time step $\Delta t_{MRG} = 0.01$, $\Delta t_{GAUSS} = 0.001$.

difference between metric and topological interaction. Even though natural flocks are known to have topological interactions [8, 13], we therefore decide to perform simulations with the metric rule, which are much less expensive computationally. In this way, we are able to study systems in $d = 3$ with N up to 3×10^5 particles. We consider a metric connectivity matrix with interaction radius $r_c = 1.2$, such that the number of nearest neighbours at the time $t = 0$ is $n_c = 6$, close to the biological value [8, 13]. We then check a posteriori that the system remains spatially homogeneous in time by computing the distribution of the number of nearest neighbours for every simulation, and verifying that it is always sharply peaked around the initial value $n_c = 6$.

Later in the simulation we measured the average number of interacting birds, to check if there was any significant change during the evolution of the system. With our choice of the interaction range, the number of interacting individuals remains around the reference value of 6. Even if there are evidences that flocks' individuals interacts in a topological fashion [8], we decided to use the metric interaction rule. This decision was made in order to speed up the simulation time, that otherwise would have been extremely long, due to the computation of topological neighbours. Our choice is justified also by the fact that, in the polarized phase, when the quasi-equilibrium approximation is valid [85] we expect the metric connectivity matrix to be almost fixed, which means that the number of neighbours stays the same, just like in the topological interaction. This hypothesis is confirmed by checking the number of particles that are into the interaction radius of a focal particle through a whole simulation. This number does not change from its starting value of 6, hence mimicking the same effect of a topological interaction.

The integration time steps $\Delta t_{MRG} = 0.01$ and $\Delta t_{GAUSS} = 0.001$ were chosen as the largest time steps possible that guarantee energy's stability (the pseudo-Hamiltonian value) during the whole simulation, an example of the procedure we used is presented through Fig. 4.5.
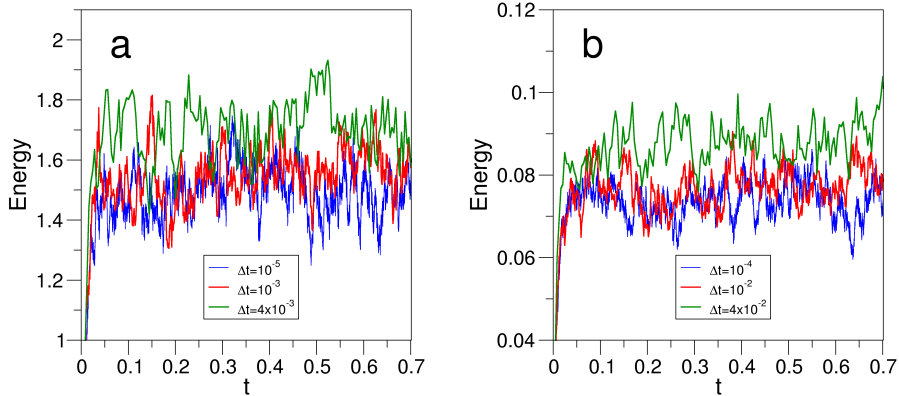
Figure 4.5. Energy as a function of time for different time steps Δt**. a**: Gaussian model. $L = 6$, $g = 10^{-3}$, $J = 10$ and $T = 1$. We can see that if we choose a time step $\Delta t = 0.001$ the energy is stable and its average value and fluctuations are compatible with the energy with a much smaller $\Delta t = 10^{-5}$. Hence we can choose the $\Delta t = 0.001$ as a reasonable time step for our simulations at this size. We repeated this procedure for all our simulations **b**: Marginal model. $L = 6$, $\lambda = 10^{-3}$, $T = 0.05$ and $J = 1$. Here the same arguments apply, a suitable time step for this model is $\Delta t = 0.01$.

4.C.1   Comparing simulation sizes with experimental sizes

We have a large set of simulations that span from a handful of particles ($N = 8$) to $O(10^6)$ individuals. We performed this simulations in a cubic box with periodic boundary conditions and we must find a sensible way to compare our simulations with experimental data.

In order to compare models and data for what concerns the average speed versus the number of particles in the system, the identification is quite straight forward: we compare the simulation with a certain number of particles N with data from a flock that has the same number of individuals $N_{bio} = N$. Since simulations are performed in cubic boxes, the box side L of a simulation corresponding to a certain N_{bio} will be the closest integer to $(N_{bio})^{1/3}$.

To compare the average speeds' values we divide every simulation speed by the reference value v_0 and we multiply it for the total mean speed of all the flocking events, which is $s_{bio} \simeq 11.9 \; m/s$. This last operation is sensible because we can consider average flocks' speeds to be independent from the number of individuals in the system. The Spearman coefficient $r_{Sp} = -0.13$ and the Spearman p-value $p_{Sp} = 0.21$ are high, which means that is highly unlikely that the average speed is correlated with the number of individuals in the system (black points of Fig. 4.2-**b** and 4.3-**b**). Using this procedure we could realize the coloured plots in Fig. 4.2-**b** and 4.3-**b**.

The situation is more sophisticated when we want to compare real sizes in meters with the arbitrary simulation units of length. We decided to use the nearest neighbours distance as the equivalence measure, hence we computed the average nearest neighbour distance in data, which is $r_c^{bio} \simeq 1.2 \; m$, and we put it equal to

the same quantity computed in simulations $r_c \simeq 1$ (simulation units). Now the procedure is similar to what we did for speeds, to convert a simulation length to compare it with an experimental length we just have to divide it by r_c and multiply it by r_c^{bio}. Now that we know how to compare lengths we must choose the same method to measure a system linear size. For natural flocks we used the largest distance between two birds in the same flock, that here we call L_{bio}, if we want to use the same rule for simulation we must take into account the fact that we are using periodic boundary conditions, hence the largest distance possible in our box of side L (already in meters) is the half diagonal of the cube $L_{sim} = \sqrt{3}L/2$. In the end if we want a correspondence from L in simulation units to L_{bio} in meters we have,

$$L_{bio} \rightarrow \frac{\sqrt{3}Lr_c^{bio}}{2r_c} \tag{4.35}$$

For the correlation length, which is computed both for simulations and for data in the same way (eq. 1.10), we just have,

$$\xi_{bio} \rightarrow \frac{\xi_{sim}r_c^{bio}}{r_c} \tag{4.36}$$

this last correspondence is, however, redundant because our goal is not to match exactly the value of the correlation length, but to capture the correlation length's linear dependence on the system's size. The precise value of the slope and intercept may vary due to specific details on how correlations are computed, the exact geometry of the system and other details we are not interested in. Given that, we are allowed to add a constant and multiply for another constant the value of the simulations' correlation length, for every model we must obviously use the same set of constants, even if we change the model's parameters. Hence, Fig. 4.2-**a** was made following this procedure: at first we matched the value of system's sizes using the correspondence 4.35, then we multiplied and added a constant to the value of the simulations correlation lengths in order to overlap the straight line points from the scale-free Gaussian model (dark red points with $g = 10^{-3}$) with the experimental ones and in the end we used the same constants to rescale the correlation lengths of the other Gaussian models (orange and yellow points). The same procedure was followed for the marginal model in Fig. 4.3-**a**.

Another aspect of simulations that must be clarified is the difference of aspect ratio between simulations and data. For every simulations we have a fixed aspect ratio that is determined by the structure of the box where the system is enclosed, in our case the volume in which the simulation takes place is a cube, the system density remains constant, hence we have that the aspect ratio is $1 : 1 : 1$. In natural flocks this is not the case, the standard situation is that flocks are elongated towards a particular direction that is perpendicular to the vertical axis [7]. However, the scale-free properties that we are analyzing do not depend on the aspect ratio [7], as we show in Fig.4.6, where the dependence of the correlation length from the system's size is shown for simulated systems with aspect ratios that vary from $1 : 1 : 6$ to $1 : 1 : 9$. We can see from the plot that the phenomenology observed for the cubic case is reproduced even if we perform simulations with a different aspect ratio. The fact that the system's interaction rule is always isotropic gives the same scale-free
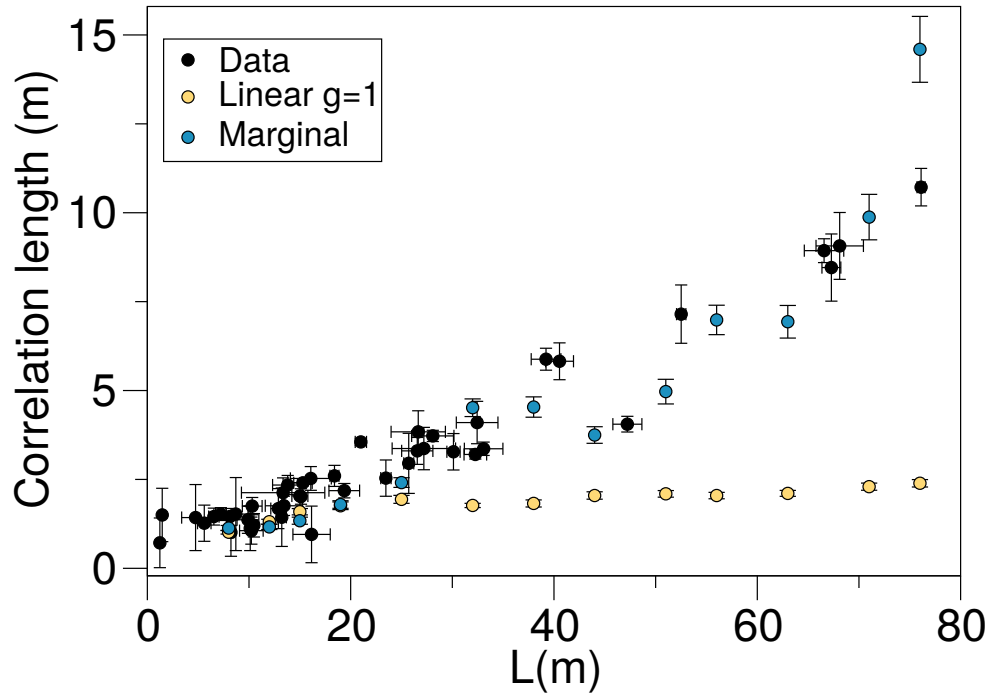
Figure 4.6. Correlation length for simulations with biologically plausible aspect ratios. We present in this plot the correlation length against the size of the system (computed as the largest distance between two individuals) for the case of non-cubic aspect ratios. Each system has a major axis and two equal minor axes, starting from the smallest systems and going up in size L the aspect ratios between the major and the minor axis are: $6, 6, 6, 6, 6.67, 6.25, 7.5, 7.78, 8, 8, 8.33, 8.62, 8.57$. These aspect ratios are comparable with natural flocks' ones, measured in [7]. We can see that the results are similar to the isotropic $1 : 1 : 1$ aspect ratio case of Fig. 4.2 and 4.3, hence the correlation length of the system is correctly compared with the system's size and does not depend on the aspect ratio of the system in a relevant way.

phenomenology, regardless of the shape of the available volume. Once we fix the speed of the Gaussian model to be physical (i.e. we choose a large enough g), no matter how elongated or not is the flock, the system does not shown scale free correlations and the correlation length for a certain small L saturates to a bulk value. On the other hand the marginal model always shows scale-free correlations for all the available experimental sizes.

Chapter 5

Renormalization Group analysis of the marginal model

In the previous chapters we introduced the marginal model (chapter 3) and we studied its non-equilibrium SPP version, comparing simulations' results with experimental data (chapter 4). We have seen that the marginal model is capable of reproducing the speed scale-free correlations that we find in experiments (chapter 1) while having reasonable values for the average speed. These peculiar properties are achieved because the marginal model possesses a critical point for $T = 0$ [27]; for vanishing temperature the system's free energy, which we computed for the equilibrium model in the mean field approximation eq. 3.52, has a zero-curvature minimum that implies a divergent modulus susceptibility.

In this chapter I go back to the equilibrium case and I study in more detail the nature of this zero-temperature critical point, casting the marginal model as a statistical field theory and using the renormalization group in the momentum shell formulation of K.G.Wilson [70, 114, 115].

5.1 Derivation of field theory

In order to build a field theory for the marginal model, we start from the fully-connected mean field approximation of the marginal model that gave us a closed form for the Gibbs free-energy (3.52) [27]. Expanding the mean-field Gibbs free energy near $m = 1$, which is the equilibrium magnetization at $T = 0$, we obtain,

$$
\begin{aligned}
g(m) =& \lambda \left(1 - m^2\right)^4 + T \left[a_2 \left(1 - m^2\right)^2 + a_3 \left(1 - m^2\right)^3 + ...\right] + \\
&+ T^2 \left[a_1 \left(1 - m^2\right) + a_4 \left(1 - m^2\right)^2 + ...\right]
\end{aligned}
\tag{5.1}
$$

where the a_n are some constants of $O(1)$, which depend on the parameters J and λ of the Hamiltonian (3.37). The free energy, given that the Hamiltonian is symmetric under space-independent rotations of all the spins, is $O(n)$ symmetric too, hence it only depends on the squared modulus of its variable m. For $T = 0$ we recover the functional form of the marginal potential, that has a zero-curvature minimum. In order to find a guide to build a consistent statistical field theory, we start from eq.

(5.1) and we reorder the terms in a different way: we write each power of $(m^2 - 1)$, keeping the lowest order in T of each constant in front of the m-dependent terms,

$$g(m) = a_1 T^2 \left(1 - m^2\right) + a_2 T \left(1 - m^2\right)^2 + a_3 T \left(1 - m^2\right)^3 + \lambda \left(1 - m^2\right)^4 + \dots$$

$$(5.2)$$

We will start from this free-energy in order to build a Landau-Ginzburg Hamiltonian [91] for our model. Since our procedure is heuristic, we do not need to know the exact value of the a_n, it suffices to know that they do not depend on the temperature T. Inspired by the functional form of the free energy (5.2) we promote the magnetization to a field $m \to \varphi(\boldsymbol{x})$. The average magnetization modulus at zero temperature is 1, hence we perform the shift $\psi(\boldsymbol{x}) = 1 - \varphi(\boldsymbol{x})$, because we are interested in the system's properties near the marginal critical point at $T = 0$. We ignore the angular degrees of freedom, focusing only on modulus fluctuations, because we know that modulus and phase fluctuations are weakly coupled [17, 93, 100]. We thus obtain the following Landau-Ginzburg Hamiltonian,

$$\beta \mathcal{H} = \frac{1}{T} \int \mathrm{d}^d x \left\{ \frac{1}{2} (\nabla \psi)^2 + \frac{aT}{2} \psi^2 + cT^2 \psi + vT \psi^3 + u \psi^4 + \dots \right\} \qquad (5.3)$$

where a,c,v and u are constants that do not depend on temperature. In conventional field theories [52] we would ignore the factor $1/T$ in front of the Hamiltonian, because at the critical point goes to a harmless constant $1/T_c$. Here, however, we should focus our attention on it because the critical point is $T_c = 0$ [27]. In the next section we show how to deal with this peculiarity.

5.1.1 Initial field rescaling

If we focus on the results of the mean-field approximation of the marginal model (chapter 3), we can see from eq. (3.144) that the modulus connected correlation function at $\boldsymbol{r} = 0$ behaves like,

$$C_0 = \left\langle s_i^2 \right\rangle - \left\langle s_i \right\rangle^2 \sim T \qquad (5.4)$$

that can also be obtained by computing the connected correlation function in the Gaussian approximation of eq. (5.3),

$$\langle \psi(\boldsymbol{k}) \psi(\boldsymbol{k}') \rangle_c^0 = \delta(\boldsymbol{k} + \boldsymbol{k}') \frac{T}{k^2 + aT} \sim \delta(\boldsymbol{k} + \boldsymbol{k}') \frac{C_0}{k^2 + aT} \qquad (5.5)$$

we can see that this situation is problematic, since in the limit of vanishing temperature the correlation function's amplitude C_0 vanishes. We want to investigate the regime of small T where the modulus correlation length is big but at the same time we do not want the amplitude of the correlation function itself to vanish. For this reason it seems natural to re-define the field ψ in this way,

$$\psi' = \frac{\psi}{\sqrt{T}} \qquad (5.6)$$

such that the correlation function of ψ' has a fixed amplitude for every temperature,

$$\langle \psi'(\boldsymbol{k})\psi'(\boldsymbol{k}') \rangle_c^0 = \delta(\boldsymbol{k} + \boldsymbol{k}') \frac{1}{k^2 + aT} \tag{5.7}$$

at least in the Gaussian (and mean-field) approximation. We do not expect great deviations of C_0 from the mean field behaviour, given the simulations results presented in chapter 3 (Fig. (3.4)). Hence if we write the Hamiltonian for ψ', following the definition (5.6), and we switch back to the name ψ the resulting Landau-Ginzburg Hamiltonian is,

$$\beta\mathcal{H} = \int \mathrm{d}^d x \left\{ \frac{1}{2} \left(\nabla \psi \right)^2 + \frac{T}{2} \psi^2 + vT^{3/2}\psi^3 + uT\psi^4 \right\} \tag{5.8}$$

where we also dropped the linear term in ψ because it is unimportant in the study of the critical behaviour of this theory. It can be eliminated with an appropriate shift of the field and, even if we include it in our theory, it doesn't give any correction to the critical exponents (see Appendix 5.A). We also dropped the higher order terms in ψ for notation's clarity, they are discussed in Appendix 5.A. The quadratic coupling a was put equal to 1, it is equivalent to a harmless redefinition of the temperature and the other couplings. The novelty of this field theory is that every coupling is composed by a certain power of T (that here plays the role of a mass) and a T-independent contribution (u and v), a rather uncommon occurrence for standard field theories where usually all the couplings (at tree level) are independent from the temperature (i.e. the mass) [14]. Now we will discuss the potential ambiguities of this situation, to see in which way the critical behaviour of this theory can be analyzed.

5.1.2 Naive dimensional analysis

First of all, we write the Landau-Ginzburg Hamiltonian in momentum space,

$$\beta\mathcal{H} = \frac{1}{2} \int \frac{\mathrm{d}^d k}{(2\pi)^d} \left[\left(k^2 + T \right) \psi_k \psi_{-k} \right] + vT^{3/2} \int \frac{\mathrm{d}^d k_1 \mathrm{d}^d k_2}{(2\pi)^{2d}} \psi_{k_1} \psi_{k_2} \psi_{-k_1 - k_2} +$$
$$+ uT \int \frac{\mathrm{d}^d k_1 \mathrm{d}^d k_2 \mathrm{d}^d k_3}{(2\pi)^{3d}} \psi_{k_1} \psi_{k_2} \psi_{k_3} \psi_{-k_1 - k_2 - k_3} \tag{5.9}$$

where every momentum integral is performed up to a cutoff Λ, that is the inverse of the microscopic lattice spacing. Using the momentum-space Hamiltonian we can compute the naive dimensions,

$$[k] = 1 \quad [\psi_k] = -\frac{d}{2} - 1 \quad [T] = 2 \quad [v] = -\frac{d}{2} \quad [u] = 2 - d \tag{5.10}$$

We immediately see that for $d > 2$ the naive scaling dimension of v and u is negative, hence one may think that for $d = 3$ our model could behave like an infrared-free theory, but at this step it is far from obvious. In fact, if we compute the naive dimensions of the products $vT^{3/2}$ and uT, which appear in front of the interaction terms of the Hamiltonian (5.9), we find,

$$[vT^{3/2}] = 3 - \frac{d}{2} \quad [uT] = 4 - d \tag{5.11}$$

hence if we consider the products above, for $d = 3$, the naive scaling dimension is positive, like a standard φ^4 theory [70]. A more careful analysis is needed to understand which point of view is more informative on the critical behaviour of our system. We need to understand in which way our theory's parameters enter in the critical exponents. We will study this property of the marginal theory using momentum shell renormalization group [114].

5.2   Renormalization group

We perform the Renormalization Group in the Wilson fashion [114], here we will briefly recall the main passages. Our probability distribution is a Boltzmann distribution [63] of the form,

$$P[\psi_{\boldsymbol{k}}] = \frac{1}{Z} e^{-\beta \mathcal{H}[\psi_{\boldsymbol{k}}]} \tag{5.12}$$

where the Hamiltonian $\mathcal{H}$ is defined in eq. 5.9. We now separate each integral over the fields in a part inside the shell (with the momentum k going from 0 to Λ/b) and a part on the shell of thickness b (with k from Λ/b to Λ). The field with momentum smaller than Λ/b will be $\psi_{\boldsymbol{k}}^{<}$ and the field in the shell will be $\psi_{\boldsymbol{k}}^{>}$. The probability distribution is then written as,

$$P\left[\psi_{\boldsymbol{k}}^{<}, \psi_{\boldsymbol{k}}^{>}\right] = \frac{1}{Z} e^{-\beta \mathcal{H}[\psi_{\boldsymbol{k}}^{<}]} e^{-\beta \mathcal{H}_G[\psi_{\boldsymbol{k}}^{>}]} e^{-\beta \mathcal{H}_{INT}[\psi_{\boldsymbol{k}}^{<}, \psi_{\boldsymbol{k}}^{>}]} \tag{5.13}$$

where we divided the original Hamiltonian eq. 5.9 in three parts: the internal $\boldsymbol{k}$ part,

$$\mathcal{H}\left[\psi_{\boldsymbol{k}}^{<}\right] = \frac{1}{2} \int\limits_{0}^{\Lambda/b} \frac{\mathrm{d}^d k}{(2\pi)^d} \left[\left(k^2 + T\right) \psi_{\boldsymbol{k}}^{<} \psi_{-\boldsymbol{k}}^{<}\right] + v T^{3/2} \int\limits_{0}^{\Lambda/b} \frac{\mathrm{d}^d k_1}{(2\pi)^d} \int\limits_{0}^{\Lambda/b} \frac{\mathrm{d}^d k_2}{(2\pi)^d} \, \psi_{\boldsymbol{k}_1}^{<} \psi_{\boldsymbol{k}_2}^{<} \psi_{-\boldsymbol{k}_1-\boldsymbol{k}_2}^{<} +$$

$$+ u T \int\limits_{0}^{\Lambda/b} \frac{\mathrm{d}^d k_1}{(2\pi)^d} \int\limits_{0}^{\Lambda/b} \frac{\mathrm{d}^d k_2}{(2\pi)^d} \int\limits_{0}^{\Lambda/b} \frac{\mathrm{d}^d k_3}{(2\pi)^d} \, \psi_{\boldsymbol{k}_1}^{<} \psi_{\boldsymbol{k}_2}^{<} \psi_{\boldsymbol{k}_3}^{<} \psi_{-\boldsymbol{k}_1-\boldsymbol{k}_2-\boldsymbol{k}_3}^{<} \tag{5.14}$$

the shell Gaussian part,

$$\mathcal{H}_G\left[\psi_{\boldsymbol{k}}^{>}\right] = \int\limits_{\Lambda/b}^{\Lambda} \frac{\mathrm{d}^d k}{(2\pi)^d} \left[\left(k^2 + T\right) \psi_{\boldsymbol{k}}^{>} \psi_{-\boldsymbol{k}}^{>}\right] \tag{5.15}$$

and the remaining interaction part $\mathcal{H}_{INT}\left[\psi_{\boldsymbol{k}}^{<}, \psi_{\boldsymbol{k}}^{>}\right]$ that contains all the cubic and quartic terms that have at least one integral over the shell. Now the first step of the momentum shell renormmalization group can take place, we integrate the exponential of the interaction Hamiltonian $\mathcal{H}_{INT}\left[\psi_{\boldsymbol{k}}^{<}, \psi_{\boldsymbol{k}}^{>}\right]$ using the Gaussian measure, defined by the Hamiltonian $\mathcal{H}_G\left[\psi_{\boldsymbol{k}}^{>}\right]$, in order to marginalize the probability distribution,

$$\begin{aligned} P[\psi_{\boldsymbol{k}}^{<}] &= \frac{1}{Z} e^{-\beta \mathcal{H}[\psi_{\boldsymbol{k}}^{<}]} \left\langle e^{-\beta \mathcal{H}_{INT}[\psi_{\boldsymbol{k}}^{<}, \psi_{\boldsymbol{k}}^{>}]} \right\rangle_G \\ &= \frac{1}{Z} \exp\left\{-\beta \mathcal{H}\left[\psi_{\boldsymbol{k}}^{<}\right] + \log \left\langle e^{-\beta \mathcal{H}_{INT}[\psi_{\boldsymbol{k}}^{<}, \psi_{\boldsymbol{k}}^{>}]} \right\rangle_G \right\} \end{aligned} \tag{5.16}$$

If we expand diagramatically the logarithm and the exponential of the interaction Hamiltonian, we obtain all the one-particle irreducible [14, 121] diagrams with external legs that are $\psi_{\boldsymbol{k}}^<$ fields, while the internal integrated legs are $\psi_{\boldsymbol{k}}^>$ fields. All this diagrams give an additive correction to the bare coupling constants that are contained in the Hamiltonian $\mathcal{H}\left[\psi_{\boldsymbol{k}}^<\right]$, thus giving a renormalized Hamiltonian that can be written as,

$$\mathcal{H}_r\left[\psi_{\boldsymbol{k}}^<\right] = \frac{1}{2}\int\limits_0^{\Lambda/b}\frac{\mathrm{d}^d k}{(2\pi)^d}\left[\left(k^2+T_r\right)\psi_{\boldsymbol{k}}^<\psi_{-\boldsymbol{k}}^<\right] + (vT^{3/2})_r\int\limits_0^{\Lambda/b}\frac{\mathrm{d}^d k_1}{(2\pi)^d}\int\limits_0^{\Lambda/b}\frac{\mathrm{d}^d k_2}{(2\pi)^d}\;\psi_{\boldsymbol{k}_1}^<\psi_{\boldsymbol{k}_2}^<\psi_{-\boldsymbol{k}_1-\boldsymbol{k}_2}^<+$$

$$+(uT)_r\int\limits_0^{\Lambda/b}\frac{\mathrm{d}^d k_1}{(2\pi)^d}\int\limits_0^{\Lambda/b}\frac{\mathrm{d}^d k_2}{(2\pi)^d}\int\limits_0^{\Lambda/b}\frac{\mathrm{d}^d k_3}{(2\pi)^d}\;\psi_{\boldsymbol{k}_1}^<\psi_{\boldsymbol{k}_2}^<\psi_{\boldsymbol{k}_3}^<\psi_{-\boldsymbol{k}_1-\boldsymbol{k}_2-\boldsymbol{k}_3}^< \tag{5.17}$$

then we rescale all the momenta $\boldsymbol{k}\to\boldsymbol{k}/b$,

$$\mathcal{H}_r\left[\psi_{\boldsymbol{k}/b}^<\right] = \frac{1}{2}\int\limits_0^{\Lambda}\frac{\mathrm{d}^d k}{(2\pi)^d}b^{-d}\left[\left(k^2 b^{-2}+T_r\right)\psi_{\boldsymbol{k}/b}^<\psi_{-\boldsymbol{k}/b}^<\right]+$$

$$+(vT^{3/2})_r\int\limits_0^{\Lambda}\frac{\mathrm{d}^d k_1}{(2\pi)^d}\int\limits_0^{\Lambda}\frac{\mathrm{d}^d k_2}{(2\pi)^d}\;b^{-2d}\psi_{\boldsymbol{k}_1/b}^<\psi_{\boldsymbol{k}_2/b}^<\psi_{-\boldsymbol{k}_1/b-\boldsymbol{k}_2/b}^<+$$

$$+(uT)_r\int\limits_0^{\Lambda}\frac{\mathrm{d}^d k_1}{(2\pi)^d}\int\limits_0^{\Lambda}\frac{\mathrm{d}^d k_2}{(2\pi)^d}\int\limits_0^{\Lambda}\frac{\mathrm{d}^d k_3}{(2\pi)^d}\;b^{-3d}\psi_{\boldsymbol{k}_1/b}^<\psi_{\boldsymbol{k}_2/b}^<\psi_{\boldsymbol{k}_3/b}^<\psi_{-\boldsymbol{k}_1/b-\boldsymbol{k}_2/b-\boldsymbol{k}_3/b}^<$$
$$\tag{5.18}$$

and finally we change variable rescaling the field $\psi_b(\boldsymbol{k}) = b^{-d/2-1}\psi_{\boldsymbol{k}/b}^<$ and including the rescaling factor (that is a power of b), inside the coupling constants, which gives,

$$\mathcal{H}_b\left[\psi_b(\boldsymbol{k})\right] = \frac{1}{2}\int\limits_0^{\Lambda}\frac{\mathrm{d}^d k}{(2\pi)^d}\left[\left(k^2+T_b\right)\psi_b(\boldsymbol{k})\psi_b(-\boldsymbol{k})\right]+$$

$$+(vT^{3/2})_b\int\limits_0^{\Lambda}\frac{\mathrm{d}^d k_1}{(2\pi)^d}\int\limits_0^{\Lambda}\frac{\mathrm{d}^d k_2}{(2\pi)^d}\;\psi_b(\boldsymbol{k}_1)\psi_b(\boldsymbol{k}_2)\psi_b(-\boldsymbol{k}_1-\boldsymbol{k}_2)+$$

$$+(uT)_b\int\limits_0^{\Lambda}\frac{\mathrm{d}^d k_1}{(2\pi)^d}\int\limits_0^{\Lambda}\frac{\mathrm{d}^d k_2}{(2\pi)^d}\int\limits_0^{\Lambda}\frac{\mathrm{d}^d k_3}{(2\pi)^d}\;\psi_b(\boldsymbol{k}_1)\psi_b(\boldsymbol{k}_2)\psi_b(\boldsymbol{k}_3)\psi_b(-\boldsymbol{k}_1-\boldsymbol{k}_2-\boldsymbol{k}_3)$$
$$\tag{5.19}$$

From the above Hamiltonian we have the resursive RG equations $T_b = T_b(b,T,u,v)$, $(vT^{3/2})_b = (vT^{3/2})_b(b,T,u,v)$ and $(uT)_b = (uT)_b(b,T,u,v)$. In the next section we will compute the terms of the recursive equations, via Feynman diagrams at one loop.

5.2.1   Diagrams and recursive equations

Considering the marginal field-theory Hamiltonian eq. 5.9, we have two vertices: the cubic one with coupling $vT^{3/2}$ (▲) and the quartic one with coupling uT (•),
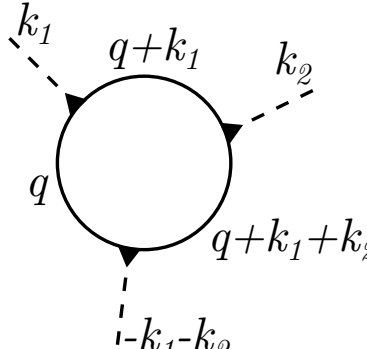
$$(5.20)$$

We can combine these two vertices, in order to form all the possible one-loop diagrams with an arbitrary number of external legs. Since we are going to evaluate the renormalized couplings only up to the term ψ^4, we stop at four external legs. All the diagrams with more than four external legs give a correction to higher order terms that we do not include in Hamiltonian (5.8) because they are all RG-irrelevant (see Appendix 5.A). Diagrams that give a contribution to the renormalization of temperature T are,

$$16uT \int\limits_{\Lambda/b}^{\Lambda} \frac{\mathrm{d}^d q}{(2\pi)^d} \frac{1}{q^2 + T} \qquad (5.21)$$

$$-18v^2 T^3 \int\limits_{\Lambda/b}^{\Lambda} \frac{\mathrm{d}^d q}{(2\pi)^d} \frac{1}{(q^2 + T)\left[(\boldsymbol{k} - \boldsymbol{q})^2 + T\right]}$$

$$(5.22)$$
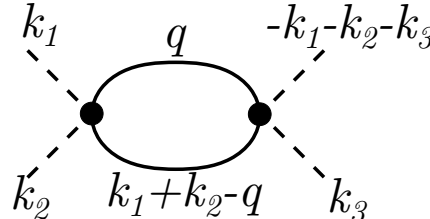
then we have contributions for $vT^{3/2}$,

$$-36uvT^{5/2} \int\limits_{\Lambda/b}^{\Lambda} \frac{\mathrm{d}^d q}{(2\pi)^d} \frac{1}{(q^2 + T)\left[(\boldsymbol{k}_1 - \boldsymbol{q})^2 + T\right]}$$

$$(5.23)$$
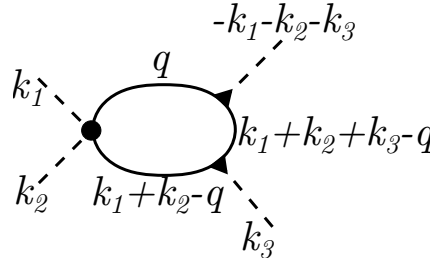
$$36v^3T^{9/2}\int\limits_{\Lambda/b}^{\Lambda}\frac{\mathrm{d}^dq}{(2\pi)^d}\frac{1}{(q^2+T)\left[(\boldsymbol{k}_1+\boldsymbol{q})^2+T\right]\left[(\boldsymbol{k}_1+\boldsymbol{k}_2+\boldsymbol{q})^2+T\right]}\tag{5.24}$$
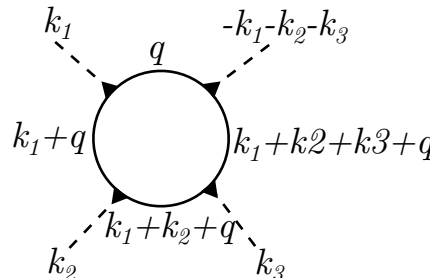
and finally for uT,

$$-36u^2T^2\int\limits_{\Lambda/b}^{\Lambda}\frac{\mathrm{d}^dq}{(2\pi)^d}\frac{1}{(q^2+T)\left[(\boldsymbol{k}_1+\boldsymbol{k}_2-\boldsymbol{q})^2+T\right]}$$

$$\tag{5.25}$$

$$216uv^2T^4\int\limits_{\Lambda/b}^{\Lambda}\frac{\mathrm{d}^dq}{(2\pi)^d}\frac{1}{(q^2+T)\left[(\boldsymbol{k}_1+\boldsymbol{k}_2-\boldsymbol{q})^2+T\right]\left[(\boldsymbol{k}_1+\boldsymbol{k}_2+\boldsymbol{k}_3-\boldsymbol{q})^2+T\right]}\tag{5.26}$$

$$-162v^4T^6\int\limits_{\Lambda/b}^{\Lambda}\frac{\mathrm{d}^dq}{(2\pi)^d}\frac{1}{(q^2+T)\left[(\boldsymbol{k}_1+\boldsymbol{q})^2+T\right]\left[(\boldsymbol{k}_1+\boldsymbol{k}_2+\boldsymbol{q})^2+T\right]}\times$$

$$\times \frac{1}{(\boldsymbol{k}_1 + \boldsymbol{k}_2 + \boldsymbol{k}_3 + \boldsymbol{q})^2 + T} \tag{5.27}$$

where dashed lines represent fields with momentum $k < \Lambda/b$ inside the shell, while solid lines represent integrated fields with momentum $\Lambda/b < k < \Lambda$ on the shell. The resulting RG recursive equations are,

$$T_b = b^2 \left[T + 12uTA_1 - 18v^2T^3A_2 \right] \tag{5.28}$$

$$\left(vT^{3/2} \right)_b = b^{3-d/2} \left[vT^{3/2} - 36uvT^{5/2}A_2 + 36v^3T^{9/2}A_3 \right] \tag{5.29}$$

$$(uT)_b = b^{4-d} \left[uT - 36u^2T^2A_2 + 216uv^2T^4A_3 - 162v^4T^6A_4 \right] \tag{5.30}$$

where we have, for a small shell with b close to 1,

$$A_l = \int_{\Lambda/b}^{\Lambda} \frac{\mathrm{d}^d q}{(2\pi)^d} \frac{1}{(q^2 + T)^l} \simeq \frac{\Omega_d \Lambda^d}{(2\pi)^d(\Lambda^2 + T)^l} \log b \simeq \frac{\Omega_d}{(2\pi)^d} \Lambda^{d-2l} \log b \left[1 - \frac{lT}{\Lambda^2} \right] \tag{5.31}$$

where Ω_d is the solid angle in d dimensions and we are computing every diagram at zero external momentum. Considering the heuristic procedure we used to build our Landau Hamiltonian eq. (5.8), where we "inherited" the constants dependence on T from the mean-field free-energy (5.2), we conclude that v and u do not depend explicitly on the temperature, nor from each other, they descend from the heuristic coarse-graining procedure [91]. For this reason it seems reasonable to combine eq.s (5.28), (5.29) and (5.30) to extract recursive equations for v_b and u_b alone (we already have eq. (5.28) for T). We write each equation for T, v and u, keeping only the lowest order terms in T, because we expect that the criticality will be present as $T \to 0$, as we already discovered through simulations and mean-field [27]. The resulting equations are,

$$T_b = b^2 \left[T + 12uTA_1 - 18v^2T^3A_2 \right] \simeq b^2 \left[T + 12uT\frac{\Omega_d}{(2\pi)^d}\Lambda^{d-2} \log b \right] \tag{5.32}$$

$$v_b = \frac{\left(vT^{3/2} \right)_b}{(T_b)^{3/2}} = \frac{b^{3-d/2} \left[vT^{3/2} - 36uvT^{5/2}A_2 + 36v^3T^{9/2}A_3 \right]}{b^3 [T + 12uTA_1]^{3/2}}$$

$$\simeq b^{-d/2} \left[v - 18uv\frac{\Omega_d}{(2\pi)^d}\Lambda^{d-2} \log b \right] \tag{5.33}$$

$$u_b = \frac{(uT)_b}{T_b} = \frac{b^{4-d} \left[uT - 36u^2T^2A_2 + 216uv^2T^4A_3 - 162v^4T^6A_4 \right]}{b^2 \left[T + 12uTA_1 \right]}$$

$$\simeq b^{2-d} \left[u - 12u^2\frac{\Omega_d}{(2\pi)^d}\Lambda^{d-2} \log b \right] \tag{5.34}$$

Then we expand the recursive equations for b close to 1, defining $b = 1 + x$ with $x \ll 1$. We end up with the equations,

$$\frac{\mathrm{d}T}{\mathrm{d}x} = 2T \left(1 + 6u\Lambda^{d-2} \right)$$

$$\frac{\mathrm{d}v}{\mathrm{d}x} = -\frac{d}{2}v - 18uv\Lambda^{d-2}$$

$$\frac{\mathrm{d}u}{\mathrm{d}x} = (2 - d)u - 12u^2\Lambda^{d-2} \tag{5.35}$$

where we have rescaled the cutoff $\Lambda^{d-2}\Omega_d/(2\pi)^d \to \Lambda^{d-2}$ (Ω_d is the solid angle in d dimensions) in order to get rid of all the numerical constants coming from the angular part of the integrals (5.31). Now we choose d to be the physical dimension of our system, i.e $d = 3$ and we solve the system (5.35), obtaining,

$$T(x) = T_0(12\Lambda u_0 + 1)e^{2x} - 12\Lambda T_0 u_0 e^x$$

$$v(x) = \frac{v_0 e^{-\frac{3}{2}x}}{(12\Lambda u_0 + 1 - 12\Lambda u_0 e^{-x})^{3/2}}$$

$$u(x) = \frac{u_0 e^{-x}}{12\Lambda u_0 + 1 - 12\Lambda u_0 e^{-x}} \tag{5.36}$$

where T_0, v_0 and u_0 are the initial values of the constants (i.e. at $x = 0$) that are the "physical" values of the theory's parameters, the starting point of the RG transformation.

5.2.2   Critical exponents

We find from the system (5.35) and also from the explicit solutions (5.36), that our flow has only a physically meaningful ($T \geq 0$ and $u \geq 0$) fixed point for $T^* = v^* = u^* = 0$. This fixed point is unstable for the direction T, and stable for the directions v and u, as we can see from the linear terms in the eq.s (5.35). Normally we could place ourselves at the fixed point and we could perturb our position to investigate the relevant eigendirection, in order to compute the critical exponent ν [70]. However, this is a quite pathological situation for our model, because the whole Hamiltonian (5.8) vanishes (except for the gradient term) if we are at the fixed point with $T = 0$. Hence we decide to proceed in a different way, we start the RG flow close to the critical manifold $T = 0$ and, by using the exact solutions eq.s (5.36), we study the critical exponents dependence on the initial conditions of T, u and v. More specifically, we fix the values of $v_0 \sim O(1)$ and $u_0 \sim O(1)$, thus selecting a particular theory, and then we try to figure out the value of T_0 such that the theory is in the critical regime that is controlled by the fixed point $T^* = v^* = u^* = 0$.

   We want to be in the critical regime for the whole flow, so we impose a "stop condition": we start the flow close enough to the critical manifold, so that the physical correlation length is way bigger than the lattice spacing $\xi_0 \gg 1/\Lambda$ and we stop the flow when the correlation length approaches the lattice spacing size,

$$\xi(x_{stop}) = \xi_0 e^{-x_{stop}} \simeq 1/\Lambda \tag{5.37}$$

Given that the fixed point of this theory is Gaussian, i.e $v^* = u^* = 0$, we assume that the critical exponent for the divergence of the correlation length is $\nu = 1/2$. This value for ν implies that $\xi_0 \sim T_0^{-1/2}$, then the stop condition becomes,

$$T_0 \sim \Lambda^2 e^{-2x_{stop}} \tag{5.38}$$

We can check the self-consistency of our assumption by computing ν [22], using eq.s (5.36) and (5.38),

$$1/\nu = \left(\frac{\mathrm{d}\log T}{\mathrm{d}x}\right)\Big|_{x_{stop}} = 2 + \frac{\sqrt{T_0}u_0}{\Lambda u_0 + 1} \tag{5.39}$$

given this result we can say that if the term $\frac{\sqrt{T_0}u_0}{\Lambda u_0+1}$ is negligible with respect to 2 our assumption holds and we have a Gaussian critical exponent for the correlation length divergence. In the worst case scenario with $\Lambda u_0 \ll 1$ we find that we should choose a physical temperature (and consequently a correlation length),

$$T_0 \ll u_0^{-2} \sim O(1) \tag{5.40}$$
$$\xi_0 \gg u_0 \sim O(1) \tag{5.41}$$

that is a completely reasonable condition for the temperature; it is essentially telling us that, given any reasonable quartic coupling u_0, we can choose a small enough temperature T_0 to place our system in the critical regime such that the correlation length diverges with $\nu = 1/2$.

We check also the critical exponent η, which is determined by the diagram with two external legs and two cubic vertices (5.22), which corrects the field scaling, at one loop. We have to compute the k^2 contribution of the diagram (5.22), which is, in $d = 3$,

$$\frac{\mathrm{d}}{\mathrm{d}k^2}\left[-18v^2T^3\int_{\Lambda/b}^{\Lambda}\frac{\mathrm{d}^3q}{(2\pi)^3}\frac{1}{(q^2+T)\left[(\boldsymbol{k}-\boldsymbol{q})^2+T\right]}\right]\Bigg|_{k=0} \tag{5.42}$$
$$= Av^2T^3\Lambda^{-3}\log b \tag{5.43}$$

where A is a numeric constant. The above term corrects the field scaling,

$$\psi_b(\boldsymbol{k}) = b^{-5/2}\left(1 + Av^2T^3\Lambda^{-3}\log b\right)^{1/2}\psi_{\boldsymbol{k}/b}^{<} \simeq b^{-5/2+Av^2T^3\Lambda^{-3}/2}\psi_{\boldsymbol{k}/b}^{<} \tag{5.44}$$

and using the scaling of the correlation function,

$$\langle\psi_b(\boldsymbol{k})\psi_b(\boldsymbol{k}')\rangle_c = \delta^3(\boldsymbol{k}+\boldsymbol{k}')C_b(k) \tag{5.45}$$
$$C(k/b) = b^{2-\eta}C_b(k) \tag{5.46}$$

we can find that the anomalous dimension is,

$$\eta \sim v^2T^3\Lambda^{-3} \tag{5.47}$$

Once we compute $v(x)$ and $T(x)$ at $x = x_{stop}$, using eq. (5.36) and (5.38) we find,

$$\eta \sim v_0^2T_0^{3/2} \tag{5.48}$$

hence we have another condition for the physical temperature to ensure that the anomalous dimension is as small as pleased,

$$T_0 \ll v_0^{-4/3} \sim O(1) \tag{5.49}$$

$$\xi_0 \gg v_0^{2/3} \sim O(1) \tag{5.50}$$

In the end we discovered that, if we have any marginal theory like (5.8) with physical values $v_0 \sim O(1)$ and $u_0 \sim O(1)$, it suffices to choose a temperature $T_0 \ll O(1)$ to be in the critical regime, that is controlled by a Gaussian fixed point with,

$$\nu = 1/2 \qquad \eta = 0 \tag{5.51}$$

These calculations can be generalized for any $d > 2$, hence we conclude that our marginal theory is infrared-free [100] with an upper critical dimension $d_c = 2$

5.3 Lattice MonteCarlo simulations and finite-size scaling

In order to check the critical exponents of the Marginal theory, we perform numerical Monte Carlo simulations ona cubic lattice, using the microscopic marginal Hamiltonian 3.36, with nearest neighbours interaction and periodic boundary conditions. We expect our theory to be infrared-free, as we have seen in the previous sections. This means that the finite-size scaling [9], which normally can be used to estimate critical exponents for theories that are not asymptotically free, is not granted [16]. However, we assume that it holds and we will see a posteriori if the result is coherent with this assumption. In general we have, for large enough L and small enough $t = T - T_c$,

$$\chi = t^{-\gamma} f(L t^\nu) \tag{5.52}$$

where $f()$ is a scaling function. With some manipulations we obtain,

$$\chi = \frac{t^{-\gamma} L^{-\gamma/\nu}}{L^{-\gamma/\nu}} f(L t^\nu) = L^{\gamma/\nu} (L t^\nu)^{-\gamma/\nu} f(L t^\nu) = L^{\gamma/\nu} g(L t^\nu) \tag{5.53}$$

where $g()$ is another scaling function. Since we are interested in the marginal model's critical point with $T_c = 0$ we obtain, for the modulus susceptibility,

$$\frac{\chi_{mod}}{L^{\gamma/\nu}} = g(L T^\nu) \tag{5.54}$$

hence if we plot $\frac{\chi_{mod}}{L^{\gamma/\nu}}$ as a function of $L T^\nu$, for all the finite systems we have simulated, with the true critical exponents γ and ν, all the curves must collapse onto each other. This is what happens in Fig. 5.1 with the choices $\gamma = 1$ and $\nu = 1/2$, that are the same critical exponents that we found via the renormalization group analysis of this chapter.

This result deserves some comments and further investigations. On one hand we see that relation (5.54) holds quite well for our theory, with the free exponents $\gamma = 1$ and $\nu = 1/2$ but on the other hand we know that usually for free theories the (5.54) does not hold. The reason of this result could be either our theory is not free and it has non-trivial critical exponents, but this is not what we expect from the renormalization group calculations and from the free exponents that produce such a good collapse (Fig. 5.1), or the theory is free and simultaneously the relation 5.54 holds. We think the second explanation could be the most plausible but we still do not have more solid evidences to prove our point. Further study on the Marginal theory is needed in order to clarify this point.
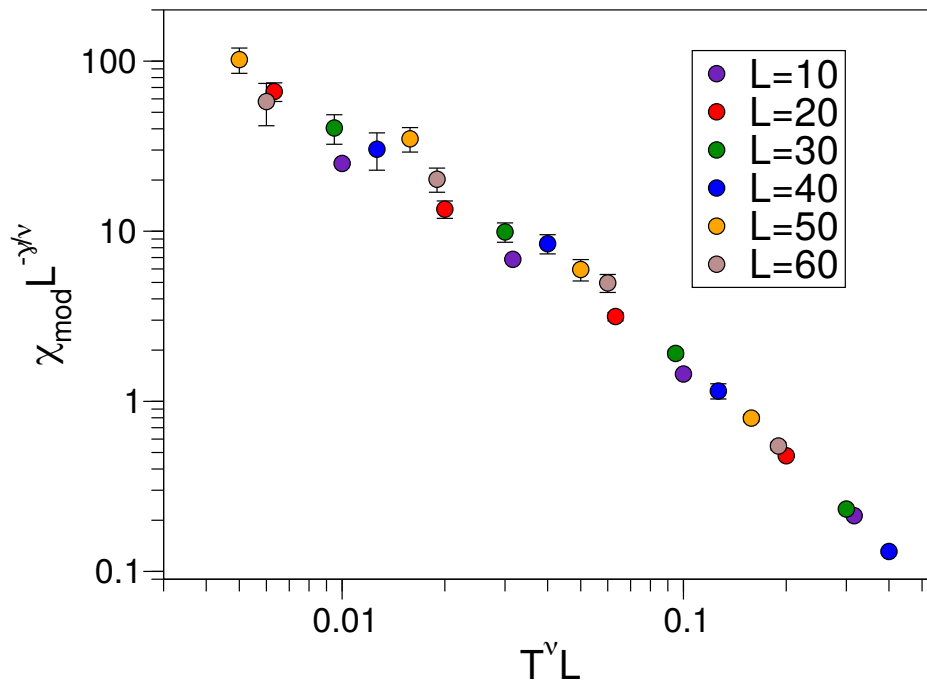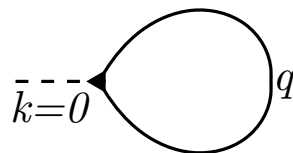
Figure 5.1. Finite size scaling for the marginal model. Plot of eq. 5.54 with $\nu = 1/2$ and $\gamma = 1$ for Monte Carlo simulations of the microscopic equilibrium marginal model 3.36 with periodic boundary conditions on a cubic lattice. The edge of the cubic lattice goes from $L = 10$ up to $L = 60$. We can observe a good collapse of the curves on top of each other, using the general finite-size scaling relation (5.54). This is peculiar since for generic free theories finite-size scaling breaks down [16]. Error bars have been computed using the blocking procedure described in [1], together with the Jackknife method.

5.A Appendix: other terms in the Landau-Ginzburg Hamiltonian

For what concerns the linear term of the statistical field theory 5.3, after the initial field rescaling 5.6 it becomes,

$$cT^{3/2}\psi \tag{5.55}$$

that gives the naive dimensions $[c] = d/2 - 2$ and $\left[cT^{3/2}\right] = d/2 + 1$. This term can be eliminated by a simple shift of the field, that must include the one-loop diagram that corrects the linear term. In this way we can get rid of the linear term and we can simplify the Hamiltonian that becomes eq. 5.3. We can also include the linear term in the field theory, without doing any field shift. The result will be the same, the linear term does not produce any diagram to correct eq.s 5.32, 5.33 and 5.34, hence eq.s 5.35 are left untouched. Which means that all our calculations to obtain the critical exponents do not change. On the other hand the linear coupling constant $cT^{3/2}$ obtains a contribution from the diagram,

$$3vT^{3/2}\int\limits_{\Lambda/b}^{\Lambda}\frac{\mathrm{d}^d q}{(2\pi)^d}\frac{1}{(q^2 + T)} \tag{5.56}$$

which gives,

$$(cT^{3/2})_b = b^{d/2+1}\left[cT^{3/2} + 3vT^{3/2}A_1\right] \tag{5.57}$$

that can be divided by $T_b^{3/2}$ to obtain, at the lowest order in T,

$$c_b = b^{d/2-2}[c + (3v - 18uc)\frac{\Omega_d}{(2\pi)^d}\Lambda^{d-2}\log b] \tag{5.58}$$

Once we expand $b \simeq 1 + x$ we have the differential equation for $c(x)$,

$$\frac{\mathrm{d}c}{\mathrm{d}x} = (\frac{d}{2} - 2)c + 3v\Lambda^{d-2} - 18uc\Lambda^{d-2} \tag{5.59}$$

which gives, for $d = 3$,

$$c(x) = \frac{c_0 e^{-x/2} + 3\Lambda v_0 e^{-x/2}(1 - e^{-x})}{(12\Lambda u_0 + 1 - 12\Lambda u_0 e^{-x})^{3/2}} \tag{5.60}$$

where $c_0 = c(x = 0)$. The behaviour of $c(x)$ during the RG flow is influenced by the other couplings initial values u_0 and v_0 but, since the coupling c does not appear in the evolution equations 5.35 of all the other couplings, it does not change the analysis we did in the previous sections.

In order to check the terms of order higher than ψ^4, we need to know the naive scaling dimension of their T-independent couplings. To see that, we need to go

back to eq. 5.2, which tells us the dependence on T of each coupling, based on the mean-field Gibbs free energy 3.52. We find that, before the rescaling 5.6, the higher order terms can be written as,

$$\beta\mathcal{H}_{high} = \frac{1}{T}\int \mathrm{d}^d x \left\{ u_5\psi^5 + u_6\psi^6 + \cdots + u_8\psi^8 + \right.$$

$$\left. + u_9 T\psi^9 + u_{10}T\psi^{10} + \cdots + u_n T\psi^n + \dots \right\} \tag{5.61}$$

where every u_l is a constant independent of T. We find this dependence on T from eq. 3.52, where we can see that the lowest order (in T) that generates the terms from $(m-1)^5$ up to $(m-1)^8$ is the first term (the bare marginal potential) hence their couplings do not depend on T. On the other hand, the lowest order term that generates powers from $(m-1)^9$ and above is the logarithm of order T. Once we perform the rescaling 5.6, we have,

$$\beta\mathcal{H}_{high} = \int \mathrm{d}^d x \left\{ u_5 T^{3/2}\psi^5 + \cdots + u_8 T^3\psi^8 + u_9 T^{9/2}\psi^9 + \cdots + u_n T^{n/2}\psi^n + \dots \right\}$$
$$\tag{5.62}$$

which can be expressed as,

$$u_n\psi^n \to \begin{cases} T^{n/2-1} & \text{for } 4 < n < 9 \\ T^{n/2} & \text{for } n \geq 9 \end{cases} \tag{5.63}$$

Using the expressions above we can compute the naive scaling dimensions of the u_n couplings, that are,

$$[u_n] = \begin{cases} 2 + d\left(1 - \frac{n}{2}\right) & \text{for } 4 < n < 9 \\ d\left(1 - \frac{n}{2}\right) & \text{for } n \geq 9 \end{cases} \tag{5.64}$$

For $d = 3$ we can see that $[u_n] < 0$ for every n, hence the Gaussian fixed point $T^* = v^* = u^* = u_n^* = 0$, for every n, is still stable.

Conclusions and perspectives

Through the marginal model, it is possible to reproduce the most important traits of starling flocks experimental phenomenology – large polarization, large correlation length, moderate speed at all group sizes – without the need of a strong size-dependent fine-tuning [34]. If we were dealing with a traditional critical point [91], at each size we would have been forced to tune the temperature in order to obtain scale-free correlations, but in the case of the marginal model this is not necessary. In the framework of this theory, given the fact that its critical point is at temperature $T = 0$, it suffices to choose a low enough temperature such that the largest finite-size system that we are observing displays scale-free correlations and automatically all the systems with smaller size will satisfy this property. This means that, at least in the case of starling flocks, we do not need to choose a size-dependent set of parameters to reproduce the system's peculiar experimental features. We have achieved the considerable result of finding a model that is suitable to reproduce biological experimental data.

We will now underline the physical and biological meaning of choosing the marginal potential over the pseudo-Gaussian. The highly non-linear marginal potential implies that small speed fluctuations elicit nearly zero restoring force (see single particle term of eq. (4.12)), while larger speed fluctuations are pushed back extremely sharply, in contrast with the constant slope of a pseudo-linear confining force (see eq. (4.11)). In bird flocks, small speed fluctuations are not prevented by biomechanical constraints, but they could be depressed by energetic expenditure concerns, as changing the speed requires extra energy consumption; however, starlings prove to be *very* liberal about their energy expenditure habits while flocking [6, 54, 61]: although their metabolic rate is dramatically higher in flight than on the roost [54], these birds will spectacularly wheel every day for half an hour before landing, expending energy at a ferocious rate; this suggests that small extra energy expenditures due to small speed fluctuations may indeed be weaker-than-linearly suppressed. On the other hand, large speed fluctuations clash against biomechanical and aerodynamic constraints, which are set very stringently by anatomy, physiology and physics [94, 98, 99]; therefore, a stronger-than-linear suppression of large speed fluctuations also seems quite reasonable. This implies that an harmonic (or quadratic) potential is not adequate to describe individual fluctuations. Our way to reproduce flocks experiments is based on a marginal potential that has zero curvature in its minimum, hence it cannot be expanded quadratically [27]. This situation seems to suggest that, if we want to build a theory on how a single individual controls its own velocity, we cannot assume Gaussian fluctuations but we have to look for a more complex explanation.

Even though we tested our conclusions on the experimental case of starling flocks, it seems that our results do not depend on that specific system: it is not just starlings data to be incompatible with linear speed control, but rather that linear control would blow the group's speed out of proportion in *any* collective system; marginal control, on the contrary, is one simple way (possibly not the only one) to reconcile data with theory. Given this expectation of generality, it would be extremely useful to test these ideas within other biological systems. Field experiments reporting the dynamical trajectories within animal groups are quite rare, especially in three dimensions, and beyond starlings the only data are for pigeons (*Columba livia*) [45, 87, 113], jackdaws (*Corvus monedula*) [69, 74, 75] and chimney swifts (*Chaetura pelagica*) [43]. Monitoring the mean speed of these groups should be straightforward, while checking the speed correlations may be somewhat more laborious, as only a study of correlation at different group's size L would reveal whether or not scale-free correlations are present also in these systems; and yet, this seems to us an essential step to establish on a firmer basis the connection between speed control and correlation, which is the cornerstone of our results.

A further crucial issue to consider when we think about real biological systems, is that the dynamical phases of natural collective behaviour are diverse: starlings' aerial display studied in our data (sometimes called *murmurations*) is characterized by a very compact drop-like structure, moving coherently over the roost, often subject to predation [96]; chimney swifts display a remarkable circling geometry [43], while the jackdaws data collected in [74] display two group-level phases, namely a cruising-to-roost dynamics and an anti-predator mobbing dynamics. It would be helpful to understand what are the properties that these different phases have in common. This is particularly relevant for correlation, which - as we have seen - is a tricky trait to sustain. Consider, for example, correlations in the *velocity orientations* of animals: statistical physics tells us [53] that when the rotational symmetry is spontaneously broken by the group, namely when out of many *equivalent* directions of motion only one is selected, scale-free correlations of the orientations emerge automatically in the system. If spontaneous symmetry-breaking seems certainly to be the relevant case for starling flocks swirling over the roost, jackdaws flocks traveling to the roost [69, 74, 75] and homing pigeons [45, 87, 113] need to follow *one* specific direction, hence there is no spontaneous symmetry breaking; similarly, in the case of migrating birds, when longer duration flight carry the individuals along one well-defined route, there is no spontaneous symmetry breaking. In these cases, correlations of the orientations could be quite different from those of starlings. However, speed requires a different correlation mechanism than orientation, as no physical reason automatically grants long-range correlation; hence, it would be really helpful to investigate the link between correlation and speed control in different phases. Our impression is that long-range speed correlations are essential to propagate information in *all* phases of collective motion, in order to keep a good degree of cohesion in the face of natural variations of the individual speeds; we therefore expect that the interplay between speed control and speed correlation is a very general concern of collective motion. But only experiments can confirm this.

Experimental data on two-dimensional collective motion are somewhat more accessible than $3D$ data. The recent study about sheep herds [51] presents a case where exactly the same interplay between correlation and speed control could be at

work, and the presence of intermittency - with its huge speed fluctuations - could make even more urgent the issue of speed control; again, obtaining correlations at different groups size could require some nontrivial work, but the two-dimensional nature of the systems makes the tracking somewhat simpler than in the case of bird flocks. Intermittent motion and large speed distributions have also been observed in locust swarms [10]. Similarly, $2D$ data of fish schools in shallow water have been studied for a long time, both numerically [64] and experimentally [62, 76]; as in the case of sheeps - and unlike the case of birds - speed fluctuations in fish schools are substantial, hence the issue of speed control can be quite different than in bird flocks. In fact, there may exist a rather profound difference between animals that *cannot* change much their speed, as birds within a flock, for which not only very large speeds are forbidden, but also very low ones, because of the very aerodynamics of flight, and animals that *can* reduce considerably their speed, down to halting, as mammal herds or fish schools, at least to a certain extent; apart from a significantly larger asymmetry in the control mechanisms, the very possibility to reduce the speed to zero could be a game changer. However, our calculation shows that - in absence of marginal control - the entropic push drives the group's speed to absurdly *large* values, not small ones, and this is something no group can afford to do. And yet again, one should check whether or not this is true at the experimental level.

We have discussed the biological plausibility of the marginal model and some possible extensions of our work for other biological systems. Furthermore it is also possible to improve our model in order to catch other peculiar aspects of the biological system that we observed. Regarding the accuracy of our model in describing the dynamics, our theory can be further improved. In systems that evolve following dynamics equations like the one we have written and used here (eq.s 4.7) information propagates very differently from how it propagates in real flocks while they perform turns [33]. In order to resemble the observed propagation, a second order differential equation for the velocity is needed [33]. A second order model, the inertial spin model (ISM), has been implemented and studied using a standard $\lambda\phi^4$ Landau Hamiltonian [33]. It would be very interesting to see what happens if we combine together the marginal potential and the second order dynamics, they might give rise to some interesting effects concerning the system's dynamics at low temperature. Furthermore, another dynamical effect that has been studied is the existence of speed waves and their interaction with density waves [25], but only for the pseudo-Gaussian model. A similar investigation could be done in order to see if any changes in the speed waves phenomenology occur if we use the marginal pseudo-Hamiltonian instead of the pseudo-Gaussian.

Another peculiar feature of flocks is that the power law decay of their connected correlation functions have a really low exponent [24], this can be explained with the presence of continuous random external perturbations and a model that reproduces them has been studied in [29]. To investigate further this topic, it would be interesting to apply random external perturbation on an artificial flock that obeys to the marginal theory's pseudo-Hamiltonian to see how correlation functions are affected by the perturbation in the marginal case.

An interesting topic that we partially addressed in the second chapter is the effect of gravity in partially breaking the $O(3)$ symmetry of the system. We decided to disregard this effect in order to simplify our work and we found that our theory

can describe the experimental system. However, a way to include this partial explicit breaking of the three dimensional rotation symmetry could be included in our model, to see if it adds some new interesting features to be studied.

Finally, beyond the horizon of broadening our study to include biological systems other than starling flocks, experiments on artificial self-organized swarms would be the next essential step forward. Artificial swarms would allow first to assess at the embodied level (which is quite different from the numerical one) to what extent group's cohesion depends on the range of the correlation: the fact that long-range correlations (quite rare a condition in physical systems) are so frequent in biological collective behaviour - from bird flocks [24], to midge swarms [4] and down to bacterial clusters [36] - has prompted biophysicists to connect this trait to collective response and cohesion, with both theoretical [84] and numerical backup [60]; yet, biology is one thing, engineering another one, and no matter how much inspiration the latter takes form the former, it is crucial to check whether the link between correlation and response holds at the technological level. Secondly, in artificial collectives it would be possible - at least to some extent - to tune the reference agents' speed v_0 and to tweak the manner individual speed can fluctuate around v_0 in a controlled way, which is impossible to achieve in natural systems. Having the possibility to operate on both arms of the problem (correlation and speed control) would be invaluable, given the growing technological relevance of self-organized collective behaviour.

Showing some examples, already some drones or vehicles make use of the pseudo-Gaussian or similar potentials to regulate the machine's speed [47, 119]. It would be fascinating to see if the speed correlation induced by the marginal potential could improve the performance of these machines. Furthermore in the flourishing field of neural networks and deep learning cost functions are often regularized by a quadratic term that has the aim of preventing overfitting by limiting the values of the network parameters to fluctuate around zero [15]. Since we have seen that a quartic term has the same effect and also grants scale-free correlations through the system it might be relevant to see if a neural network with a quartic regularization term showed some differences with respect to networks with standard regularization.

Bibliography

[1] AMIT, D. J. AND MARTIN-MAYOR, V. *Field theory, the renormalization group, and critical phenomena: graphs to computers.* World Scientific Publishing Company (2005).

[2] ANDERSON, P. W. More is different. *Science*, **177** (1972), 393. `doi:10.1126/science.177.4047.393`.

[3] ATTANASI, A., ET AL. Collective behaviour without collective order in wild swarms of midges. *PLoS Comput Biol*, **10** (2014), e1003697.

[4] ATTANASI, A., ET AL. Finite-size scaling as a way to probe near-criticality in natural swarms. *Physical Review Letters*, **113** (2014), 238102.

[5] ATTANASI, A., ET AL. Greta-a novel global and recursive tracking algorithm in three dimensions. *IEEE transactions on pattern analysis and machine intelligence*, **37** (2015), 2451.

[6] BAJEC, I. L. AND HEPPNER, F. H. Organized flight in birds. *Animal Behaviour*, **78** (2009), 777.

[7] BALLERINI, M., ET AL. Empirical investigation of starling flocks: a benchmark study in collective animal behaviour. *Anim Behav*, **76** (2008), 201. `doi:10.1016/j.anbehav.2008.02.004`.

[8] BALLERINI, M., ET AL. Interaction ruling animal collective behavior depends on topological rather than metric distance: Evidence from a field study. *Proceedings of the national academy of sciences*, **105** (2008), 1232.

[9] BARKEMA, G. AND NEWMAN, M. *Monte Carlo methods in statistical physics.* Oxford University Press (2001).

[10] BAZAZI, S., ROMANCZUK, P., THOMAS, S., SCHIMANSKY-GEIER, L., HALE, J. J., MILLER, G. A., SWORD, G. A., SIMPSON, S. J., AND COUZIN, I. D. Nutritional state and collective motion: from individuals to mass migration. *Proceedings of the Royal Society B: Biological Sciences*, **278** (2011), 356.

[11] BENZI, R., PARISI, G., SUTERA, A., AND VULPIANI, A. A theory of stochastic resonance in climatic change. *SIAM Journal on applied mathematics*, **43** (1983), 565.

[12] Bialek, W., Cavagna, A., Giardina, I., Mora, T., Pohl, O., Silvestri, E., Viale, M., and Walczak, A. M. Social interactions dominate speed control in poising natural flocks near criticality. *Proceedings of the National Academy of Sciences*, **111** (2014), 7212. Available from: https://www.pnas.org/content/111/20/7212, arXiv:https://www.pnas.org/content/111/20/7212.full.pdf, doi:10.1073/pnas.1324045111.

[13] Bialek, W., Cavagna, A., Giardina, I., Mora, T., Silvestri, E., Viale, M., and Walczak, A. M. Statistical mechanics for natural flocks of birds. *Proc Natl Acad Sci USA*, **109** (2012), 4786. doi:10.1073/pnas.1118633109.

[14] Binney, J. J., Dowrick, N., Fisher, A., and Newman, M. *The theory of critical phenomena: an introduction to the renormalization group*. Oxford University Press, Inc. (1992).

[15] Bishop, C. M. Pattern recognition. *Machine learning*, **128** (2006).

[16] Brézin, E. An investigation of finite size scaling. *Journal de Physique*, **43** (1982), 15. Available from: https://hal.archives-ouvertes.fr/jpa-00209373, doi:10.1051/jphys:0198200430101500.

[17] Brézin, E. and Wallace, D. Critical behavior of a classical heisenberg ferromagnet with many degrees of freedom. *Physical Review B*, **7** (1973), 1967.

[18] Brézin, E., Wallace, D., and Wilson, K. G. Feynman-graph expansion for the equation of state near the critical point. *Physical Review B*, **7** (1973), 232.

[19] Burstedde, C., Klauck, K., Schadschneider, A., and Zittartz, J. Simulation of pedestrian dynamics using a two-dimensional cellular automaton. *Physica A: Statistical Mechanics and its Applications*, **295** (2001), 507.

[20] Cammarota, C., Cavagna, A., Giardina, I., Gradenigo, G., Grigera, T. S., Parisi, G., and Verrocchio, P. Phase-separation perspective on dynamic heterogeneities in glass-forming liquids. *Phys. Rev. Lett.*, **105** (2010), 055703. Available from: https://link.aps.org/doi/10.1103/PhysRevLett.105.055703, doi:10.1103/PhysRevLett.105.055703.

[21] Caracciolo, S., Edwards, R. G., Pelissetto, A., and Sokal, A. D. Wolff-type embedding algorithms for general nonlinear ?-models. *Nuclear Physics B*, **403** (1993), 475. Available from: https://www.sciencedirect.com/science/article/pii/055032139390044P, doi:https://doi.org/10.1016/0550-3213(93)90044-P.

[22] Cardy, J. *Scaling and renormalization in statistical physics*, vol. 5. Cambridge university press (1996).

[23] Cavagna, A., Cimarelli, A., Giardina, I., Orlandi, A., Parisi, G., Procaccini, A., Santagati, R., and Stefanini, F. New statistical tools for analyzing the structure of animal groups. *Math Biosci*, **214** (2008), 32. doi:10.1016/j.mbs.2008.05.006.

[24] CAVAGNA, A., CIMARELLI, A., GIARDINA, I., PARISI, G., SANTAGATI, R., STEFANINI, F., AND VIALE, M. Scale-free correlations in starling flocks. *Proc Natl Acad Sci USA*, **107** (2010), 11865. `doi:10.1073/pnas.1005766107`.

[25] CAVAGNA, A., CONTI, D., GIARDINA, I., AND GRIGERA, T. S. Propagating speed waves in flocks: A mathematical model. *Phys. Rev. E*, **98** (2018), 052404. Available from: `https://link.aps.org/doi/10.1103/PhysRevE.98.052404`, `doi:10.1103/PhysRevE.98.052404`.

[26] CAVAGNA, A., CREATO, C., DEL CASTELLO, L., GIARDINA, I., MELILLO, S., PARISI, L., AND VIALE, M. Error control in the set-up of stereo camera systems for 3d animal tracking. *The European Physical Journal Special Topics*, **224** (2015), 3211. Available from: `http://dx.doi.org/10.1140/epjst/e2015-50102-3`, `doi:10.1140/epjst/e2015-50102-3`.

[27] CAVAGNA, A., CULLA, A., DI CARLO, L., GIARDINA, I., AND GRIGERA, T. S. Low-temperature marginal ferromagnetism explains anomalous scale-free correlations in natural flocks. *Comptes Rendus Physique*, **20** (2019), 319. Available from: `https://www.sciencedirect.com/science/article/pii/S1631070519300374`.

[28] CAVAGNA, A., CULLA, A., GIARDINA, I., AND GRIGERA, T. S. Renormalization group analysis of the marginal model. *In preparation.*

[29] CAVAGNA, A., GIARDINA, I., AND GINELLI, F. Boundary information inflow enhances correlation in flocking. *Physical review letters*, **110** (2013), 168107.

[30] CAVAGNA, A., GIARDINA, I., AND GRIGERA, T. S. The physics of flocking: Correlation as a compass from experiments to theory. *Physics Reports*, **728** (2018), 1.

[31] CAVAGNA, A., GIARDINA, I., ORLANDI, A., PARISI, G., AND PROCACCINI, A. The starflag handbook on collective animal behaviour: 2. three-dimensional analysis. *Anim Behav*, **76** (2008), 237. `doi:10.1016/j.anbehav.2008.02.003`.

[32] CAVAGNA, A., GIARDINA, I., ORLANDI, A., PARISI, G., PROCACCINI, A., VIALE, M., AND ZDRAVKOVIC, V. The starflag handbook on collective animal behaviour: 1. empirical methods. *Anim Behav*, **76** (2008), 217. `doi:10.1016/j.anbehav.2008.02.002`.

[33] CAVAGNA, A., ET AL. Flocking and turning: a new model for self-organized collective motion. *Journal of Statistical Physics*, **158** (2015), 601.

[34] CAVAGNA, A., CULLA, A., FENG, X., GIARDINA, I., GRIGERA, T. S., KION-CROSBY, W., MELILLO, S., PISEGNA, G., POSTIGLIONE, L., AND VILLEGAS, P. Marginal speed confinement resolves the conflict between correlation and control in natural flocks of birds. *Submitted to Nature Communications*, (2021). `arXiv:2101.09748`.

[35] CHATÉ, H., GINELLI, F., GRÉGOIRE, G., PERUANI, F., AND RAYNAUD, F. Modeling collective motion: variations on the Vicsek model. *The European Physical Journal B*, **64** (2008), 451.

[36] CHEN, X., DONG, X., BE?ER, A., SWINNEY, H. L., AND ZHANG, H. Scale-invariant correlations in dynamic bacterial clusters. *Physical review letters*, **108** (2012), 148101.

[37] CHIBBARO, S., RONDONI, L., AND VULPIANI, A. *Reductionism, emergence and levels of reality* (2014).

[38] COUZIN, I. AND KRAUSE, J. Self-organization and collective behavior in vertebrates. *Advances in the Study of Behavior*, **32** (2003), 1.

[39] DI LEONARDO, R., ANGELANI, L., DELL?ARCIPRETE, D., RUOCCO, G., IEBBA, V., SCHIPPA, S., CONTE, M. P., MECARINI, F., DE ANGELIS, F., AND DI FABRIZIO, E. Bacterial ratchet motors. *Proceedings of the National Academy of Sciences*, **107** (2010), 9541.

[40] D?ORSOGNA, M. R., CHUANG, Y.-L., BERTOZZI, A. L., AND CHAYES, L. S. Self-propelled particles with soft-core interactions: patterns, stability, and collapse. *Physical review letters*, **96** (2006), 104302.

[41] DYSON, F. General theory of spin-wave interactions. *Physical review*, **102** (1956), 1217.

[42] ERDMANN, U., EBELING, W., SCHIMANSKY-GEIER, L., AND SCHWEITZER, F. Brownian particles far from equilibrium. *The European Physical Journal B-Condensed Matter and Complex Systems*, **15** (2000), 105.

[43] EVANGELISTA, D. J., RAY, D. D., RAJA, S. K., AND HEDRICK, T. L. Three-dimensional trajectories and network analyses of group behaviour within chimney swift flocks during approaches to the roost. *Proceedings of the Royal Society B: Biological Sciences*, **284** (2017), 20162602.

[44] FRANGIPANE, G., VIZSNYICZAI, G., MAGGI, C., SAVO, R., SCIORTINO, A., GIGAN, S., AND DI LEONARDO, R. Invariance properties of bacterial random walks in complex structures. *Nature communications*, **10** (2019), 1.

[45] FREEMAN, R., MANN, R., GUILFORD, T., AND BIRO, D. Group decisions and individual differences: route fidelity predicts flight leadership in homing pigeons (columba livia). *Biology letters*, **7** (2011), 63.

[46] GABRIÉ, M., MANOEL, A., LUNEAU, C., BARBIER, J., MACRIS, N., KRZA-KALA, F., AND ZDEBOROVÁ, L. Entropy and mutual information in models of deep neural networks. *Journal of Statistical Mechanics: Theory and Experiment*, **2019** (2019), 124014.

[47] GARRELL, A., GARZA-ELIZONDO, L., VILLAMIZAR, M., HERRERO, F., AND SANFELIU, A. Aerial social force model: A new framework to accompany people using autonomous flying robots. In *2017 IEEE/RSJ International*

Conference on Intelligent Robots and Systems (IROS), pp. 7011–7017 (2017). `doi:10.1109/IROS.2017.8206627`.

[48] Gautrais, J., Ginelli, F., Fournier, R., Blanco, S., Soria, M., Chaté, H., and Theraulaz, G. Deciphering interactions in moving animal groups. *PLoS Comput Biol*, **8** (2012), e1002678.

[49] Ginelli, F. The physics of the Vicsek model. *The European Physical Journal Special Topics*, **225** (2016), 2099.

[50] Ginelli, F. and Chaté, H. Relevance of metric-free interactions in flocking phenomena. *Physical Review Letters*, **105** (2010), 168103.

[51] Ginelli, F., Peruani, F., Pillot, M.-H., Chaté, H., Theraulaz, G., and Bon, R. Intermittent collective dynamics emerge from conflicting imperatives in sheep herds. *Proceedings of the National Academy of Sciences*, **112** (2015), 12729.

[52] Goldenfeld, N. *Lectures on Phase Transitions and the Renormalization Group.* Perseus Books, Reading, Massachusetts (1992).

[53] Goldstone, J. Field theories with superconductor solutions. *Il Nuovo Cimento (1955-1965)*, **19** (1961), 154.

[54] Hamilton III, W. J., Gilbert, W. M., Heppner, F. H., and Planck, R. J. Starling roost dispersal and a hypothetical mechanism regulating rhthmical animal movement to and from dispersal centers. *Ecology*, **48** (1967), 825.

[55] Hanke, T., Weber, C. A., and Frey, E. Understanding collective dynamics of soft active colloids by binary scattering. *Physical Review E*, **88** (2013), 052309.

[56] Hartley, R. and Zisserman, A. *Multiple view geometry in computer vision.* Cambridge University Press (2004).

[57] Hasselmann, K. Stochastic climate models part i. theory. *tellus*, **28** (1976), 473.

[58] Hemelrijk, C. K. and Hildenbrandt, H. Self-organized shape and frontal density of fish schools. *Ethology*, **114** (2008), 245. Available from: `https://onlinelibrary.wiley.com/doi/abs/10.1111/j.1439-0310.2007.01459.x`, `arXiv:https://onlinelibrary.wiley.com/doi/pdf/10.1111/j.1439-0310.2007.01459.x`, `doi:https://doi.org/10.1111/j.1439-0310.2007.01459.x`.

[59] Hemelrijk, C. K. and Hildenbrandt, H. Some causes of the variable shape of flocks of birds. *PloS one*, **6** (2011), e22479.

[60] Hemelrijk, C. K. and Hildenbrandt, H. Scale-free correlations, influential neighbours and speed control in flocks of birds. *Journal of Statistical Physics*, **158** (2015), 563.

[61] HEPPNER, F. H. Avian flight formations. *Bird-banding*, **45** (1974), 160.

[62] HERBERT-READ, J. E., PERNA, A., MANN, R. P., SCHAERF, T. M., SUMPTER, D. J. T., AND WARD, A. J. W. Inferring the rules of interaction of shoaling fish. *Proc Natl Acad Sci USA*, **108** (2011), 18726. `doi:10.1073/pnas.1109355108`.

[63] HUANG, K. *Introduction to statistical physics.* Chapman and Hall/CRC (2009).

[64] HUTH, A. AND WISSEL, C. The simulation of the movement of fish schools. *Journal of theoretical biology*, **156** (1992), 365.

[65] ISACCHINI, G., WALCZAK, A. M., MORA, T., AND NOURMOHAMMAD, A. Deep generative selection models of t and b cell receptor repertoires with sonnia. *Proceedings of the National Academy of Sciences*, **118** (2021).

[66] JACKSON, J. D. Classical electrodynamics (1999).

[67] JAYNES, E. T. Information theory and statistical mechanics. *Physical Review*, **106** (1957), 620. Available from: `http://adsabs.harvard.edu/cgi-bin/nph-data_query?bibcode=1957PhRv..106..620J&link_type=ABSTRACT`, `doi:10.1103/PhysRev.106.620`.

[68] JAYNES, E. T. Information theory and statistical mechanics. ii. *Physical Review*, **108** (1957), 171. Available from: `http://adsabs.harvard.edu/cgi-bin/nph-data_query?bibcode=1957PhRv..108..171J&link_type=ABSTRACT`, `doi:10.1103/PhysRev.108.171`.

[69] JOLLES, J. W., KING, A. J., MANICA, A., AND THORNTON, A. Heterogeneous structure in mixed-species corvid flocks in flight. *Animal Behaviour*, **85** (2013), 743.

[70] KARDAR, M. *Statistical Physics of Fields.* Cambridge University Press (2007). `doi:10.1017/CBO9780511815881`.

[71] KARDAR, M., PARISI, G., AND ZHANG, Y.-C. Dynamic scaling of growing interfaces. *Phys. Rev. Lett.*, **56** (1986), 889. Available from: `https://link.aps.org/doi/10.1103/PhysRevLett.56.889`, `doi:10.1103/PhysRevLett.56.889`.

[72] KOSTERLITZ, J. M. AND THOULESS, D. J. Ordering, metastability and phase transitions in two-dimensional systems. *Journal of Physics C: Solid State Physics*, **6** (1973), 1181.

[73] LE BELLAC, M. *Quantum and Statistical Field Theory.* Clarendon Press Oxford (1991).

[74] LING, H., MCLVOR, G. E., WESTLEY, J., VAN DER VAART, K., VAUGHAN, R. T., THORNTON, A., AND OUELLETTE, N. T. Behavioural plasticity and the transition to order in jackdaw flocks. *Nature communications*, **10** (2019), 1.

[75] Ling, H., Mclvor, G. E., Westley, J., Van der Vaart, K., Yin, J., Vaughan, R. T., Thornton, A., and Ouellette, N. T. Collective turns in jackdaw flocks: kinematics and information transfer. *Journal of the Royal Society Interface*, **16** (2019), 20190450.

[76] MacGregor, H. E., Herbert-Read, J. E., and Ioannou, C. C. Information can explain the dynamics of group order in animal collective behaviour. *Nature communications*, **11** (2020), 1.

[77] Manabe, S. and Wetherald, R. T. Thermal equilibrium of the atmosphere with a given distribution of relative humidity. *Journal of the Atmospheric Sciences*, (1967).

[78] Marconi, U. M. B., Puglisi, A., Rondoni, L., and Vulpiani, A. Fluctuation–dissipation: response theory in statistical physics. *Physics reports*, **461** (2008), 111.

[79] Mermin, N. D. and Wagner, H. Absence of ferromagnetism or antiferromagnetism in one- or two-dimensional isotropic heisenberg models. *Phys. Rev. Lett.*, **17** (1966), 1133. Available from: `http://link.aps.org/doi/10.1103/PhysRevLett.17.1133`, `doi:10.1103/PhysRevLett.17.1133`.

[80] Meshulam, L., Gauthier, J. L., Brody, C. D., Tank, D. W., and Bialek, W. Collective behavior of place and non-place neurons in the hippocampal network. *Neuron*, **96** (2017), 1178.

[81] Meshulam, L., Gauthier, J. L., Brody, C. D., Tank, D. W., and Bialek, W. Coarse graining, fixed points, and scaling in a large population of neurons. *Physical review letters*, **123** (2019), 178103.

[82] Mezard, M., Parisi, G., and Virasoro, M. *Spin Glass Theory and Beyond: An Introduction to the Replica Method and Its Applications*, vol. 9. World Scientific (1987).

[83] Mora, T. and Bialek, W. Are biological systems poised at criticality? *Journal of Statistical Physics*, **144** (2011), 268.

[84] Mora, T. and Bialek, W. Are biological systems poised at criticality? *J Stat Phys*, **144** (2011), 268. `doi:10.1007/s10955-011-0229-4`.

[85] Mora, T., Walczak, A. M., Del Castello, L., Ginelli, F., Melillo, S., Parisi, L., Viale, M., Cavagna, A., and Giardina, I. Local equilibrium in bird flocks. *Nature Physics*, **12** (2016), 1153.

[86] Murugan, A., Mora, T., Walczak, A. M., and Callan, C. G. Statistical inference of the generation probability of t-cell receptors from sequence repertoires. *Proceedings of the National Academy of Sciences*, **109** (2012), 16161.

[87] Nagy, M., Vásárhelyi, G., Pettit, B., Roberts-Mariani, I., Vicsek, T., and Biro, D. Context-dependent hierarchies in pigeons. *Proceedings of the National Academy of Sciences*, **110** (2013), 13049.

[88] NIWA, H.-S. Self-organizing dynamic model of fish schooling. *Journal of theoretical Biology*, **171** (1994), 123.

[89] PARISI, G. Infinite number of order parameters for spin-glasses. *Phys. Rev. Lett.*, **43** (1979), 1754. Available from: `https://link.aps.org/doi/10.1103/PhysRevLett.43.1754`, `doi:10.1103/PhysRevLett.43.1754`.

[90] PARISI, G. Asymmetric neural networks and the process of learning. *Journal of Physics A: Mathematical and General*, **19** (1986), L675.

[91] PARISI, G. *Statistical field theory.* Frontiers in Physics. Addison-Wesley, Redwood City, CA (1988). Available from: `https://cds.cern.ch/record/111935`.

[92] PATASHINSKII, A. AND POKROVSKII, V. Longitudinal susceptibility and correlations in degenerate systems. *Zh. Eksp. Teor. Fiz*, **64** (1973), 1445.

[93] PATASHINSKII, A. Z. AND POKROVSKII, V. L. *Fluctuation Theory of Phase Transitions.* Pergamon Press (1979).

[94] PENNYCUICK, C. J. Mechanical constraints on the evolution of flight. *Memoirs of the California Academy of Sciences*, **8** (1986), 83.

[95] PESKIN, M. E. *An introduction to quantum field theory.* CRC press (2018).

[96] PROCACCINI, A., ET AL. Propagating waves in starling, sturnus vulgaris, flocks under predation. *Animal behaviour*, **82** (2011), 759.

[97] RAPAPORT, D. C. *The art of molecular dynamics simulation.* Cambridge University Press, 2nd edn. (2004).

[98] RAYNER, J. M. Form and function in avian flight. In *Current ornithology*, pp. 1–66. Springer (1988).

[99] RAYNER, J. M. Biomechanical constraints on size in flying vertebrates. In *Symposia of the Zoological Society of London*, 69, pp. 83–110. London: The Society, 1960-1999. (1996).

[100] RYDER, L. H. *Quantum field theory.* Cambridge university press (1996).

[101] SOLON, A. P. AND TAILLEUR, J. Revisiting the flocking transition using active spins. *Phys. Rev. Lett.*, **111** (2013), 078101. Available from: `https://link.aps.org/doi/10.1103/PhysRevLett.111.078101`, `doi:10.1103/PhysRevLett.111.078101`.

[102] STANLEY, H. E. Dependence of critical properties on dimensionality of spins. *Phys. Rev. Lett.*, **20** (1968), 589. Available from: `https://link.aps.org/doi/10.1103/PhysRevLett.20.589`, `doi:10.1103/PhysRevLett.20.589`.

[103] STANLEY, H. E. *Introduction to Phase Transitions and Critical Phenomena* (1987).

[104] TAKAHASHI, Y. On the generalized ward identity. *Il Nuovo Cimento (1955-1965)*, **6** (1957), 371.

[105] TKACIK, G., MORA, T., MARRE, O., AMODEI, D., BERRY II, M. J., AND BIALEK, W. Thermodynamics for a network of neurons: Signatures of criticality. *arXiv preprint arXiv:1407.5946*, (2014).

[106] TONER, J. AND TU, Y. Long-range order in a two-dimensional dynamical xy model: How birds fly together. *Phys Rev Lett*, **75** (1995), 4326.

[107] TONER, J. AND TU, Y. Flocks, herds, and schools: A quantitative theory of flocking. *Physical review E*, **58** (1998), 4828.

[108] TONER, J., TU, Y., AND RAMASWAMY, S. Hydrodynamics and phases of flocks. *Annals of Physics*, **318** (2005), 170.

[109] TU, Y., TONER, J., AND ULM, M. Sound waves and the absence of galilean invariance in flocks. *Phys. Rev. Lett.*, **80** (1998), 4819. `doi: 10.1103/PhysRevLett.80.4819`.

[110] VICSEK, T., CZIRÓK, A., BEN-JACOB, E., COHEN, I., AND SHOCHET, O. Novel type of phase transition in a system of self-driven particles. *Phys Rev Lett*, **75** (1995), 1226.

[111] VICSEK, T. AND ZAFEIRIS, A. Collective motion. *Physics Reports*, **517** (2012), 71.

[112] WARD, J. C. An identity in quantum electrodynamics. *Phys. Rev.*, **78** (1950), 182. Available from: `https://link.aps.org/doi/10.1103/PhysRev.78.182`, `doi:10.1103/PhysRev.78.182`.

[113] WATTS, I., NAGY, M., BURT DE PERERA, T., AND BIRO, D. Misinformed leaders lose influence over pigeon flocks. *Biology letters*, **12** (2016), 20160544.

[114] WILSON, K. G. Renormalization group and critical phenomena. i. renormalization group and the kadanoff scaling picture. *Physical review B*, **4** (1971), 3174.

[115] WILSON, K. G. Renormalization group and strong interactions. *Physical Review D*, **3** (1971), 1818.

[116] WILSON, K. G. Problems in physics with many scales of length. *Scientific American*, **241** (1979), 158.

[117] WILSON, K. G. AND FISHER, M. E. Critical exponents in 3.99 dimensions. *Physical Review Letters*, **28** (1972), 240.

[118] WILSON, K. G. AND KOGUT, J. The renormalization group and the ϵ expansion. *Physics Reports*, **12** (1974), 75.

[119] YANG, D., OZGUNER, U., AND REDMILL, K. Social force based microscopic modeling of vehicle-crowd interaction. In *2018 IEEE Intelligent Vehicles Symposium (IV)*, pp. 1537–1542 (2018). `doi:10.1109/IVS.2018.8500499`.

[120] ZEE, A. V. *Group Theory in a Nutshell for Physicists.* Princeton Univ P (2016).

[121] ZINN-JUSTIN, J. Quantum Field Theory and Critical Phenomena (2002). International Series of Monographs on Physics 113, 1054 pp. (2002), Fourth Edition. Available from: `https://hal.archives-ouvertes.fr/hal-00120423`.

[122] ZINN-JUSTIN, J. *Phase transitions and renormalization group.* Oxford University Press on Demand (2007).

[123] ZWANZIG, R. *Nonequilibrium statistical mechanics.* Oxford university press (2001).